WARSAW UNIVERSITY
OF TECHNOLOGY

Faculty of Automotive and Construction Machinery Engineering

Ph.D. THESIS

Jacek Mateusz Bajkowski, M.Sc.
jm.bajkowski@gmail.com

Vibrations of sandwich beams controlled by smart materials

Supervisor
Professor Czesław Bajer
Auxiliary supervisor
Ph.D. Bartłomiej Dyniewicz

Warsaw 2014

ABSTRACT

The study presents results of a research on a semi-active control method of damping of vibration of a beam structure, treated with smart materials. Two materials were considered as damping elements: magnetorheological elastomer controlled with magnetic field and granular structures, subjected to controlled underpressure. Mathematical models of the systems are represented by the equations of three layered sandwich beam with core of controllable shear modulus and a phenomenological model of the granular material. For such models the optimal control problem was posed, considering the concept of intermediate switching of the systems' parameters instead of the damping turned constantly on. The resulting control was verified experimentally in free vibrations of a sandwich cantilever beam. The laboratory research proved that the appropriate, periodic switching of the properties of the considered materials enables to reduce the vibration more effectively than if the material is treated passively. The surplus reaches 20%–30% or more. The range of applicability and limitations of the proposed solution has been given, as well as the benefits from the application. The proposed semi-active control can be directly applied to engineering vibrating structural elements.

STRESZCZENIE

W pracy przedstawiono wyniki badań półaktywnego tłumienia drgań układu belkowego za pomocą sterowanych materiałów inteligentnych. Rozpatrzono dwa rodzaje materiałów wykorzystanych do budowy elementów tłumiących: elastomer magnetoreologiczny sterowany polem magnetycznym oraz specjalną strukturę granulowaną sterowaną za pomocą podciśnienia. Matematyczny opis układów reprezentowany jest przez model belki trójwarstwowej z odkształcalnym rdzeniem o sterowanym module ścinania oraz model fenomenologiczny struktury granulowanej. Sformułowano zagadnienie optymalnego sterowania układem, korzystając z koncepcji okresowego przełączania parametrów układu zamiast tłumienia załączonego w sposób ciągły. Teoretycznie wyznaczoną strategię sterowania zaadaptowano w rzeczywistym układzie laboratoryjnym. Badania eksperymentalne potwierdziły, że okresowe załączanie w odpowiednich chwilach sygnału sterowania elastomerem magnetoreologicznym lub strukturą granulowaną, pozwala na skuteczniejsze tłumienie drgań układu, niż w przypadku tłumienia działającego w sposób pasywny. W zależności od zastosowanego materiału i wybranej strategii sterowania, drgania udaje się wytłumić w czasie krótszym o 20%–30%. Określono zakres stosowalności i ograniczenia proponowanych rozwiązań oraz strategii sterowania. Wskazano korzyści wynikające z ich zastosowania oraz możliwe docelowe aplikacje inżynierskie.

Acknowledgements

For helping me to complete this work I would like to thank Prof. Mariusz Pyrz for advices and the SIMR Faculty authorities for supporting the research.

Contents

List of Figures

CHAPTER 1

Introduction

1.1 | Motivation

In the process of designing mechanical systems and structures, a major concern should be dedicated to face the challenge of unwanted vibration reduction. Exposing the structure to excessive stresses and strains caused by vibrations may lead to a catastrophic failures.

One of the most spectacular examples of such a failure is the collapse of the suspension bridge that spanned the Tacoma Narrows with the Kitsap Peninsula in USA, which was named the "Galloping Gertie" after the incident in 1940. The underdamped structure of the bridge was exposed to a wind excitation, which frequency was close to the natural frequency of a bridge and thus the amplitude of the forced system grew without a bound, eventually causing the bridge to fall (Figure 1.1a). The unexpected, dangerous vibrations still occasionally plague modern designs. The concrete girder bridge over the Volga River had been inaugurated in October 2009, and closed by the authorities to all motor traffic on May 2010, due to severe, wind-driven twisted mode vibrations (Figure 1.1b). During the opening day of the London Millennium Footbridge in 2000, unexpected synchronous lateral movements occurred when thousands of people were crossing the bridge at one time. Since day one, the bridge remained closed for almost 2 years.

In the design of machinery and structures, whether bridges, buildings, cranes, suspension of a car or an airplane's wing, actions leading to vibration attenuation help to prevent the system from the risky states and failures, assure its robustness, reduce the noise level, enhance the fatigue life and the comfort of use. As the possibility of reducing the source of vibrations and isolating the system members is highly limited, the additional damping members need to be introduced. **The development of the modern smart materials motivates to study the possibility of improving the damping properties of structures, by utilizing their unique controllable properties.**

To face undesired dynamical effects, either passive, active or semi-active damping method needs to be put into practice. The passive control involves selection of the mass,

(a) Tacoma Narrows Bridge

(b) Volga Bridge

Figure 1.1: Examples of mechanical systems plagued by unwanted oscillations.

stiffness or damping properties of the system, to make it less susceptible to vibrations, without requiring an external power source to operate. The obvious drawback of such a system is the lack of possibility to actively adjust its parameters. Once the system is configured, the parameters cannot be changed easily and passive vibration damping strategies become ineffective when the dynamics of the system or frequency of the disturbance varies with time. Materials mostly used in passive damping are composites [51], polymers, urethanes and synthetic rubber [21, 22, 99] or viscous fluids [90].

The active damping solutions require an external power source to operate properly. Usually they are based on the force actuators attached to the vibrating structure. The parameters of the system can be controlled in real time to increase the stability or perform desired trajectories of motion [56, 89]. Nevertheless, the poorly designed or malfunctioning active system can act in anti-phase, supplying the energy that may rapidly cause the damage of a structure [31]. A variable damping is widely used in vehicle suspension systems, improving the travel comfort by keeping the passage trajectory as smooth as possible (Figure 1.2), resulting in a greater performance than in case of a classic passive suspension.

The most interesting damping method seems to be the semi-active control. It utilizes the motion of the vibrating mechanical system to develop the control forces, so the energy requirement is lower than in the typical active damping treatment and the system is safer in the case of malfunction. Nevertheless, the semi-active solutions are usually less efficient than the active. The recent trend is to replace the active force actuators with adjustable rheological dampers or devices utilizing smart materials like magneto- and electrorheological fluids with controllable rheological properties, shape memory alloys or piezoelectric devices.

(a) Passive (b) Semi-active

Figure 1.2: Comparison of the vertical displacement of a car with different types of suspension passing a road bump.

This work introduces a semi-active control strategy of a three-layer beam, treated with the damping member made of magnetorheological elastomer (MRE) or special granular structure. The sandwich beam comprises thin, aluminium face sheets bonded to one of the two types of smart damping elements. The parameters of the damping member may be controlled by altering the magnetic field (for the MRE) or the underpressure (for the special granular structure). The parameters of the mechanical system, such as the stiffness or the coefficients of damping can be modified in real time to increase the stability of the system or to obtain the desired dynamical response. This type of an adaptive structure allows damping at much higher level than its equivalent traditional passive damping system.

Choosing the material, which properties best suits the particular application, is only small part of contribution in developing practical system with high efficiency of energy dissipation. The appropriate control strategy of the properties of the smart material is as much important as the material development itself. **When properly designed, the semi-active modulation of the system parameters can raise the damping capacity and at the same time decrease the amount of the energy required by the system to operate, making it more efficient.**

The damping solution presented in this work can lead to further improvements of existing damping systems and increase the number of applications utilizing properties of magnetorheological elastomers and special granular structures. It gives a chance of fabricating high-quality and cost-efficient damping systems that enable certain design flexibility.

1.2 | Thesis

Magnetorheological elastomers and special granular structures use different mechanisms to achieve the damping behaviour. For both of these materials the real time parameters of the damping element of a proposed sandwich beam can be controlled. The purpose of placing the lightweight member between the face materials is to sustain its deformations. It is assumed that as a result of the instantaneous local change of the stiffness in the inner layer, the entire beam starts to oscillate with higher modes. A controlled switching of the damping and stiffness leads to a faster energy dissipation, which means a quicker convergence to a steady state. No additional energy is introduced to the system, as the semi-active control utilizes the motion of the structure to develop the control forces.

The thesis of the work states that
switching at selected moments the damping properties of the magnetorheological elastomer or special granular structure, allows attenuating the vibration of the beam more effectively than when the damping is turned on constantly.

1.3 | Objectives

The main objective of this study is to design an efficient semi-active control method for free vibrations of a layered-cantilever with a smart material used as a damping element. Two materials of different mechanical and structural properties are considered: the magnetorheological elastomers controlled by the augmentation of the magnetic field, and the granular structures subjected to controlled underpressure. **The efficient control is the one that allows limiting the displacement amplitude and provides shorter stabilization time than the passive treatment.** The designed control system should be easy to adapt in a practical realization.

The optimal stabilization is the initially considered control objective. To solve the optimal control problem, the observed phenomena require development of an appropriate mathematical formulation of a sandwich beam with a core of variable parameters. The goal is to design the control laws that provide, with respect to some assumed metric, the fastest convergence of the beam vibration towards the equilibrium point. Prior to solving the optimal control problem, the identification of the parameters of the structure has to be performed.

The theoretically obtained control strategy needs to be verified and evaluated on a real object, hence the laboratory stand needs to be developed. Different control strategies, including the theoretically obtained one, need to be adapted as programmable logic con-

troller algorithm.

The outcome of this work will be the experimentally verified optimal control strategy for layered beams with the semi-actively controlled damping treatment and suggestions for improvements to existing applications and engineering solutions.

1.4 | Research Scope

The scope of the research was limited to the experimental and analytical investigation of the free decay of a three-layered sandwich beam in a free-clamped configuration. The scope includes:

- the literature review on the topic of vibration damping with the particular smart materials to settle the problem among the existing levels of knowledge,
- the mathematical modelling of a sandwich beam with controllable core for two materials: a magnetorheological elastomer and a special granular structure,
- solving the optimal control problem for both considered cases of layered beams,
- designing and implementing the switching control method with the reduced number of switchings; the control variables are the moments for turning on and off the damping properties of the material (changing the intensity of the chosen parameter of the system),
- transient response analysis of the real beam structure with passive and semi-active damping, for parameter identification.

The following problems are out of the scope, and they may be dedicated to the future works:

- the problem of composing and manufacturing the magnetorheological elastomer with properties providing the most efficient damping performance,
- fabrication of the granular damping element with the optimal parameters considering the geometry, topology and material properties of the granules, suited for particular application,
- investigation of the influence of size and location of the damping elements on the overall performance of the damping system,
- multi-physics modelling of the particle interactions of the special granular structure,

- studying the response and efficiency of the system for different types of excitations like dynamic or impulse loads.

1.5 | Dissertation Outline

The dissertation is divided into six main chapters and the appendices. The content of the chapters is as follows.

Chapter 1: Introduction

A short overview of the problem of vibration abatement is given, as well as the overview of the damping treatment methods. The main problem of the dissertation is introduced and the thesis is formulated. The objectives and scope of the research are stated in dedicated sections.

Chapter 2: Literature Background

This chapter provides literature background and information on application of the smart materials in vibration damping. The properties of magnetorheological elastomers and granular materials are characterized in **Section 2.1**. Exemplary applications for both types of materials are given. A short review of the approach to modelling of the sandwich structures is presented in **Section 2.2**.

Chapter 3: Problem Formulation and System Modelling

Chapter 3 focusses on the mathematical modelling of the proposed damping system. First, the method of periodically switching the parameters of a vibrating structure is described. A detailed principals of the mathematical analysis are discussed. Mathematical model of the layered beam with controllable MRE core and the mathematical model of a layered beam with the granular damping structure are formulated. Optimal control problems are posed and solved. The interpretation of numerical results is provided as well as the computed optimal control strategy.

Chapter 4: Experimental Setup and Calibration

This chapter provides technical information on the designed laboratory stand. The operation of the experimental equipment is covered along with the calibration of the measurement apparatus and the data acquisition system. The operation of the control system for the beam with magnetorheological elastomer and the beam with underpressure granular structure is covered with details. The geometrical and material parameters of the specimens are enclosed. Dedicated section describes important field of the signal processing of experimental data with the examples of data extraction, smoothing and filtering procedures.

Chapter 5: Experimental Results

The content of **Chapter 5** is based on the experiments carried on sandwich beams with smart dampers composed of materials with controllable material properties. The in-depth look at the most important results and parameters influencing performance of the damping members are critically reviewed. Identification of the parameters of the granular structure is given. Results from the theory and the experiments are compared. Observations concerning the proposed technique for the damping enhancements are made. The switching control strategy is thoroughly examined.

Chapter 6: Conclusions

The overview of the work and the final conclusions are drawn and discussed. The scope of applicability and the limitations of the proposed solutions, as well as the benefits from using that type of structures are defined. The dissertation concludes with possible engineering applications, perspectives and recommendations on the topic of the dissertation. Finally, the directions for further work are recommended.

Appendices

Following the main chapters, **Appendices** provide an extended experimental results which were omitted in the main part of the work with some additional remarks. The programmable logic controller ladder diagram algorithms, used to compute the real output signal for the actuating electromagnets and electrovalve are enclosed.

CHAPTER 2

Literature Background

The topic concerned in this dissertation is a multidisciplinary problem, which combines mainly the mechanics of layered structures and the semi-active control of beams vibration. Literature on these issues is extensive and it would be a major challenge to create the full list, whereas the studies on damping properties of the magnetorheological elastomers and vacuum packed granules are very rare. Therefore, the author decided to shorten the list of the well described issues on layered beams and elaborate on the ones dealing with the unique properties of the materials of interest. More examples of possible applications of the discussed materials were formulated on the basis of the acquired research results, and discussed in **Section 6.1:Perspectives** in **Chapter 6: Conclusions**.

2.1 | Smart Materials in Vibration Damping

2.1.1 Magnetorheological Elastomers

Since the discovery of magnetorheological (MR) effect by Rabinow in 1948 [74, 75], these smart materials have developed into a family with MR fluids, foams, greases, gels, and elastomers. Generally, the MR materials are ferromagnetic, micrometer-sized carbonyl iron particles suspended in a carrier medium. The most common in this group are the fluids, with particles suspended in a silicone oil [6].

Elastomers are the new branch in the group of magnetorheological materials. They are the structural solid analogues of the fluids but the magnetizable particles are dispersed in a non-magnetic, solid polymer matrix. Usually they are composed by randomly mixing particles in the matrix or alternatively, using strong uniaxial magnetic field to induce dipole moments in the particles pointing along the constant magnetic field. When the elastomer matrix is cured, the ferrous particles chains are locked and embedded in the matrix, as shown in Figure 2.1.

The magnetorheological elastomers exhibit unique mechanical performance compared

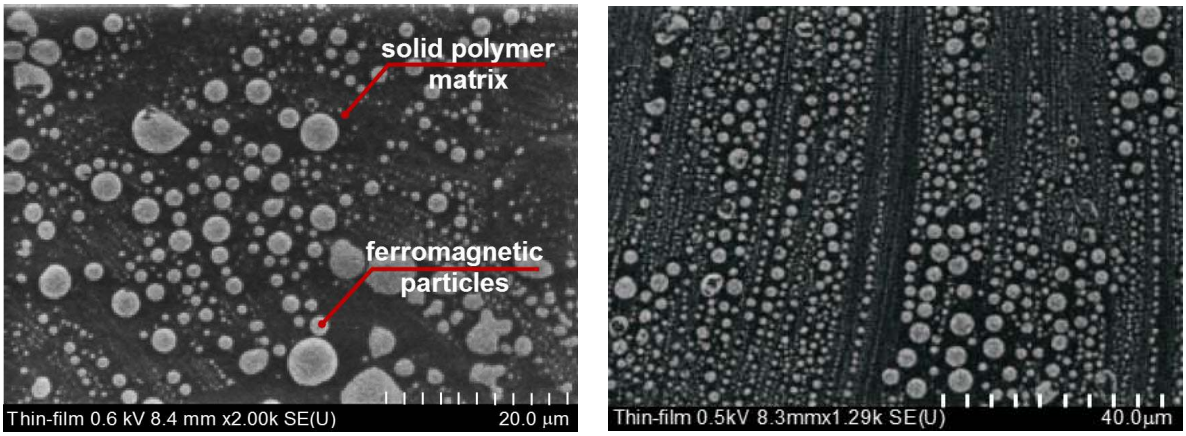

(a) Randomly dispersed particles (b) Aligned particles

Figure 2.1: SEM images of the alignment of ferromagnetic particles in a matrix of a cured magnetorheological elastomer [37].

to other materials. When exposed to a magnetic field, the properties of the material change rapidly and reversibly in a matter of several milliseconds [30].

Shearing of the cured elastomer causes particle displacement from the low net energy state. It requires additional work, which increases with the applied magnetic field, thus resulting in a field dependent shear modulus (Figure 2.2a), while fluids have a field-dependent yield stress (Figure 2.2b). The particles within elastomers typically operate in the pre-yield regime while MR fluids typically operate in the post-yield continuous shear or flow regime. This makes the MR fluids and elastomers complementary materials, rather than competitive to each other. From Figure 2.2a it can be seen that the shear modulus for elastomer is increasing with the magnetic field intensity, until the material reaches the magnetic saturation. Further enhance of the magnetic field got no effect on the value of the shear modulus. The fraction of the magnetizable particles should be sufficient to provide the required on-state mechanical properties.

The main advantage of MR elastomers over the fluids is their stability against sedimentation, coagulation and particle clustering [47]. As a consequence of the fact that the chain-like particle structures have been locked in the matrix material during the process of curing, the rearrangement of the particles is eliminated when the external magnetic field is applied. Consequently the response time of MRE is much quicker than for the fluids.

Elastomers are easy to process, which gives possibility of embedding them between beams or plates to obtain a layered structure. Furthermore, the size and shape of the pad can be designed to fit particular requirements. The urge for container to keep the MR fluid in place is eliminated for the elastomers. Also they do not change their prop-

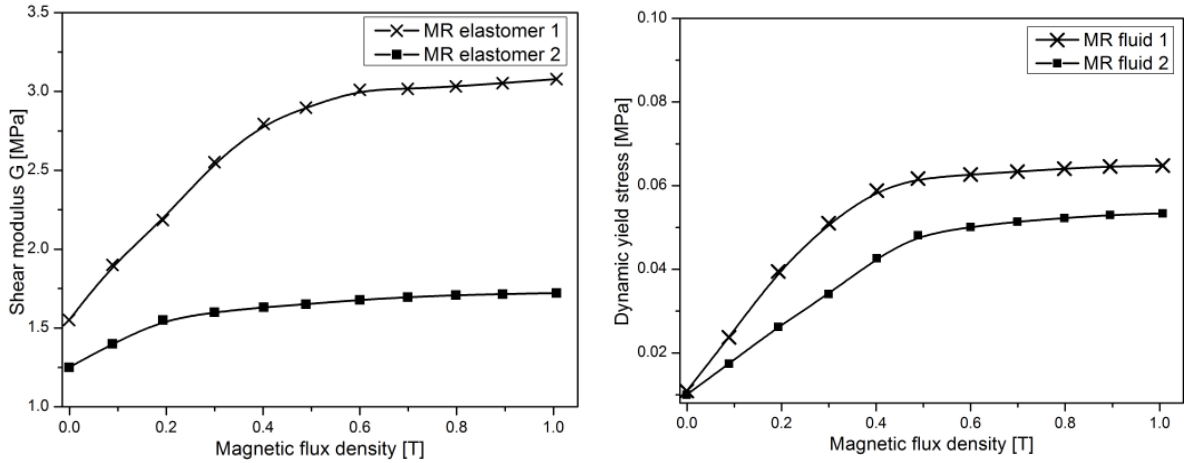

(a) MR elastomer (b) MR fluid

Figure 2.2: Comparison of typical characteristics of different MR materials.

erties rapidly with temperature, as it can be observed for the fluids [6]. Nevertheless, MRE compared with MR fluids have only found limited applications, mainly due to the fact that the field-dependent modulus change is not wide enough to meet the demands of particular applications. Several groups of researchers have taken efforts to improve the parameters, reporting on elastomers with magnetorheological effect enhanced several times [19, 72, 85]. Further material technology development is crucial to significantly improve the characteristics of these materials.

Although much research on MRE is still at a primary stage, undoubtedly they predestined for the applications focused on three main areas that can make use of controllable stiffness:

- **sound and vibration control**, especially for the vehicle applications, like the tuned vibration absorbers [23, 24, 94, 106] (Figure 2.3a),
- **controllable stiffness change and deformation**, like in the stiffness tunable mounts and suspensions [3] used to stabilize buildings (Figure 2.3b), variable impedance surfaces [18, 20], or adaptive spring elements for the system's natural frequency shift [39],
- **sensors and magnetoactive actuators applications** like in US20056877193 [68] and US20040074066 [91] which describe the complex releasable fastener system with MRE hooks that provide change in shape, orientation or flexural modulus of the fastener elements.

The solutions utilizing MRE as damping layers for the vibration control of flexible sandwich structures are rare. In US7086507 [32], the authors came up with the device for

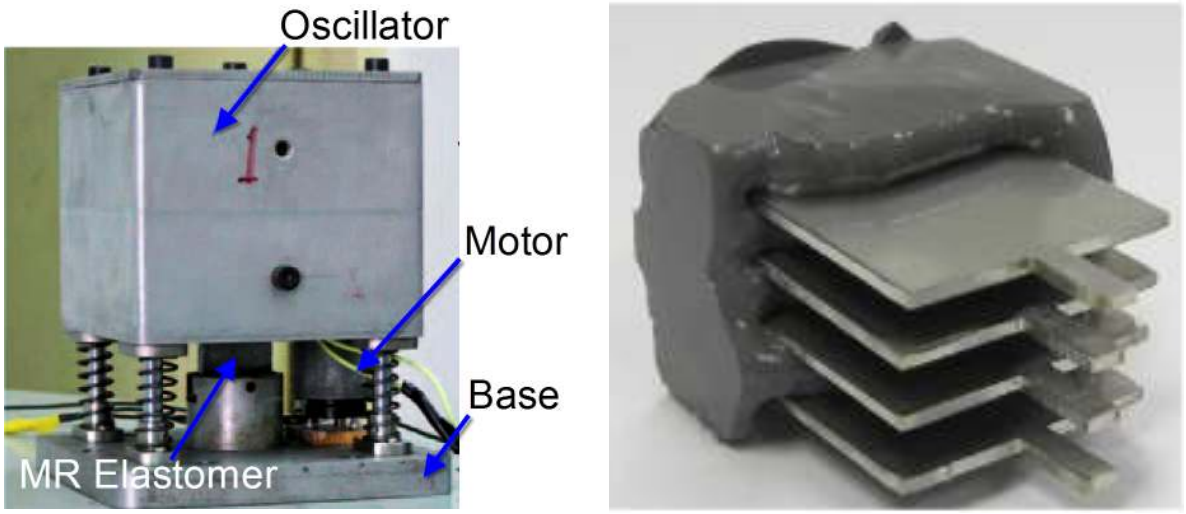

(a) Vibration absorber

(b) Laminated MRE isolator

Figure 2.3: Exemplary, prototype applications of magnetorheological elastomers.

vibration isolation of mechanical systems for random shock events by changing the storage and loss modulus of the MRE core embodied between magnetic activation layers. In [61] authors study the transverse deflection of a three-layered magnetorheological elastomer embedded viscoelastic cored sandwich beam with conductive and non-conductive skins. The authors investigated how the size and locations of the MRE patches influence the vibration properties of the structure. Ying and Ni [102] adapted MRE for damping of the micro-vibration of a clamped-free sandwich beam under stochastic micro-motion excitation. In several studies the influence of the magnetic field on the vibration suppression capabilities of such beams is described in the form of variations in loss factors [44, 93, 101], vibration amplitudes [76, 98] and shifts in natural frequency values [100].

2.1.2 Granular Materials

Different methods for reducing vibration are based on the dissipative nature of particle collisions in the granular material. It may be compared to a derivative of a single-mass impact damper (Figure 2.4a). This is a relatively simple concept, where particles of a small size are placed in a container that is attached to the structure, as illustrated in Figure 2.4b. In typical applications the movement of the loose grains inside the enclosure causes the dissipation of part of the energy through non-conservative collisions among the grains, and the grains against the container walls.

This mechanism was applied in linear particle impact dampers like the one presented in [82, 83, 86] and further used for damping of the beams vibrations, by placing the stiff box at the tip of an oscillating cantilever [52] (Figure 2.5a). Furthermore, the solution

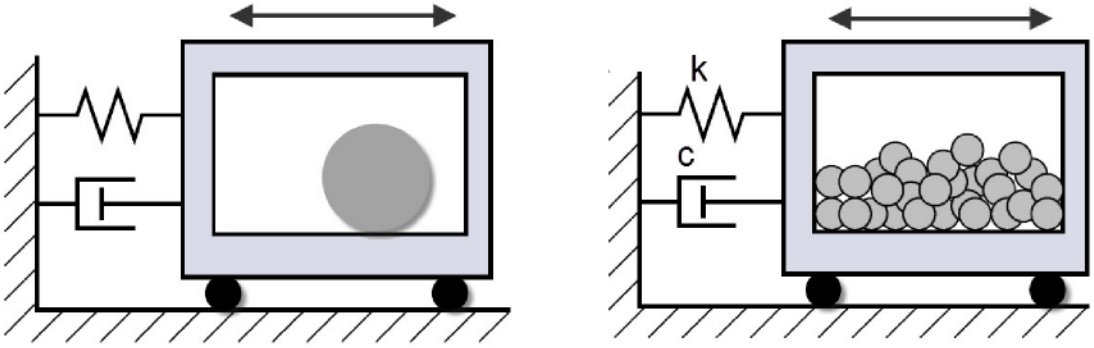

(a) Impact damper (b) Particle damper

Figure 2.4: Schematics of different types of particle impact dampers.

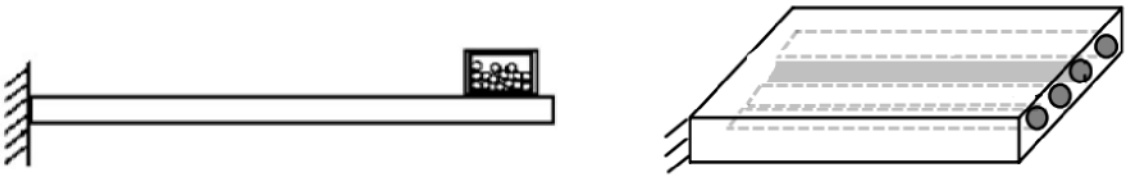

(a) Damping of transverse vibrations (b) Longitudinal particle damping

Figure 2.5: Schematics of granular material used a damping medium for cantilever beams.

was found to be effective for the beams under centrifugal loads [29].

Park and Palumbo in [69] described the structural vibration damping capabilities of the loose, lightweight particles, filling cavities in aluminum sandwich beams. The vibration of the structure induces vibration of the micro particles in the cavities, which dissipate energy into the heat due to the internal damping. In [53] authors investigated vibration damping of beams filled with tightly packed elastomeric beads. In [62] authors described a set of empirical studies on vibration of aluminum beams filled with 65 μm granules, whose total mass is only 3% of the unfilled beam. The authors in [92] investigated damping behaviour of laminated honeycomb cantilevers with fine solder balls placed in the transversal or longitudinal cells (Figure 2.5b). The displacement attenuation was achieved by the exchange of momentum through the repeated collisions between the balls and the face sheets. The mechanism was found to be effective in reducing the amplitude without significantly shifting the natural frequency of the cantilever. In all of the mentioned studies it was shown that the conduction of the energy into the micro-sized granular material and the following dissipation increase the vibration damping significantly.

The damping solution utilizing granular material subjected to underpressure is notably different from the solutions in the publications mentioned above, and it uses completely different principle. Placing the granular material

in the hermetic and elastic envelope with the remaining possibility of adjusting the underpressure value among the granules (Figure 2.6), gives such obtained structure features typical for smart materials.

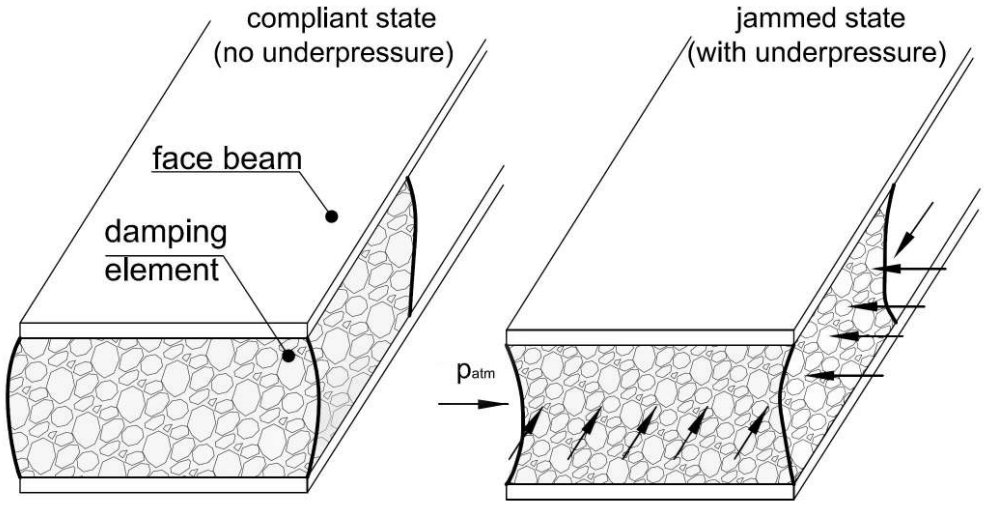

Figure 2.6: Construction of the beam with the granular damping member controlled by the underpressure value (compliant state and jammed state).

Unlike in [62] or [69], the particles are much larger, with the diameter of several millimeters and **their movement is significantly limited by the boundary conditions, forced by an elastic envelope**. The proposed pneumatic structure exploits fluid-like to solid-like reversible phase transition of the granular material, known as the jamming [13, 17]. **The transition to a jammed state is forced by subjecting the structure to an underpressure, and the properties of the structure can be real-time controlled by adjusting the value of the partial vacuum**. The details covering the fabrication, dimensions and principles of operation of the discussed beam are presented in **Chapter 5**.

According to the definition of smart material formulated by Ahmad [2], this special granular structure may be concerned *smart*, as the material *is capable of responding to the stimulus in a predetermined manner and extent, in a short time, and reverting to its original state as soon as the stimulus is removed*, which is a feature unattainable by the classic granular dampers.

The negative pressure intensifies the mechanisms which enhance the rigidity of the structure and the energy of dissipation, like the friction and slips among the particles and between the particles and the enclosure [36], hence it enables the reduction of the free transverse vibrations. Other mechanisms, such as the particle intrusion, occur when the granules change their position or orientation. The particle can also be pushed over

an underlying layer as the particle hopping takes place [16]. The particle deformation can promote or inhibit the total deformation [46]. The level of deformation of particles depends on the hardness and stiffness of the granular material [38]. The stability of the packing and the probability distributions of the forces depend on the number of layers up to a certain limit and were examined in [1].

The applications of underpressure granular materials in elastic envelopes are mainly limited to medical services like the vacuum medical pillows, mattresses [49] or splints [14] which form a firm, uniform support for parts of the body (Figure 2.7a). Furthermore interesting prototype constructions are developed, like the vacuum granular endoscope guide [46], laparoscopy camera shaft [35] or upper-arm orthotic [55]. By controlling the inside air pressure, the orthotic can exert a stiffness or viscosity on the joints. The interesting field of research are the soft robots that move respectively to the underpressure [88] or the universal robotic gripper with an elastic cell filled with granules (Figure 2.7b), which allows picking differently shaped objects [15].

(a) Medical stiffener (b) Universal robotic gripper Versaball

Figure 2.7: Example of applications of granular structures subjected to underpressure.

Despite the medical applications and prototype robots, there are only a few studies dealing with the potential of using such structures subjected to underpressure as a damping material with smart properties. Broad overview of the models for loose and compacted granular materials is presented in books [63, 81]. However, the connection between these models and the case when the granular material is dynamically switched between two states is somehow unsettled.

The concept itself was introduced and briefly characterized in papers [7, 8]. Main research effort was directed towards determination of the damping and elastic properties of the pneumatic granular structure used in a linear damper, subjected to axial forces [9, 10]. The rheological models of granular conglomerates under partial vacuum were presented in [103]. The constitutive model was later expanded to a six parameters rheological model

capable of capturing the response of the conglomerate subjected to an axial cyclic loading [105]. Nevertheless these models do not translate directly for the sandwich beams. The experimental approach to the analysis of the vibration of a steel beam, fully covered with a sleeve filled with granules was given in [104] and later compared with a simplified model of the dynamics in [11].

2.2 | Modelling of Sandwich Structures

One of the usual solutions for beam damping are the composite sandwich sheets into which a thin layers of viscoelastic materials has been placed between the face layers. Usually the structure comprises outer metal skins to enhance their bulk zero-field flexural rigidity and utilizes the soft core properties to alter their bulk flexural rigidity due to the transverse shear modulus. The integrated viscoelastic cores were proven to be effective in reducing vibration response of lightweight and flexible structures [58, 59]. Over the years many different mathematical models were employed to describe the dynamic response of such structures.

Since when Kerwin in 1959 in his pioneering work [41] examined the possibility of utilizing properties of viscoelastic material sandwich structures to reduce vibration and initiated modelling studies, the theoretical investigation of a three-layer damped beams has received considerable attention. In his work, Kerwin refers to the transverse vibration of an infinitely long beam with the damping layer. A simply supported sandwich beam was considered, supposing only transverse shear for the core and negligible bending rigidity for the core and the constraining layer. The solution was obtained in the form of the travelling waves.

The work was continued by Ross et al. [80], who derived an expression describing the loss factor and complex bending stiffness of a beam from relationship of the displacements and forces, and compared theoretical and experimental results. In the RKU model called after Ross, Kerwin and Ungar, the vibratory energy is dissipated through the predominant mechanism of shearing of the viscoelastic layer. The RKU model was later extended by Ditaranto [25, 26], who derived a sixth-order differential equation which could predict the longitudinal vibration response of a three-layered damped plate. The equation was solved in the form of the standing waves for arbitrary boundary conditions. The performed calculations showed that the parameters responsible for the efficiency of the damping layer described in [41], limited to the analysis of an infinite beam, can also be used for any non-dissipative boundary conditions and forced vibrations.

Mead and Markus [54] came up with the sixth-order differential equation for general-

ized boundary conditions of viscoelastically damped transversal oscillations of a sandwich beam. The model was experimentally verified by Lu and Douglas [48] who proved that it adequately predicts the damped resonance frequencies and damping inherent in the low-order modes of relatively thin three-layer laminates. Formulation proposed in [27] includes thickness deformation of the core layer and deals with the case where only a portion of the base structure receives the treatment. Later, in [95, 96] Mead and Markus model was extended to homogeneous and non-homogeneous adaptive beam with smart damping layers for various boundary conditions. In [97], the energy method was used to predict and compare the vibration responses of adaptive structures.

The vast majority of further work makes use of a mathematical basis from the solutions presented above, identifying the loss factor [77] or stability of the system [40]. In [12] a non-uniform shear stress variation across the thickness of each layer was assumed. The proposed approach enabled to determine the loss factor of the simply supported sandwich beam. Numerical results showed that the existing models are not suited when the shear modulus of the core is small. The analytical model that takes into account the compressional vibration of the layered beam is shown in [87]. Attempts to describe the sandwich beams with simple models were given in [4]. By implementing the frequency-dependent parameters, the vibration of sandwich composite beams can be approximated by using a simple fourth-order beam theory. A higher-order sandwich beam model is used to obtain estimates for frequency-dependent flexural stiffness and shear modulus corresponding to Euler and Timoshenko models. In [73] Posiadała presented the solution of the free vibration problem of a Timoshenko beam with different disturbing elements attached like elastic supports, rigidly or elastically mounted masses, etc. In [50] the theoretical five-layered beam model, which incorporates thin adhesive layers connecting the face-plates to the core was examined.

In order to take into account large amplitude vibrations of sandwich structures, the nonlinear modelling is also carried out. In [33] the harmonic forced vibration of a clamped-clamped sandwich beam with viscoelastic core was analyzed. The proposed model takes into account the geometric nonlinearity introduced by von Karman strain. The theoretical analysis confirmed the super-harmonic type of the resonance observed in the experiment. Likewise in [42] von Karman non-linear dependence between deformation and displacement was assumed for the beam subjected to periodic distributed load. The gained load in combination with a sharp increase of deflection (loss of stability) results in change from regular to chaotic oscillations.

CHAPTER 3

Problem Formulation and System Modelling

3.1 | Switched Parameters Damping Method

The essence of this work is to combine two components into a single entity: the layered structure with a core of variable dynamic properties and a concept of semi-active control strategy, aimed at mitigation of the displacement amplitude. Numerous variants of semi-active methods have been already considered in the literature on structural control, as well as the concept of periodical modification of the system parameters [5, 57, 65]. However, since many new adaptive materials were developed just quite recently, the possibility of practical application of it remains somehow unexplored. This section will elaborate on the unique solution for the beams with magnetorheological elastomers and special granular structures, which was not studied elsewhere. **For both materials the strategy of periodical switching of the parameters is assumed, although different parameters are altered because of the differences in the dissipation mechanisms.** For the elastomer the change of the value of the shear modulus is realized by altering the magnetic field. For the granular materials we are periodically jamming and unjamming the structure by changing the underpressure, thus the rigidity, damping and friction change. The proposed models were later confronted with the experimental results.

The worth-mentioning papers on the variable stiffness devices are in the field of tunable vibration isolators. Despite the papers that describe theoretical solutions, mostly for a single degree of freedom system like in [34, 43, 64], only a few consider beam-like structures. In [60] authors studied simply supported beam equipped with a piezoelectric actuator, which realized two functions: full adhesion between two beam layers and full delamination. The study proved that the strategy can be very effective in mitigating of the fundamental mode of the structure, as the vibrations were fully damped in just four cycles. In [66] and [67] Ostachowicz et al. used counteracting shape memory alloys to suppress forced vibration of smart beams. Each of actuators was activated only under compression, while at the same time the opposite actuator remained inactivated, which resulted in fine

damping performance. In [78] the switched stiffness method was applied to a flexible beam with a moving base. In [79] the author proposed a simple semi-active vibration control algorithm for free vibrations of the beam filled with MR fluid. The method was based on switching the yield stress between two distinct values.

In a nutshell, the strategy of periodical switching of the parameters aims at converting the strain energy of a vibrating system into kinetic energy, which is then released from the system by the means of a dissipative device during its deformation. The process consists of two main stages. In the first phase some kinematic constraints imposed on the system are released when the maximum strain energy can be converted to the kinetic energy. It usually results in a local, higher frequency of vibrations. In the second phase kinematic constraints are reimposed. It leads to conversion of the part of the kinetic energy into other, non-mechanical form, for example heating-up of the actuator device. This can be compared to periodically switching the equilibrium position of the whole system. The system returns to its initial configuration, but with the declined amplitude of vibration. The process is semi-active as it does not require adding any substantial amount of energy into the system.

Let's demonstrate the idea considering a simple mass with spring system as shown in Figure 3.1. The spring posses the possibility of step-variable stiffness switching between

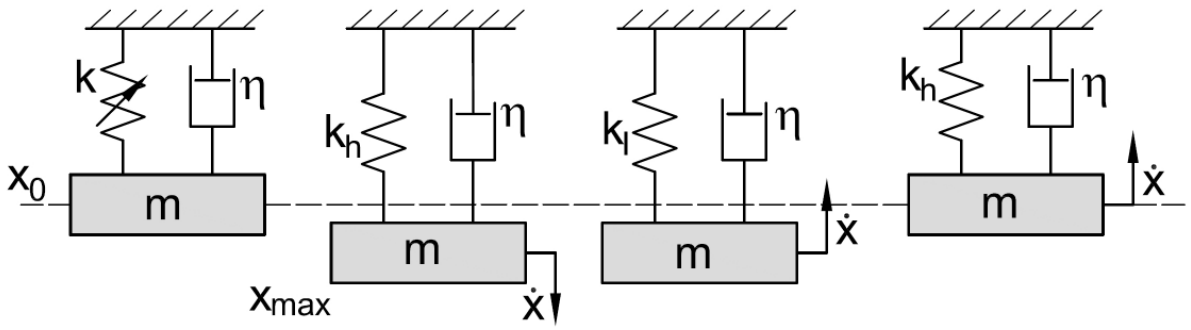

Figure 3.1: Single mass with variable stiffness spring system.

the high value k_h and the low value k_l. **One can imagine, that there are particular points of switching the parameters that will result in a better damping behaviour than others.**

For an idealized case of free vibrations, neglecting the inertia of the spring, the motion is governed by the equation

$$m\ddot{x}(t) + \eta\dot{x}(t) + kx(t) = 0\,. \tag{3.1}$$

Let's switch the stiffness of the spring to k_h when the mass is moving away from the equilibrium position $x = 0$, so the potential energy is maximized. The potential energy of a spring is equal to the work of the elastic force which acted along the displacement. The maximum potential energy occurs at the point of maximum displacement of the mass where $\dot{x} = 0$, thus at this point the kinetic energy vanishes

$$E_{p\,\max} = \int_0^{x_{\max}} k_h x dx = \frac{k_h {x^2}_{\max}}{2}\,. \tag{3.2}$$

When the potential energy reaches maximum, the stiffness is switched to the low value k_l and kept until the mass reaches back the equilibrium position. The loss in the potential energy caused by switching of the stiffness is equal to

$$\Delta E_p = \frac{\Delta k {x^2}_{\max}}{2}\,, \tag{3.3}$$

where $\Delta k = k_h - k_l$. The loss in potential energy results in a declined kinetic energy, and is proportional to the absolute change in the stiffness of a spring. During the following phase, the system acts same as before, however, a considerable part of the total vibration amplitude is gradually diminished in each following cycle. If the desired effectiveness is reached then the operation of switching can be repeated again near the initial equilibrium position, resulting in returning to the initial configuration.

In practice part of the released strain energy is dissipated by the device which performs switching of the stiffness and the remaining part introduces higher frequency vibrations, nevertheless, it can be suppressed with natural damping of the system. For both types of the smart damping elements considered in this dissertation, the mathematical models of layered beams were formulated taking into consideration their unique characteristics in order to obtain the optimal moments for switching the system parameters.

3.2 | Beam with Magnetorheological Elastomer

3.2.1 Model of the Beam with MRE

Theoretical analysis can not be performed for arbitrary structures with equal simplicity. For the analytical solution, we choose the simply supported beam as one of the most representative structures. The governing set of differential equations for the vibrating sandwich beam was derived in [54]. The necessary assumptions and simplifications of the

analytical model are described below.

Let us consider a three-layered sandwich beam. Its cross-sectional geometry has the characteristic width b and the thicknesses of each layer is h_1, h_2, and h_3 (Figure 3.2). Longitudinal displacements u in the x direction and transversal displacements w in the z direction of the beam were taken into account. The face-plates are assumed to be purely

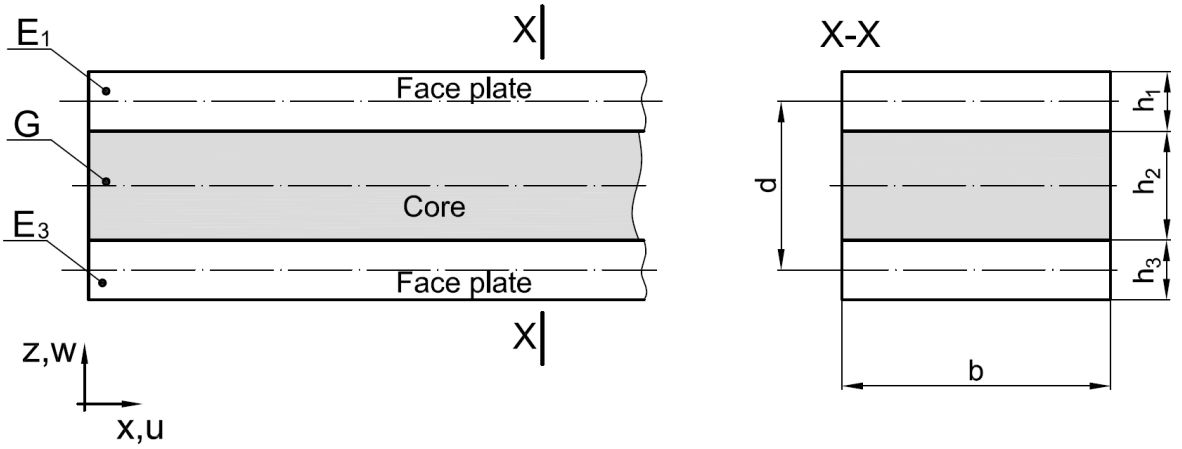

Figure 3.2: Dimensions and coordinate system of a three-layered beam with a viscoelastic core.

elastic, with Young modules E_1 and E_3, respectively. The core is linearly viscoelastic and defined by the shear modulus G. The obtained mathematical model is the result of some physically simplifying assumptions. The shear strains in the outer layers and the stresses in the longitudinal direction in the core were neglected. Moreover, the transversal direct strains in each layer were neglected as well, so the displacements w of the entire cross-section of the beam are constant (Figure 3.3a).

The shear strain in the core is given by the formula

$$\gamma = \frac{\partial w}{\partial x} + \frac{\partial u}{\partial z}\,. \tag{3.4}$$

The geometrical relationships in the deformed beam allows describing the term $\partial u/\partial z$ by the displacement pattern u_1, u_3 and $\partial w/\partial x$ of the face plates

$$\frac{\partial u}{\partial z} = \frac{1}{h_2}\left[\left(u_1 + \frac{h_1}{2}\frac{\partial w}{\partial x}\right) - \left(u_3 - \frac{h_3}{2}\frac{\partial w}{\partial x}\right)\right]\,. \tag{3.5}$$

It should be mentioned that the applied dependency has certain restrictions and is accurate for h_2 tending to zero. Otherwise, for large h_2, we should expect some discrepancies

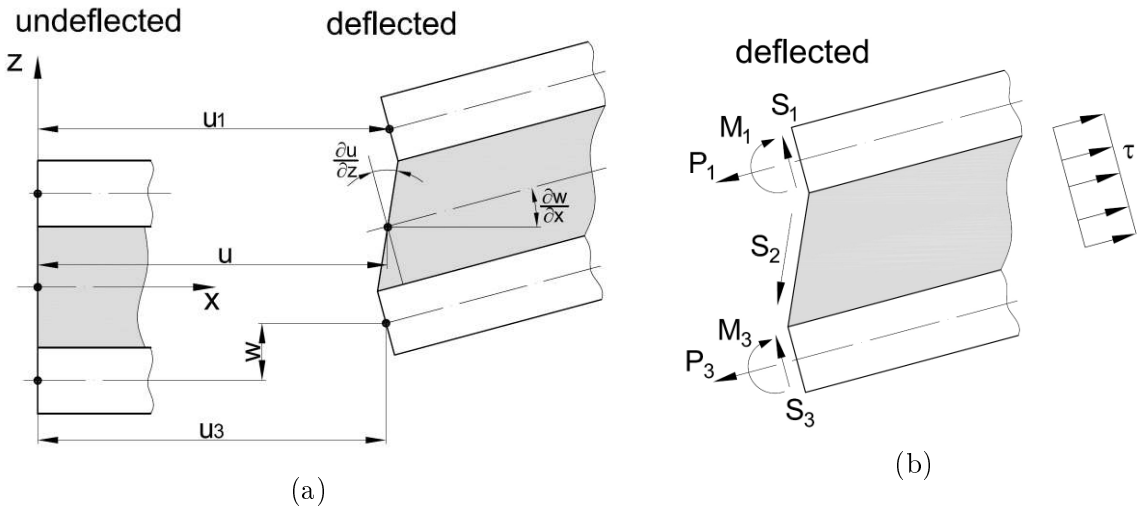

(a) (b)

Figure 3.3: Displacements of the beam element (a), forces, moments and loads acting on a beam element (b).

between the computed results and the real motion. By subjecting Equation 3.5 into Equation 3.4, and after some rearrangements we obtain

$$\gamma = \frac{d}{h_2}\frac{\partial w}{\partial x} + \frac{u_1 - u_3}{h_2}\,, \tag{3.6}$$

where $d = (h_1 + 2h_2 + h_3)/2$ is the distance between the mid-planes in the outer face plates. If we know the explicit form of γ, we can determine the shear force in the core. The shear forces in both remaining layers are also computed. We assume zero longitudinal direct stress in the core

$$\tau = G \cdot \gamma\,. \tag{3.7}$$

The total shear force consists of three main components. The shear force of the upper beam and shear force on the lower beam (Figure 3.3b) is

$$S_1 = D_1\frac{\partial^3 w}{\partial x^3}\,, \tag{3.8}$$

$$S_3 = D_3\frac{\partial^3 w}{\partial x^3}\,, \tag{3.9}$$

and the force caused by the core shear stress

$$S_2 = -\tau d b\,, \tag{3.10}$$

where D_1 and D_3 are the flexural rigidities of the face layers.

The total force is the sum of three forces

$$S = S_1 + S_2 + S_3 = (D_1 + D_3)\frac{\partial^3 w}{\partial x^3} - Gdb\left[\frac{d}{h_2}\frac{\partial w}{\partial x} + \frac{u_1 - u_3}{h_2}\right]. \tag{3.11}$$

The assumption that the transverse load is carried by the total shear force $p = \partial S/\partial x$ on the section after rearrangements gives the following formula

$$p = D_t\frac{\partial^4 w}{\partial x^4} - G\frac{d^2 b}{h_2}\frac{\partial^2 w}{\partial x^2} - G\frac{db}{h_2}\left(\frac{\partial u_1}{\partial x} - \frac{\partial u_3}{\partial x}\right), \tag{3.12}$$

where $D_t = EI_1 + EI_3$ is the sum of the flexural rigidities of the top and the bottom face plates.
Let us denote the longitudinal force in the face plates P_1 and P_3. They act in the midplane and are connected with the longitudinal displacements by the relations

$$P_1 = E_1 h_1 b\frac{\partial u_1}{\partial x}, \tag{3.13}$$

and

$$P_3 = E_3 h_3 b\frac{\partial u_3}{\partial x}. \tag{3.14}$$

The total longitudinal force along the section equals to 0, so $P_1 = -P_3$ and hence we obtain the relation

$$\frac{\partial u_1}{\partial x} = \frac{-E_3 h_3}{E_1 h_1}\frac{\partial u_3}{\partial x}. \tag{3.15}$$

Considering the physical system we can write

$$E_1 h_1 u_1 = -E_3 h_3 u_3. \tag{3.16}$$

Finally the Equation 3.12 can be rewritten as

$$p = D_t\frac{\partial^4 w}{\partial x^4} - \frac{bGd^2\partial^2 w}{h_2\partial x^2} + \frac{bGd}{h_2}\left(\frac{E_1 h_1 + E_3 h_3}{E_1 h_1}\right)\frac{\partial u_3}{\partial x}. \tag{3.17}$$

The second equation connecting w and u_3 is derived from the equilibrium of the longitudinal forces on an infinitesimal element of the lower face

$$\delta P_3 = -\tau\delta x. \tag{3.18}$$

This equation assumes the equilibrium of the axial forces in the outer layer and the longitudinal force resulting from the shear stress in the core. With respect to the longitudinal

force on the lower face plate, Equation 3.18 can be written in the following form

$$-\tau = E_3 h_3 b \frac{\partial^2 u_3}{\partial x^2} \,. \tag{3.19}$$

In order to determine the relationship between the longitudinal displacements u_1 and u_3, and the relationship between their derivatives with the respect to x, the condition of no resultant axial force on the whole section was assumed

$$\frac{\partial^2 u_3}{\partial x^2} - \frac{G\left(E_3 h_3 + E_1 h_1\right)}{E_1 h_1 h_2 E_3 h_3 b} u_3 = -\frac{Gd}{h_2 E_2 h_3 b} \frac{\partial w}{\partial x} \,. \tag{3.20}$$

Finally, we obtain the couple of differential equations

$$\frac{\partial^4 w}{\partial x^4} - gY \frac{\partial^2 w}{\partial x^2} + g \frac{db}{D_t} E_3 h_3 \frac{\partial u_3}{\partial x} = \frac{p}{D_t} \,, \tag{3.21}$$

$$\frac{\partial^2 u_3}{\partial x^2} - \frac{g}{b} u_3 = -gY \frac{D_t}{E_3 h_3 b^2 d} \frac{\partial w}{\partial x} \,, \tag{3.22}$$

where

$$g = \frac{G}{h_2} \left(\frac{1}{E_1 h_1} + \frac{1}{E_3 h_3} \right) \,, \tag{3.23}$$

$$Y = \frac{d^2 b}{D_t} \frac{E_1 h_1 E_3 h_3}{E_1 h_1 + E_3 h_3} \,. \tag{3.24}$$

are the shear and stiffness parameters. This mathematical formulation is used for the simply supported three-layered beam with a controllable core.

3.2.2 Vibration of the Beam with MRE

Let us consider a simply supported, three-layered beam, of mass density μ and length l, with point mass m placed in the middle of the structure. The considered sandwich beam is depicted in Figure 3.4. The following boundary conditions were assumed

$$w(0,t) = w(l,t) = 0 \,, \qquad M(0,t) = M(l,t) = 0 \,, \qquad u_3'(0,t) = u_3'(l,t) = 0 \,, \tag{3.25}$$

where the total bending moment of the sandwich beam model from the previous section is given by the formula

$$M = M_1 + M_2 + M_3 = D_t \frac{\partial^2 w}{\partial x^2} + E_3 h_3 db \frac{\partial u_3}{\partial x} \,. \tag{3.26}$$

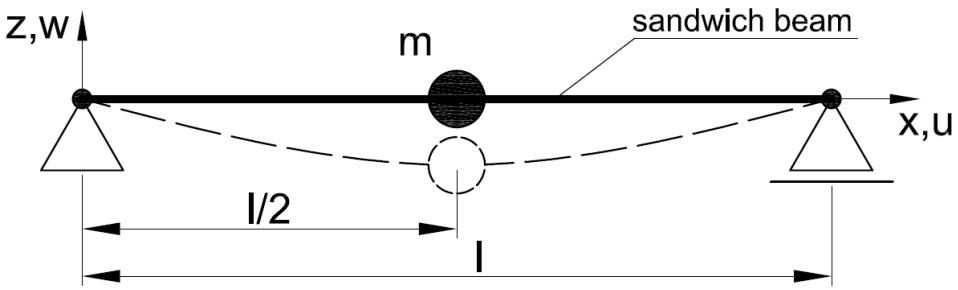

Figure 3.4: Simply supported sandwich beam.

The vibrations of the beam are initiated by the kinematic excitation. The structure is initially deflected according to the formula

$$w_0(x) = 4\bar{w}_0 \frac{x}{l}\left(1 - \frac{x}{l}\right) . \tag{3.27}$$

Then the following initial conditions were taken into account

$$w(x,0) = w_0(x) , \quad \dot{w}(x,0) = 0 , \quad u_3(x,0) = 0 . \tag{3.28}$$

The equations of motion of the sandwich beam of Figure 3.4 are described by Equations 3.21 and 3.22, where the transverse loading is written in the following form

$$p = -\mu \frac{\partial^2 w}{\partial t^2} - \delta\left(x - \frac{l}{2}\right) m \frac{\partial^2 w}{\partial t^2} . \tag{3.29}$$

Finally, the governing equations of the considered problem are

$$\begin{aligned} &\frac{\partial^4 w}{\partial x^4} - gY\frac{\partial^2 w}{\partial x^2} + \frac{g}{\eta b}\frac{\partial u_3}{\partial x} + \left[\frac{\mu}{D_t} + \delta\left(x - \frac{l}{2}\right)\frac{m}{D_t}\right]\frac{\partial^2 w}{\partial t^2} = 0, \\ &\frac{\partial^2 u_3}{\partial x^2} - \frac{g}{b}u_3 + gY\eta\frac{\partial w}{\partial x} = 0 . \end{aligned} \tag{3.30}$$

The simplification of the above formula is accomplished with the substitution

$$\eta = \frac{D_t}{E_3 h_3 d b^2} . \tag{3.31}$$

The system of partial differential Equations 3.30 can be solved by the separation of variables. The transversal displacement is developed into the Fourier sine series

$$w(x,t) = \frac{2}{l}\sum_{j=1}^{n} U_j(t) \sin\frac{j\pi x}{l} , \tag{3.32}$$

while the longitudinal displacement is developed into the Fourier cosine series

$$u_3(x,t) = \frac{1}{l}V_0(t) + \frac{2}{l}\sum_{j=1}^{n} V_j(t)\cos\frac{j\pi x}{l}\,, \tag{3.33}$$

where

$$U_j(t) = \int_0^l w(x,t)\sin\frac{j\pi x}{l}\mathrm{d}x\ , \qquad V_j(t) = \int_0^l u_3(x,t)\cos\frac{j\pi x}{l}\mathrm{d}x\,. \tag{3.34}$$

These series satisfy the boundary conditions (3.25). As a result of the Fourier transformation of (3.30), we obtain

$$\begin{aligned} &\frac{j^4\pi^4}{l^4}U_j(t) + gY\frac{j^2\pi^2}{l^2}U_j(t) - \frac{g}{\eta b}\frac{j\pi}{l}V_j(t) + \frac{\mu}{D_t}\ddot{U}_j(t) + \frac{m}{D_t}\sin\frac{j\pi}{2}\left.\frac{\partial^2 w}{\partial t^2}\right|_{x=\frac{l}{2}} = 0,\\ &-\frac{j^2\pi^2}{l^2}V_j(t) - \frac{g}{b}V_j(t) + gY\eta\frac{j\pi}{l}U_j(t) = 0\,. \end{aligned} \tag{3.35}$$

According to (3.32), the acceleration of the concentrated mass m in the middle of the beam is given by the series

$$\left.\frac{\partial^2 w}{\partial t^2}\right|_{x=\frac{l}{2}} = \frac{2}{l}\sum_{k=1}^{n}\ddot{U}_k(t)\sin\frac{k\pi}{2}\,. \tag{3.36}$$

After rearrangement, the set of Equations 3.35 can be written as one equation, dependent on $U_j(t)$:

$$\frac{\mu}{D_t}\ddot{U}_j(t) + \frac{2m}{D_t l}\sin\frac{j\pi}{2}\sum_{k=1}^{n}\ddot{U}_k(t)\sin\frac{k\pi}{2} + \omega_j^4\left(1 + \frac{gYb}{\omega_j^2 b + g}\right)U_j(t) = 0\,, \tag{3.37}$$

where

$$\omega_j = \frac{j\pi}{l}\,. \tag{3.38}$$

The sine Fourier transformation of the initial condition of the sandwich beam (3.27) is

$$U_j = \int_0^l w_0(x)\sin\frac{j\pi x}{l}\mathrm{d}x = 8\bar{w}_0\frac{l}{j^3\pi^3}\left[1-(-1)^j\right] = U_j(0)\,. \tag{3.39}$$

The initial deflection of the beam is symmetrical, so the even terms of the resulting series are zero. The system of Equations 3.37 can be written in a matrix form and solved numerically for an unrestricted number of terms in the solution. Figure 3.5 presents the solution of the problem for 1 and 10 terms of the Fourier sine expansion (3.32). We see that the first term gives sufficiently accurate results.

In order to enable the analytical solution of Equation 3.37, the solution was confined

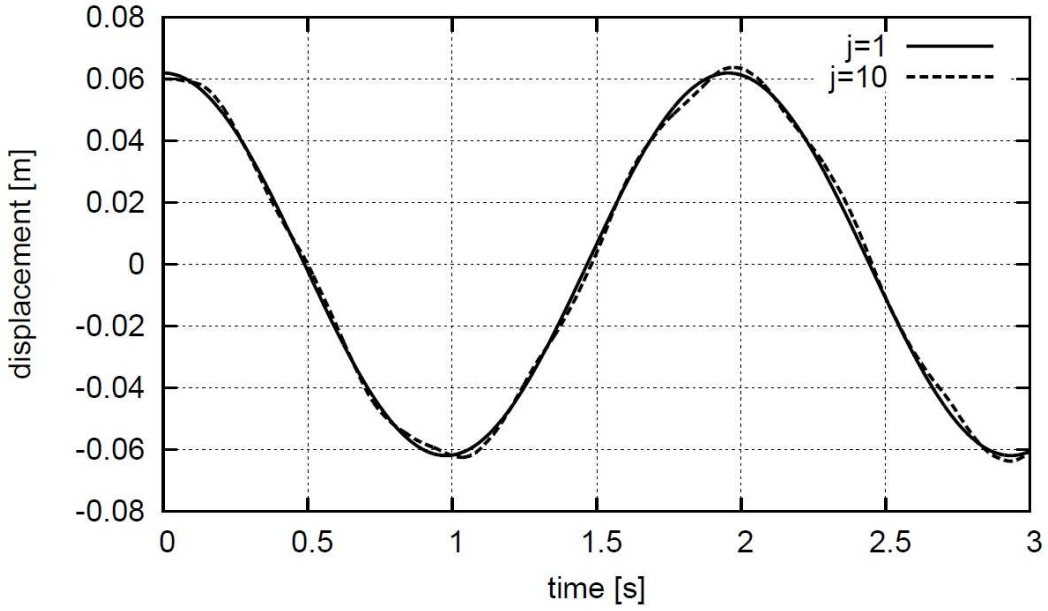

Figure 3.5: Free vibrations response of the sandwich beam with 1 and 10 terms of the Fourier expansion.

to the first term of the series (3.32). The resulting ordinary differential equation takes the form

$$\left(\frac{\mu}{D_t}+\frac{2m}{D_t l}\right)\ddot{U}_1(t)+\omega_1^4\left(1+\frac{gYb}{\omega_1^2 b+g}\right)U_1(t)=0\,. \tag{3.40}$$

After Laplace transformation, we obtain

$$\left(\frac{\mu}{D_t}+\frac{2m}{D_t l}\right)\left[s^2\hat{U}_1(s)-sU_1(0_+)\right]+\omega_1^4\left(1+\frac{gYb}{\omega_1^2 b+g}\right)\hat{U}_1(s)=0\,. \tag{3.41}$$

The solution of the algebraic form (3.41) is given by

$$\hat{U}_1(s)=\frac{s}{s^2+\beta^2}U_1(0_+)\,, \tag{3.42}$$

with the coefficient

$$\beta=\omega_1^2\sqrt{\frac{D_t l}{\mu l+2m}\left(1+\frac{gYb}{\omega_1^2 b+g}\right)}\,. \tag{3.43}$$

Now the Equation 3.42 can be transformed back to the time variable

$$U_1(t)=U_1(0_+)\cos\beta t\,. \tag{3.44}$$

Finally, with the Equation 3.32 the first term of the transversal displacement can be

written

$$w(x,t) = 32\bar{w}_0 \frac{1}{\pi^3} \cos \beta t \sin \frac{\pi x}{l} \,. \tag{3.45}$$

This formula is the basis for optimization. The parameter β contains all the material and geometrical data. We can now simply derive the velocity and the acceleration of the layered structure.

3.2.3 Control Strategy for MRE

In general case the control strategy depends on the type of the structure, its geometry and topology, boundary and initial conditions and type of excitation. In our research the efficiency of a controlled damping is related to the permanently damped beam in a cantilever configuration.

Here, we will consider a vibrating beam in $\Omega = \{x\colon\ 0 \le x \le l\}$, subjected to initial displacement. The displacement field being reduced $w(x,u,t)$ depends on the control input $u(x,t)$ that influences the shear stiffness of the filling material. The objective of the control is to distribute the shear stiffness $G(x,t)$ over time to achieve the highest damping. In our problem, the filling core material has a shear stiffness that is uniform over its length. It can only vary in time. We assume a finite time horizon. The optimization problem can be written in the following form:

$$\begin{aligned} \text{Minimize} \quad J = &\frac{1}{2} \int_0^T \int_0^l \left[w(x,u,t) - w_d(x,t)\right]^2 \,\mathrm{d}x\,\mathrm{d}t + \\ &+ \frac{\alpha}{2} \int_0^T \int_0^l \left[u(x,t)\right]^2 \,\mathrm{d}x\,\mathrm{d}t \,, \end{aligned} \tag{3.46}$$

subject to the constraints

$$\begin{aligned} &\frac{\partial^4 w}{\partial x^4} - gY\frac{\partial^2 w}{\partial x^2} + \frac{g}{\eta b}\frac{\partial u_3}{\partial x} + \left[\frac{\mu}{D_t} + \delta\left(x - \frac{l}{2}\right)\frac{m}{D_t}\right]\frac{\partial^2 w}{\partial t^2} = 0, \\ &\frac{\partial^2 u_3}{\partial x^2} - \frac{g}{b}u_3 + gY\eta\frac{\partial w}{\partial x} = 0 \,, \\ &w(x,0) = w_0(x) \quad \text{on} \quad \Omega \,, \\ &w = 0 \quad \text{on} \quad \partial\Omega \,, \\ &u \in U \,. \end{aligned} \tag{3.47}$$

This problem is a linear quadratic hyperbolic problem with distributed control. The treatment of this type of a problem is much more difficult, due to the weaker smoothing

properties of the associated solutions.

Most of the numerical algorithms developed for the optimization of partial differential equations are designed for convex problems. Their solution is simply obtained if the objective function is quadratic. There are a few reasons for this. The most important one is that a convex problem has a unique solution and, therefore, less or more efficient gradient methods can be used. Moreover, quadratic functions enable us to derive simple formulas for the gradients by introducing the adjoint state.

For practical reasons, we assume an objective function which minimizes the amplitudes of the displacement at the midpoint, which is equal to the full length of the experimental beam. We will take n time intervals per observation time T and denote by u_i, $i = 1, 2, ..., n$ the control variable in each period i. Then our problem is defined as follows:

$$\begin{aligned} \text{Minimize} \quad J \;=\; & \frac{1}{2}\int_0^T \left[w(l/2,u,t) - w_d(l/2,t)\right]^2 \,\mathrm{d}t \;+ \\ & + \frac{\alpha}{2}\int_0^T \left[u(l/2,t)\right]^2 \,\mathrm{d}t\,, \end{aligned}$$

$$\begin{aligned} & \Omega = \{x\colon\, 0 \le x \le l\}\ , \\ & \partial\Omega = \{0, l\}\ , \\ & 0 \le u_i \le 1,\ G_i = G_{\text{low}} \cdot (1 + 0.2\, u_i) \quad i = 1, 2, ..., n\ , \\ & \text{with the governing Equation 3.47.} \end{aligned} \tag{3.48}$$

In our numerical implementation of the optimization problem, we divide the limited period of observation into short intervals of identical lengths. In each interval, the control function is assumed to be constant. We search for values in these intervals. The higher the number of intervals used, the more precise is the resulting control function. In the case of steady state vibrations subjected to an oscillatory force, we can successfully adjust the control to a single period of vibrations. In the case of free vibrations being controlled by a chosen material parameter, each action modifies the form of vibrations in the next cycle. Both the period of the vibrations and the function of displacements in time are changed. For this reason, we must consider several successive cycles and the entire process must be treated homogeneously.

Our problem is characterized by the following features:

- the change of one control variable at a particular time influences the response of the remaining process, starting from the moment of a decision,
- a less acceptable local response can result in a response that is, on the whole, advantageous,
- the neighbouring values can be radically different, although usually they are similar,
- optimum solutions can be achieved for zero-one control variables,
- the objective function is very sensitive to the control variables.

An elongated observation requires a higher number of control variables. The observation of four cycles, divided into 40–400 intervals is proposed. Since the objective functions are not convex, the known computational methods for minimization are ineffective, as for example the IPopt package, devoted to optimization by the interior point method.

The first attempts showed the efficiency of random methods. The simple Monte Carlo method is, unfortunately, inefficient. The increased number of variables dramatically diminishes the convergence rate. Genetic algorithms, which seem to be good for some minimization problems, also fail in our case. One can explain the limited efficiency of the known algorithms by particular features of our task. The process is continuous in time and a locally estimated control function can be demolished by a few variables re-established in the subsequent moments. The change of the period of vibrations is a sufficient reason for such a scenario. That is why we optimize the problem in small groups of variables, usually defining the values of the control function in successive moments. Such subsequences of variables have alternating lengths and move along the time of simulation, and from time to time these subsequences contain variables from the entire set, i.e. inconsecutive.

The control problem (Equations 3.46–3.47) was computed with two levels of shear stiffness of the core: G_{low}=45·10^3 Pa and G_{high}=1.2×G_{low}. The remaining data are: length l=1.44 m, width b=0.04 m, height h_1=0.5·10^{-3} m, h_2=5·10^{-3} m, h_3=0.5·10^{-3} m, point mass m=0.740 kg, and the Young modulus of the outer layers E_1=E_3=69·10^9 Pa. The initial deflection of the end of the beam is w_0=0.06 m.

The small number of decision variables results in a sufficiently accurate normalized control function (Figure 3.6a). The increasing precision improves the sharpness of the slopes in the diagram (Figure 3.6b,c,d). All the normalized values practically vary between extreme values, i.e. zero and one. This can be simplified to an "On/Off" or "bang-bang" class of control strategies, where the actuator can assume only two states, which

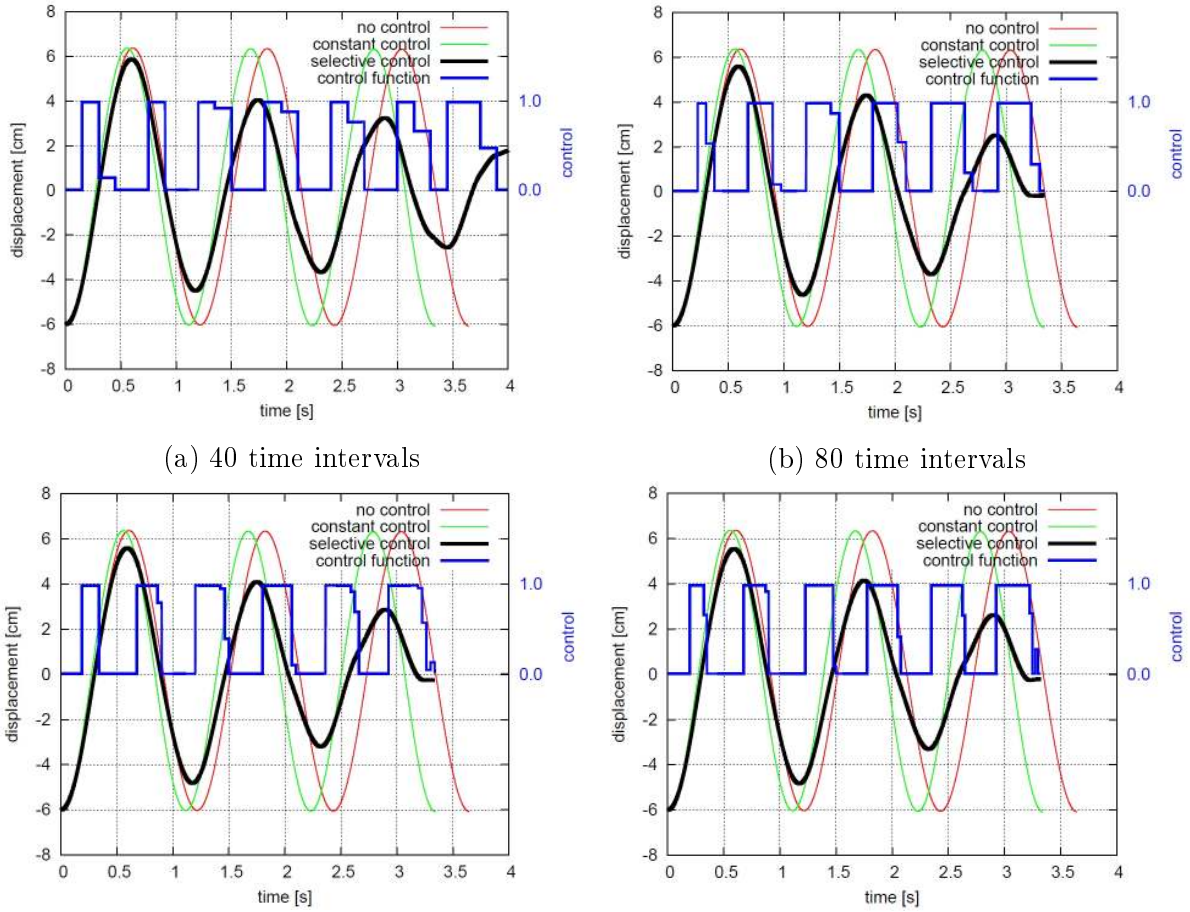

(a) 40 time intervals

(b) 80 time intervals

(c) 160 time intervals

(d) 240 time intervals

Figure 3.6: Resulting control function trace computed with partition of the time horizon into different number of time intervals.

is a condition easy to apply on a physical object by using electromechanical relays. Our control requires activation at times of the extreme displacements and switching off at times of the static equilibrium, i.e. after 1/4 of the vibration cycle (Figure 3.6 and 3.7).

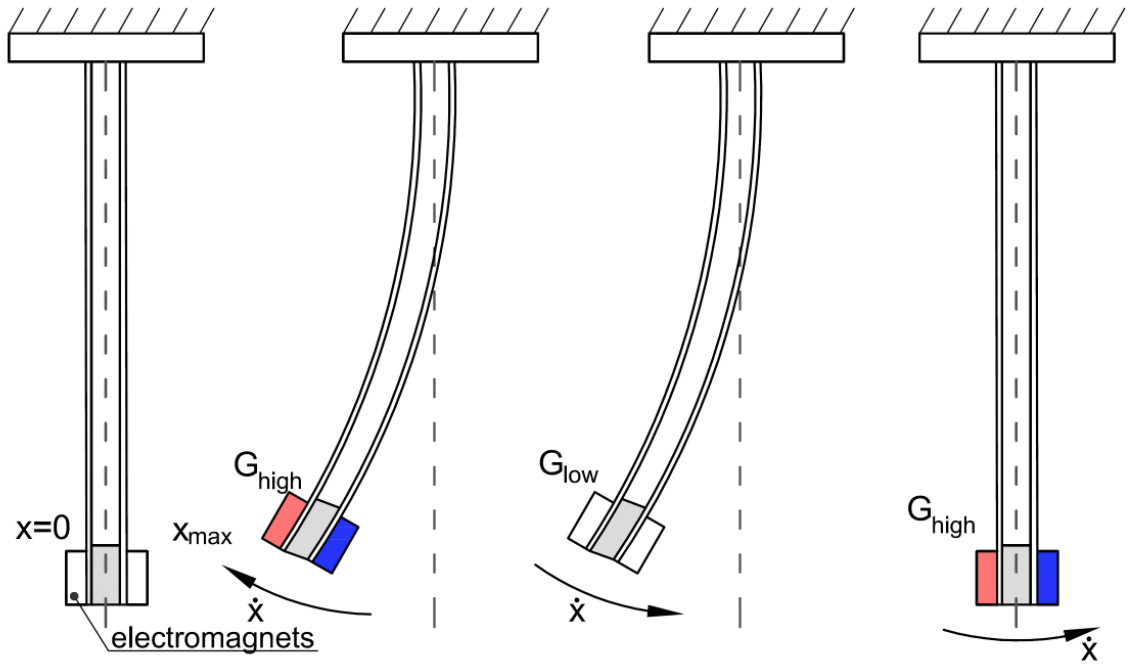

Figure 3.7: Moments for switching the shear modulus of the beam with MRE.

The action of activating the magnetorheological elastomer is carried on for one-half of the total time. For comparison, Figure 3.6 depicts the vibrations without any control (red line) and with the permanent control (green line). It is obvious that the structure vibrating with the constant-in-time low or high shear stiffness of the inner layer and excited with the same initial deflection differs only in the periods of its vibration.

If the form of the control function is known, we can replace the great number of variables that constitute it with a much smaller number of variables that define the limits of a zero-one rectangular cycle. This technique was previously applied to a beam supported with a set of dampers, controlled semi-actively [70, 71].

The control function, which enables the reduction of the amplitudes, differs from the solution of a similar problem described in [28]. Its enhanced damping of a rotating shaft controlled with magnetorheological dampers occurred with a sinusoidal control function.

3.3 | Beam with Granular Structure

The second variant of the complex beam incorporates the granular structure that allows changing the damping characteristics by varying the underpressure value inside the struc-

ture. To analyse the properties of such a material we need to consider interactions among the granules, i.e. the stress in a plane section of the granular structure. For simplicity, a section with only two granules in contact is specified (Figure 3.8).

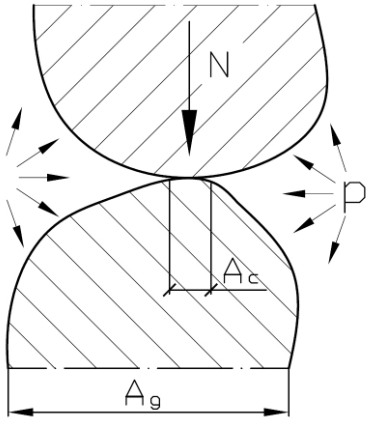

Figure 3.8: Contact between two granules of the structure.

The following force equation can be stated

$$N = A_c p_c + A_u p\,, \tag{3.49}$$

where A_c is the contact area between the granules, p is the pressure of the air among the granules and p_c is the stress on the contact surface of the granules.
The area A_u from the Equation 3.49 is equal to

$$A_u = A_g - A_c\,, \tag{3.50}$$

where A_g is the single granule's area.
The total stress value is obtained from the Equation 3.49,

$$\sigma = \frac{A_c}{A_g} p_c + \left(1 - \frac{A_c}{A_g}\right) p\,. \tag{3.51}$$

According to Terzaghi's principle, all the measurable effects caused by the change of stress, such as compression, distortion and a change in the shearing resistance are due to changes in the effective stress. The effective stress describes the forces inside the skeleton, and in our case may be expressed as

$$\sigma' = \frac{A_c}{A_g} p_c\,. \tag{3.52}$$

If we note that $A_c/A_g << 1$, then we get

$$\sigma' = \sigma - p\,. \tag{3.53}$$

In the case considered in this work, a partial vacuum is applied to change the properties of the airtight structure. The value of the pressure p is negative, so the effective stress increases. The underpressure intensifies the mechanisms which enhance the rigidity of the structure and the dissipation of the system. As a result, we obtain a new type of structural material with the possibility of changing its parameters.

3.3.1 Model of the Beam with Granular Structure

Software packages like LGMC90, PFC3D or YADE are capable of modelling collections of deformable or rigid particles of various shapes and sizes, defining interaction laws (contact, friction, cohesion, fracture, wear, etc.) including multiphysic coupling. However, at this point, an in-depth look on the particle interactions of the granular structure encapsulated in an elastic envelope would be a complex and time consuming issue by itself. Such meticulous model would be impractical to pose and solve the optimal control problem. The mechanical properties of granular materials were modeled by constitutive laws of the equivalent, simplified system.

Let us consider two parallel cantilevers coupled by the dynamical system at free ends (Figure 3.9). Different models coupling the beams were considered: Zener, simple Maxwell and Kelvin–Voigt. Here the Kelvin–Voigt model is considered, as it enables easy analytical computations and describes the global properties of the granular structure with fair accuracy. The justification for this choice , and comparison of the performance for different models and parameter identification is thoroughly described in **Chapter 5:Experimental Results: Parameter Identification**, after the experimental results were collected.

The vibrations of the system were described by the set of the discrete-continuous equations of motion. In order to obtain a closed analytical solution of the problem the inertia of the beams was neglected. Stiffness of the continuous beam can be represented by the discrete spring. The problem was reduced to a two degrees of freedom (Figure 3.9).

The simplified problem concerns vibration of the coupled ends of the beams. According to the above scheme, each of the beams' length is L and the flexural stiffness is EI. The transversal displacements of each of two beams were described by the functions w_1 and w_2, respectively. The conjugated two degrees of freedom system can be defined by the parameters m, c and k.

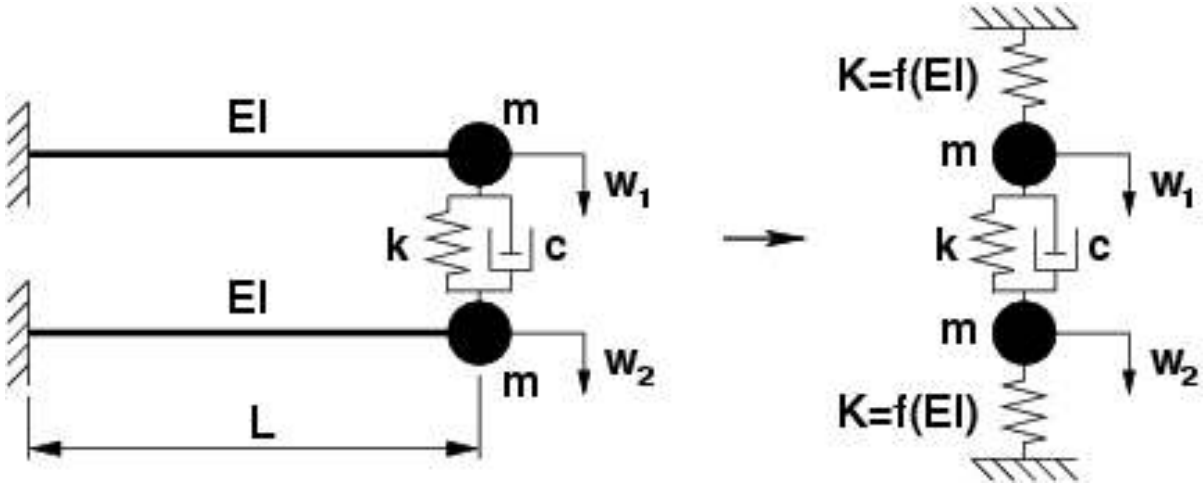

Figure 3.9: Phenomenological model of the two cantilever beams coupled with the granular damping structure.

All the considered parameters are real numbers and their values are greater than zero. The partial differential equations describing the discrete-continuous case are given by the following set of equations

$$\begin{aligned} EI\, w_1'''' &= f_1(x,t), \\ EI\, w_2'''' &= f_2(x,t)\,, \end{aligned} \tag{3.54}$$

where

$$\begin{aligned} f_1(x,t) &= -\delta(x-L)\left[m\ddot{w}_1 + c\left(\dot{w}_1 - \dot{w}_2\right) + k\left(w_1 - w_2\right)\right], \\ f_2(x,t) &= -\delta(x-L)\left[m\ddot{w}_2 + c\left(\dot{w}_2 - \dot{w}_1\right) + k\left(w_2 - w_1\right)\right]. \end{aligned} \tag{3.55}$$

Boundary conditions for the cantilever are as follows

$$w_i(0,t) = w_i'(0,t) = w_i''(L,t) = w_i'''(L,t) = 0, \quad i = 1,2\,. \tag{3.56}$$

Vibrations of the system were initiated by the kinematic excitation. The initial conditions are given as follows

$$w_i(x,0) = w_i(0), \quad \dot{w}_i(x,0) = \dot{w}_i(0), \quad i = 1,2\,. \tag{3.57}$$

In order to replace the discrete-continuous model with the simplified approach, the theory of distribution was applied. The properties of convolution were used to calculate the reduced stiffness for the massless cantilever beam

$$w(x,t) = G(x,s) * f(s,t) = \int_0^L G(x,s) f(s,t) \mathrm{d}s\,, \tag{3.58}$$

where $G(x,s)$ is the influence Green function, which is obtained by solving the basic equation. It was produced by replacing the right hand side of Equation 3.54 by the Dirac's delta $\delta(x-s)$. The solution to the complete equation is the convolution of the fundamental solution and the inhomogeneity (3.55). Finally, according to Equation 3.58 we obtain

$$\begin{aligned} m\ddot{w}_1 + c\,(\dot{w}_1 - \dot{w}_2) + k\,(w_1 - w_2) + Kw_1 = 0, \\ m\ddot{w}_2 + c\,(\dot{w}_2 - \dot{w}_1) + k\,(w_2 - w_1) + Kw_2 = 0\,, \end{aligned} \tag{3.59}$$

where

$$K = \frac{3EI}{L^3}, \quad K > 0\,, \tag{3.60}$$

is the substitute stiffness of the beams in the simplified model.
In order to solve Equations 3.59 the integral Laplace-Carson transformation was applied. According to initial conditions (3.57) the set of equations can be written in the following form

$$\begin{aligned} &\left(ms^2 + cs + k + K\right)\hat{w}_1(s) - (cs+k)\,\hat{w}_2(s) = ms\left[sw_1(0_+) + \dot{w}_1(0_+)\right] + \\ &-cs\left[w_2(0_+) - w_1(0_+)\right], \\ &\left(ms^2 + cs + k + K\right)\hat{w}_2(s) - (cs+k)\,\hat{w}_1(s) = ms\left[sw_2(0_+) + \dot{w}_2(0_+)\right] + \\ &+cs\left[w_2(0_+) - w_1(0_+)\right]\,. \end{aligned} \tag{3.61}$$

The solutions of the above set of algebraic equations describe the response of individual degrees of freedom.

3.3.2 Vibration of the Beam with Granular Structure

For the first degree of freedom we obtain

$$\begin{aligned}\hat{w}_1(s) = &\frac{ms^2\left(ms^2+cs+k+K\right)+cs\left(ms^2+K\right)}{\left(ms^2+cs+k+K\right)^2-\left(cs+k\right)^2}\,w_1(0_+)+\\ &+\frac{ms\left(ms^2+cs+k+K\right)}{\left(ms^2+cs+k+K\right)^2-\left(cs+k\right)^2}\,\dot{w}_1(0_+)+\\ &+\frac{s\left(kms-cK\right)}{\left(ms^2+cs+k+K\right)^2-\left(cs+k\right)^2}\,w_2(0_+)+\\ &+\frac{ms\left(cs+k\right)}{\left(ms^2+cs+k+K\right)^2-\left(cs+k\right)^2}\,\dot{w}_2(0_+)\,.\end{aligned} \tag{3.62}$$

To return to the time domain the inverse transformation must be performed

$$w_1(t) = \frac{1}{2\pi i}\int_{a-i\infty}^{a+i\infty}\frac{\hat{w}_1(s)}{s}\,e^{ts}\,\mathrm{d}s\,. \tag{3.63}$$

In order to perform the inverse Laplace-Carson transform we must apply the decomposition of the integrand into simple fractions. The roots of the polynomial of the denominator of Equation 3.62 are as follows

$$s_{1,2} = \pm i\sqrt{\frac{K}{m}},\quad s_{3,4} = -\frac{c}{m}\pm\frac{\sqrt{c^2-m(K+2k)}}{m}\,. \tag{3.64}$$

Identification of the parameters of a granular material limits the solutions which fulfill the condition

$$c^2 - m(K+2k) < 0\,. \tag{3.65}$$

Finally, displacements of the first degree of freedom can be written in the following form

$$\begin{aligned}w_1(t) = &\frac{w_1(0_+)+w_2(0_+)}{2}\cos\left(t\sqrt{\frac{K}{m}}\right)+\\ &+\frac{\dot{w}_1(0_+)+\dot{w}_2(0_+)}{2}\sqrt{\frac{m}{K}}\sin\left(t\sqrt{\frac{K}{m}}\right)+\\ &+\exp\left(-\frac{c}{m}t\right)\left\{\frac{w_1(0_+)-w_2(0_+)}{2}\left[\cos\left(\frac{\beta}{m}t\right)+\frac{c}{\beta}\sin\left(\frac{\beta}{m}t\right)\right]+\right.\\ &\left.+\frac{\dot{w}_1(0_+)-\dot{w}_2(0_+)}{2}\frac{m}{\beta}\sin\left(\frac{\beta}{m}t\right)\right\},\end{aligned} \tag{3.66}$$

where

$$\beta = \sqrt{m(K+2k) - c^2}\,. \tag{3.67}$$

According to (3.65) the parameter β is a real number and greater than zero.
For the second degree of freedom the displacement is given by the formula

$$\begin{aligned} w_2(t) = {} & \frac{w_1(0_+) + w_2(0_+)}{2} \cos\left(t\sqrt{\frac{K}{m}}\right) + \\ & + \frac{\dot{w}_1(0_+) + \dot{w}_2(0_+)}{2}\sqrt{\frac{m}{K}} \sin\left(t\sqrt{\frac{K}{m}}\right) + \\ & + \exp\left(-\frac{c}{m}t\right)\left\{\frac{w_2(0_+) - w_1(0_+)}{2}\left[\cos\left(\frac{\beta}{m}t\right) + \frac{c}{\beta}\sin\left(\frac{\beta}{m}t\right)\right] + \right. \\ & \left. + \frac{\dot{w}_2(0_+) - \dot{w}_1(0_+)}{2}\frac{m}{\beta}\sin\left(\frac{\beta}{m}t\right)\right\}. \end{aligned} \tag{3.68}$$

The closed form solutions for the individual degrees of freedom (Equation 3.66 and 3.68) allow us to derive the formulas for the velocities and accelerations. We know the evolution of the structure at the selected time without the necessity to calculate the entire problem. It allows us to elaborate the proper semi-active control strategy of the damping parameter c and stiffness k easily.

3.3.3 Control Strategy for Granular Structure

First we will solve the problem of finding the control strategy for the case when the stiffness k is the only variable that we modify over time. Then, we can analyse the case when stiffness k and damping coefficient c are controlled simultaneously. The particular moments for switching the variables that will result in an better damping behaviour need to be computed. We assume the time of observation equal to 1.5 of the main period of vibrations, which is divided into n number of time intervals. Then, the m successive amplitudes are to be minimized, preserving the oscillatory form of the displacements. The objective function I for the switched stiffness is formulated as

$$I = \frac{1}{m}\sum_{i=1}^{m} A(k)_i^2\,. \tag{3.69}$$

For the switched stiffness and damping coefficient, the objective function depends on two variables

$$I = \frac{1}{m} \sum_{i=1}^{m} A(k,c)_i^2 \,. \tag{3.70}$$

The damping is efficient when the sum of the squared values of the amplitudes significantly decreases. The number of successive amplitudes taken into account should be low to keep the problem simple. The larger number m would introduce adverse local minima and increase computational time. This would lower the regularity of the observed periodic motion of the beam, as additional cycles would be considered in the optimization problem, making the solution complicated.

Figure 3.10 shows how do the discrete control of variable k and simultaneous control of k and c affect the results. It is clear, that altering the number of time intervals highly influences the results of the optimization, so picking up the right number of n time intervals seems difficult. The first candidate is $n = 10$ (on both plots), where the curves reach first local minimum. The next minimum indicating better results is achieved for $n = 20$ and $n = 21$ for the Figure 3.10a and b, respectively. Higher number of time intervals does not result in much of an additional improvement. The 80 time intervals are taken as the last case.

Figure 3.11 presents the simulation results without any control (black line) and with the applied control (red line), obtained for the analytical solution of Equations 3.66 and 3.68. The plots in the left column show displacement over time for the case when the stiffness k is the only decision variable. Three different time resolutions of the control function are considered: 10, 20, and 80 time intervals. The plots in the right column show respective results for the case when k and c are the controlled variables. The time was split into 10, 21, and 80 intervals.

It may be noted that the change of the stiffness k is the major component that contributes significantly to the vibration abatement. The additional influence of the damping c is rather marginal. The resulting form of the control signal may be simplified by distinguishing dominant stages. In the first stage, when the vibration starts, the control signal is turned constantly on (blue line). The control variables (whether is k or k and c simultaneously) are maximum. Then, after some time, the control signal is rapidly turned off and the control variables are equal to zero. Then, depending on the time intervals considered, the process is repeated, but the moments for switching the control on and off changes.

For 10 time intervals the tendency is very clear, and the particular moments for switching can be estimated from the graphs. The control requires activation at times of the

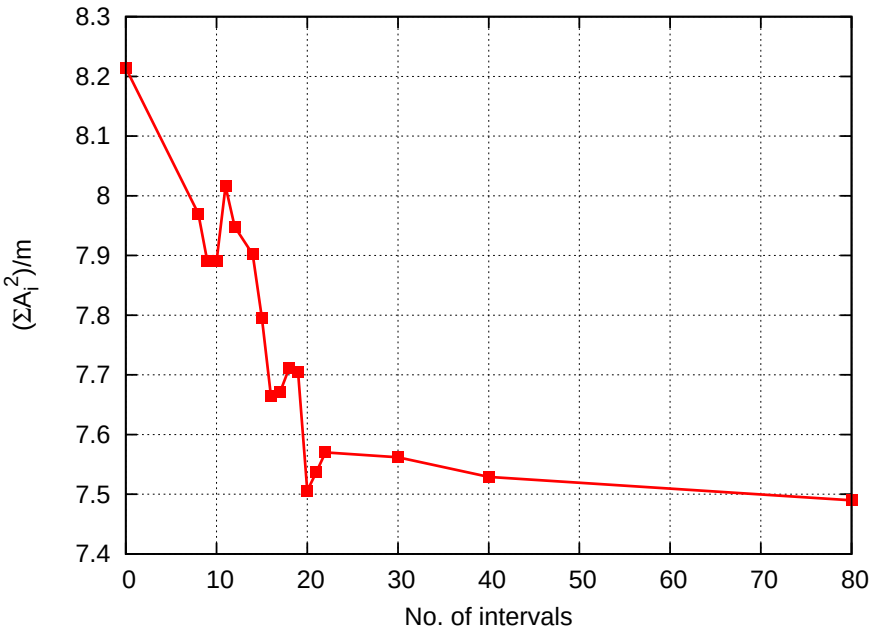

(a) Switching of k

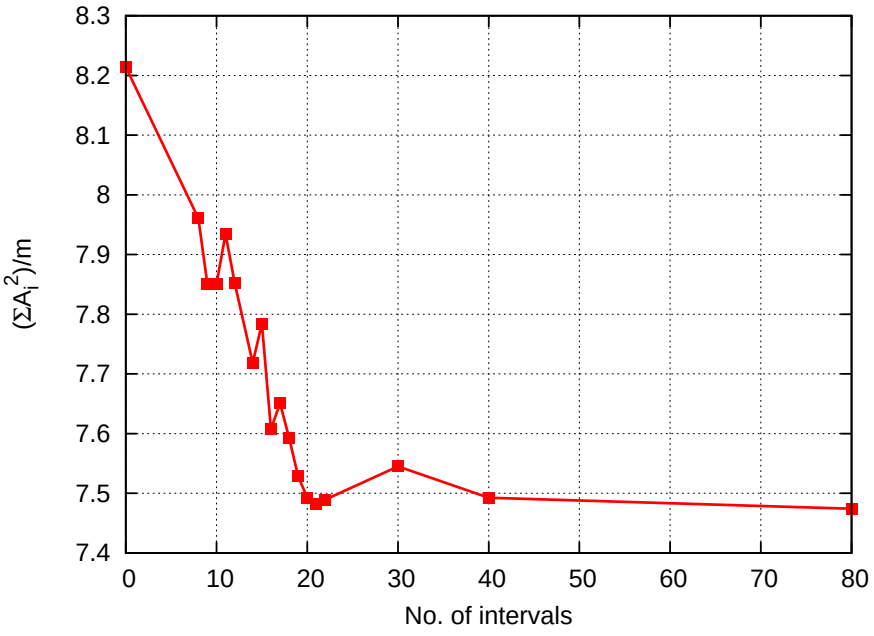

(b) Switching of k and c

Figure 3.10: Results of the optimization performed for different cases of permitted control variables.

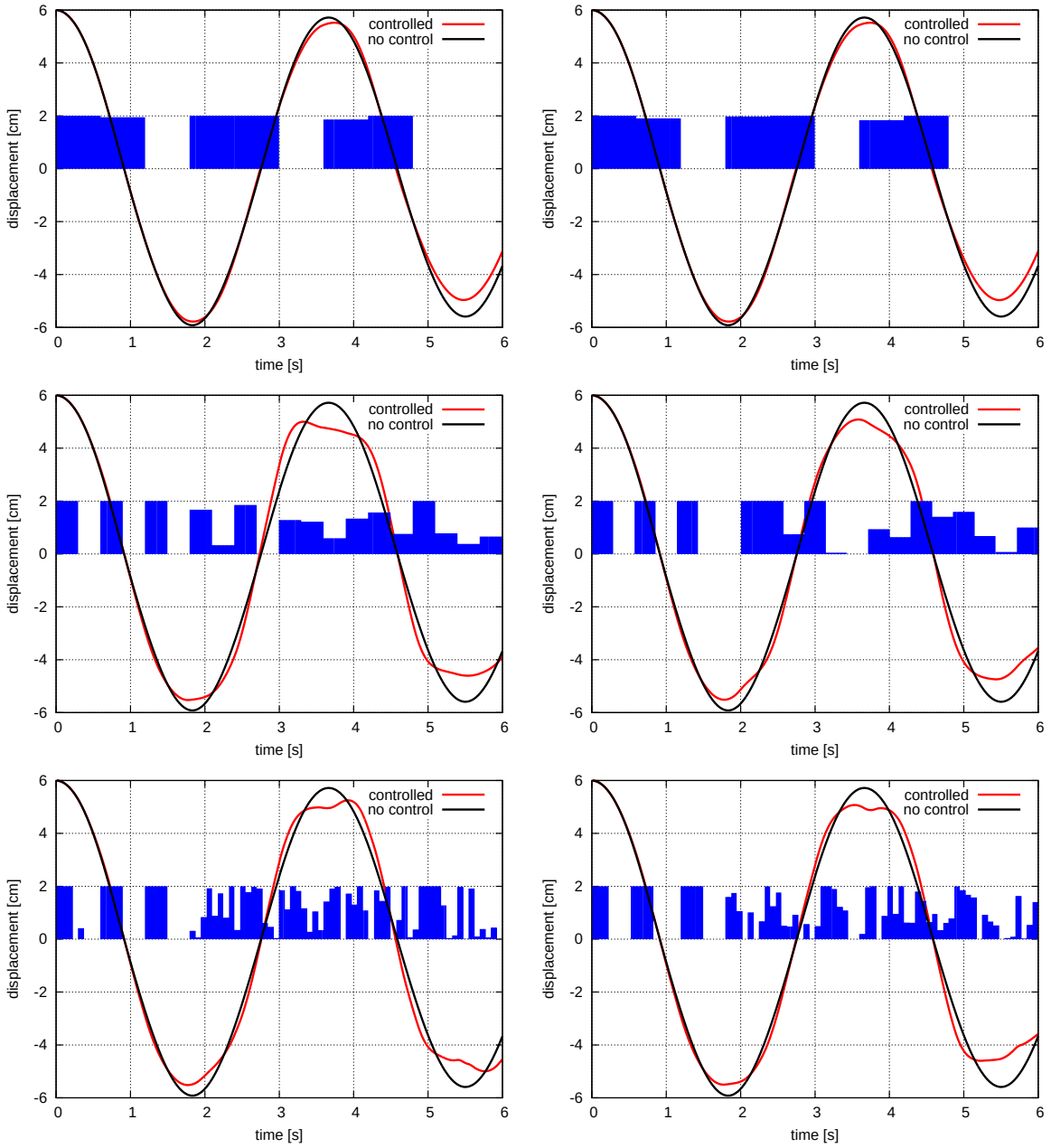

Figure 3.11: Displacements in time for the control of variable k performed in 10, 20, and 80 intervals (left column – a) and simultaneous control of k and c performed in 10, 21, and 80 intervals (right column – b).

extreme displacements ($x = \max$, $\dot{x} = 0$) and keeping the signal turned on, until the beam passes the equilibrium point $x = 0$. Shortly after passing the equilibrium, the control signal can be switched off until the beam reaches another maximum. The proposed control algorithm may be classified as an "On/Off" control strategies, where the actuator can assume only two states: on and off.

For larger number of time intervals (20, 21 and 80) the points of switching are not so easy to pick, but some conclusions can be derived. First of all we see that the higher modes of vibration manifest when the control is applied. For the first cycle of the response, when the sinusoidal waveform is regular, it is recommended to keep the underpressure constantly activated at the first stage, and turn it off three times, before the beam reaches another maximum deflection point. After that cycle, further control introduces higher modes of vibration. The movement of the beam is less regular and thus the control strategy becomes complicated.

Optimal damping of higher modes introduces not only switching between the extreme values (on and off), but also between intermediary values. That type of strategy would be hard to adapt in real structure and made it less operative. Also at some stages, the moments for turning signal on and off are very short. This would be impractical to achieve on a physical object, shortening the live time of the electromechanical actuators controlling the underpressure. By assuming some hysteresis, the real control signal may be simplified. The switching between two extreme values of vacuum is easy to achieve, and eliminates the necessity to continuously measure and adjust the underpressure in short periods of time. By keeping the control algorithm simple we avoid introducing higher modes of vibrations, nevertheless the solution is less efficient. For the experimental results, the algorithm achieved for 10 time intervals was examined, and the first cycle of the algorithm for 20 and 80 time intervals.

CHAPTER 4

Experimental Setup and Calibration

The purpose of the experimental research was to determine whether the change of the beam's smart damping member parameters can be sufficiently large to be effectively used in vibration reduction. Also the experiments were necessary for the parameter identification and to find how the magnetic field or the underpressure among the granules influences the damping capacity of the system. The theoretical analysis and the mathematically obtained control strategies for both types of materials were confronted with the experimental results. The construction and principle of operation of the manufactured laboratory stand and specimens is described below.

4.1 | Laboratory Stand for the Beam with MRE

The laboratory stand presented in Figure 4.1 consists of a fixture frame, supported firmly by a steady base plate. A proper care was taken to ensure a perfect cantilever condition. A massive mount, acting as a mechanical vice attached to the frame, allows suspending the tested beam vertically in a clamped-free configuration. In order to set the initial displacement of the beam, a holding band was connected to the free tip of the beam. The band was strained to give an initial transverse displacement of the tip 0.06 m. The data acquisition starts when the holding band is released and the beam is free to oscillate around its equilibrium point.

The component of the displacement of the amplitude was the basic, directly measured variable. The displacement was measured at three points (top, middle and bottom of the beam) with dedicated laser sensors, with a resolution up to 8 μm and 10 kHz maximum sampling frequency. The design of the test bench allowed easily setting the position of the displacement sensors, so it was possible to acquire data for a desired point on the beam.

The measurement system featured functions for compensating the inaccuracy of measurements up to 15° of inclination angle. Such inaccuracy may occur for large displacements, as the laser beam is reflected from the deformed surface of the beam. The reflected

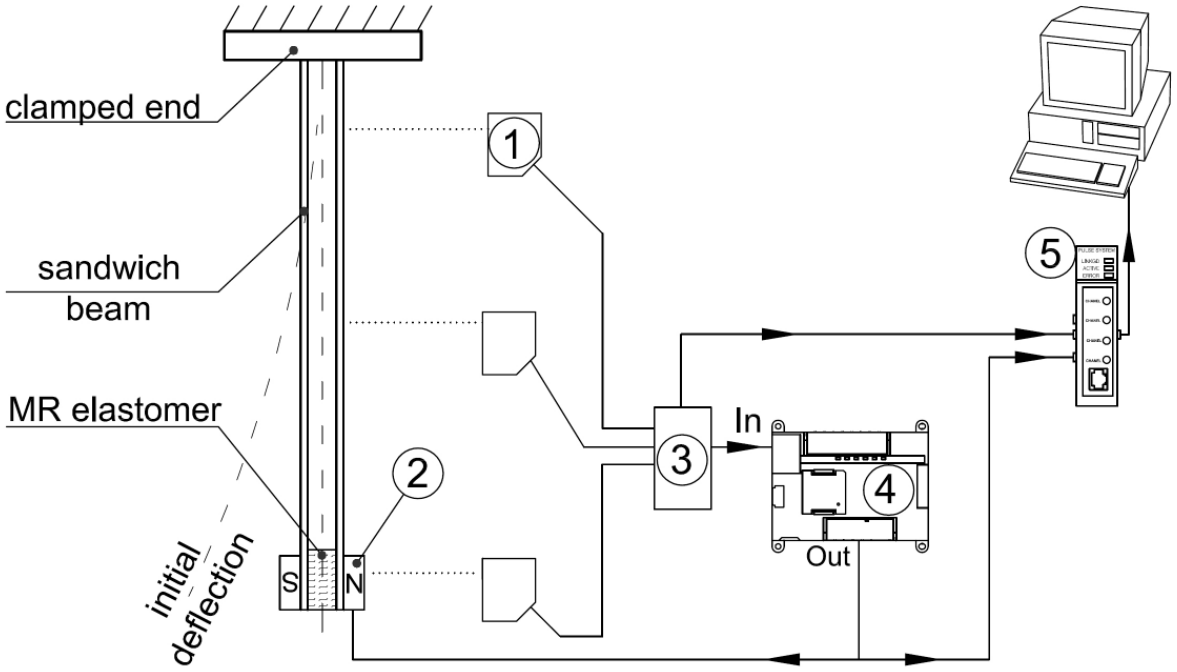

Figure 4.1: Scheme of the experimental setup: 1 – laser displacement sensors, 2 – electromagnets, 3 – displacement signal amplifier, 4 – PLC controller, 5 – data acquisition system.

beam may not be pointing directly into the CMOS sensor which may causes imprecise measurements if no compensation is performed. A 16-bit National Instruments 6210 data acquisition card connected to a computer was used to record the measurement results. The supported software features programmable graphical interface for configuration, operation and access to the real-time analysis of the signals by means of Fourier's transform, data filtration, smoothing and other tools. A Programmable Logic Controller (PLC) Omron CP1L-L14DR-A with built-in relay outputs and additional analogue In/Out module CP1W-MAD11 allows directly programming the cycles of turning the electromagnetic actuators on and off, depending on the control strategy. The test bench is equipped with two DC current power supplies, additional signal amplifiers and digital value displays, with the necessary wiring. A photo of the designed test bench is presented in Figure 4.2.

The preliminary test results were conducted to confirm the proper operation and configuration of the measuring equipment, calibration of the sensors and the data acquisition system, confirming that the boundary conditions are clamped-free, and to acquire data used as a base for the results of the beam with the embedded smart damping member.

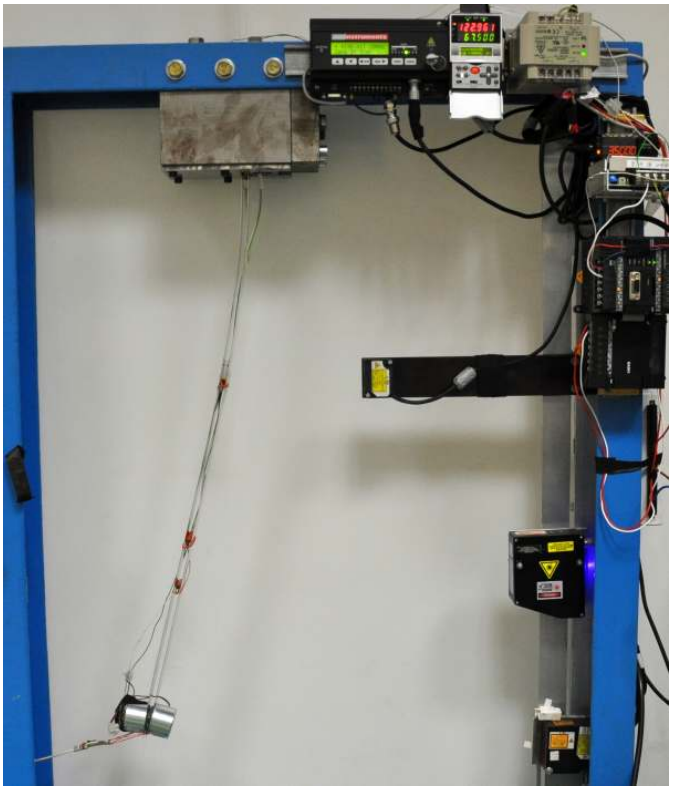

Figure 4.2: Test assembly with the deflected sandwich beam with the embedded magnetorheological elastomer ready for tests.

4.1.1 Configuration of the Beam with MRE

A photo of the real, deflected specimen and measurement system is presented in Figure 4.2. The thin face beams are made of aluminum PA4 of Young modulus E=69 GPa. Both of them are 720 mm long with a rectangular cross-section of 40×0.5 mm (Figure. 4.3). Aluminum was chosen for this purpose because of its low damping properties and the higher stiffness when compared to that of the MRE material. Moreover, the relative magnetic permeability of aluminum is equal to zero, which prevents the magnetic field from being trapped in the face layers rather than passing through the elastomer.

The beams are connected at the tip by the magnetorheological elastomer element of dimensions 40×40×20 mm, which weighs 20 g. The magnetorheological elastomer was a custom fabricated, isotropic material of density 3560 kg/m^3. The fraction of iron particles was 8% by volume. Particles were randomly dispersed in the matrix. The matrix was made of rubber, cured for 20 min at 145°C. The measured shear modulus of the elastomer is G=310 kPa for no magnetic field, and G=340 kPa for a magnetic field of 700 mT, which is the maximum value, limited by the magnetic saturation of the elastomer.

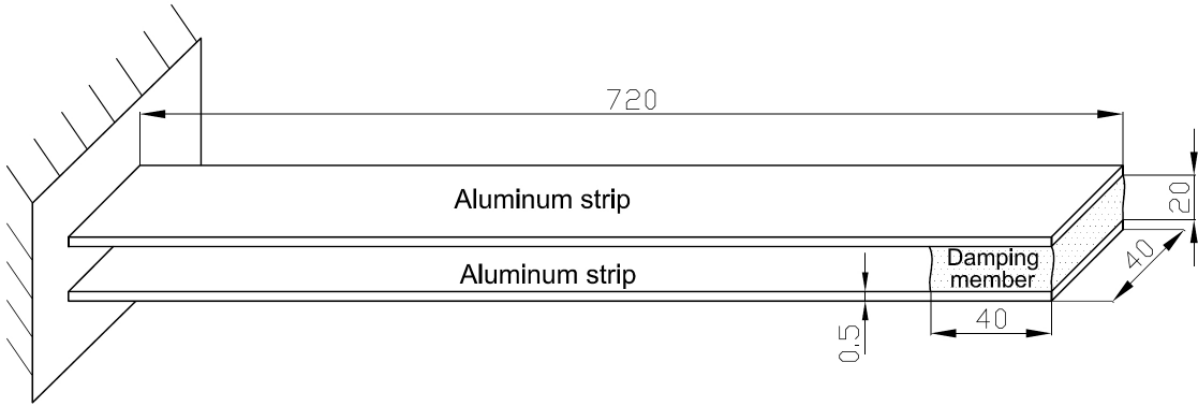

Figure 4.3: Dimensions (in mm) of the sandwich beam with the MRE damping member.

Two island-pole, 24 V DC electromagnets were used as actuators to control the properties of the smart core in the desired manner. They were also treated as a 0.37 kg point mass, which decreases the natural frequency of the system. The magnets were placed on opposite sides of the beam. The magnets were circuited in such a way that the first magnet's pole was N-type polarized, while the other magnet's pole was S-type. That type of configuration (Figure 4.4) increases the maximum value of the induced magnetic field flux density between poles up to 700 mT, and creates a field flux Φ that is normal to the sheared area of the elastomer.

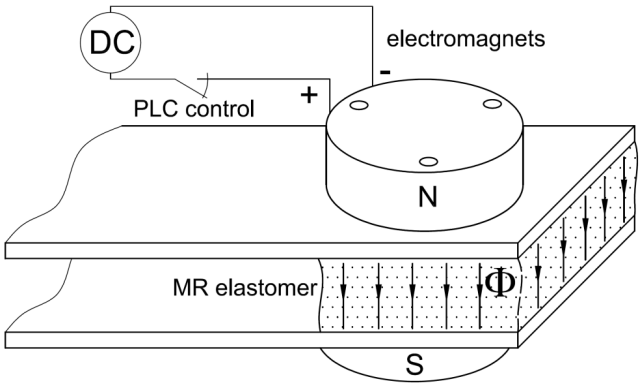

Figure 4.4: Polarization and placement of the electromagnets on the cantilever beam with the embedded magnetorheological elastomer.

4.2 | Laboratory Stand for the Beam with Granular Structure

The laboratory stand used for the studies on beams with granular damping element was the modified version of the previously introduced one, used in the studies on MRE. Nevertheless, to allow the control of the underpressure among the granules several crucial modifications were necessary (Figure 4.5).

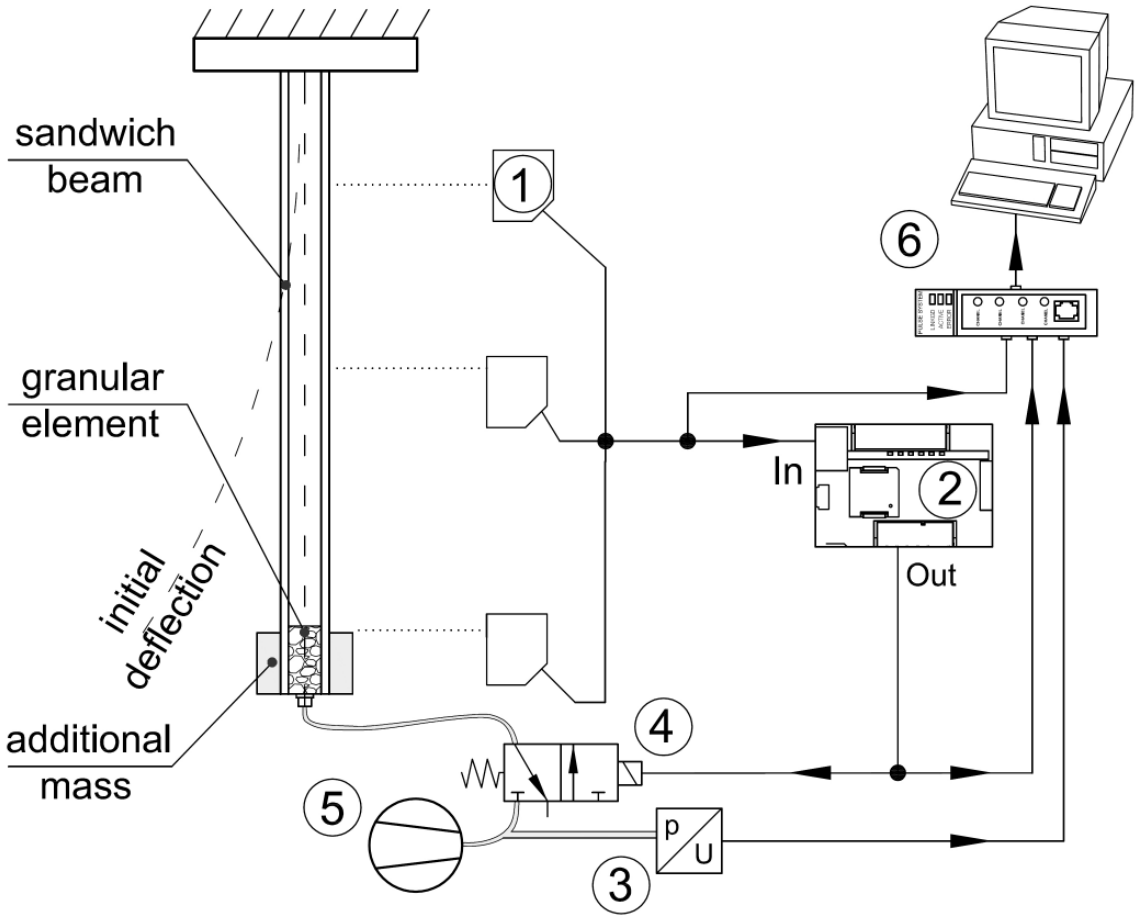

Figure 4.5: Schematic diagram of the experimental setup: 1 – laser displacement sensors, 2 – PLC controller, 3 – digital underpressure sensor, 4 – electromagnetic valve, 5 – vacuum pump with underpressure accumulator, 6 – data acquisition system.

The pressure inside the hermetically sealed envelope is controlled by a vacuum pump which is connected to the hose of the underpressure accumulator. The PLC with relay outputs was used to control the electromagnetic valve and thus to control the jamming in the granular element. When the electrovalve is in the closed position, the inlet of the damping element is connected to atmospheric pressure - the structure is in its compliant

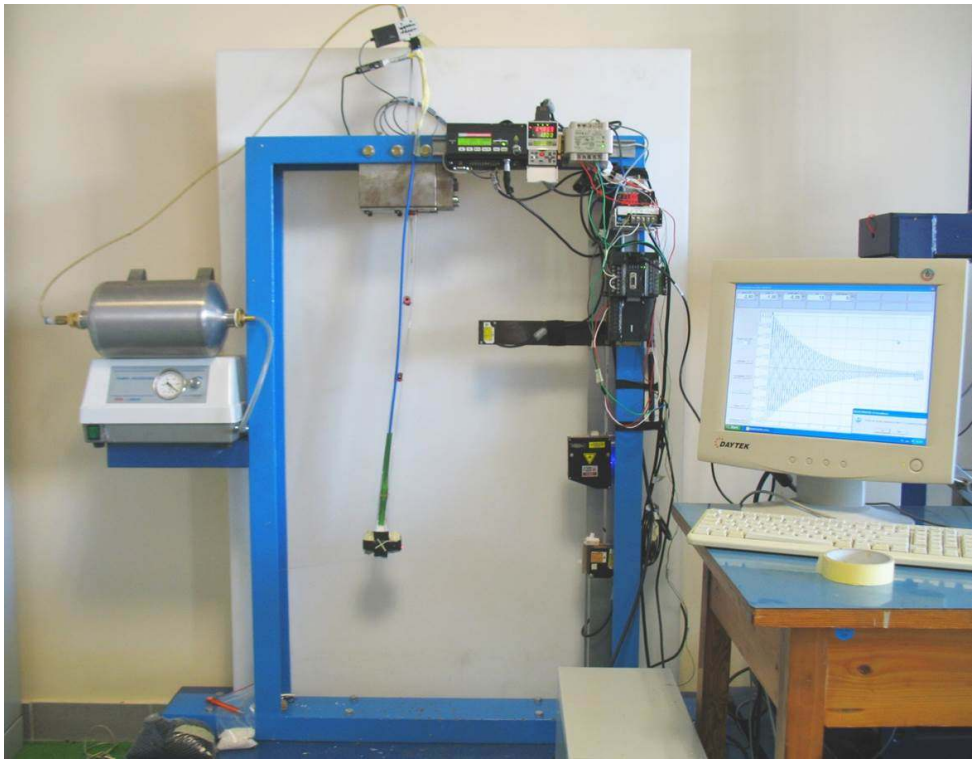

Figure 4.6: Photo of the laboratory stand for the granular beam investigation.

state and the beam can easily bent. When the valve is actuated, the inlet is connected to the underpressure accumulator, and the air is rapidly removed from the envelope, the granular material becomes jammed. The characteristic of the valve and the parameters of the pneumatic components allowed switching between the partial vacuum and the compliant state of the material in time shorter than 50 ms. The experimental setup was integrated with sensing, amplifying and signal analysis equipment. The instruments include laser displacement sensors described previously and a digital underpressure sensor that constantly measures underpressure value inside the airtight envelope. A photo of the laboratory stand with the specimen connected to a vacuum pump with the accumulator is presented in Figure 4.6.

4.2.1 Configuration of the Beam with Granular Structure

The parallel face beams of the specimen are made of aluminium of Young's modulus E=69 GPa. Both of them are 720 mm long, and have a rectangular cross-section 40×0.5 mm, the same as in Figure. 4.3. The beams are connected at the end by a thin (0.5 mm) elastomer layer made of PVC foil, which forms a hermetic envelope. The envelope is filled with a homogeneous granular material. Four test specimens were made and each one was filled with a distinct type of granule, which differed in size, shape or

structural material. Figure 4.7 presents macro photographs of the granules. The final dimensions of the damping element were 50×40×20 mm.

Figure 4.7: Types of the tested granular materials, from the left: plastic rollers, plastic spheres, steel spheres and plastic cubes.

In order to minimize the influence of the filling method, all of the granular damping elements were made in the same manner: the envelope was left open at one end and filled tightly with particles. The open end was then temporarily sealed. The beam vibrated for some time to rearrange the grains and the remained volume was further filled with particles. After that the open end of the envelope was sealed with silicone. Certain properties of the granular materials used for the experimentation are collected and presented in Table 4.1. From now on, the names listed in Table 4.1 are used whenever

Table 4.1: Properties of the types of granular material filling

Name	Material	Grain dimensions [mm]	Specimen weight [g]	Surface
Rollers	acrylonitrile butadiene styrene	ϕ2x3	30	matt
Plastic spheres	PVC with barium carbonate	ϕ6	65	polished
Steel spheres	steel	ϕ4	130	polished
Cubes	polymethyl	ϕ2x2x2	40	polished

referring to the particular filling type. A total mass of 0.37 kg was added to the tip of the beam to decrease the natural frequency of the system (the electromagnets were used as weights).

4.3 | Data Processing and Analysis

The recorded experimental data, even though that the signal transducers provided hardware signal filtering, was burdened with noise and interferences. To obtain reliable and accurate experimental results it was necessary to use additional software tools at the stage of data processing. The experimental data was then used for the parameter identification procedures. To make the numerical computations faster and more accurate proper preparation of the experimental curves is inevitable.

The used filtering method developed by Savitzky and Golay [84] is based on the use of local polynomial regression for the particular point of time series without significantly distorting the signal. An example of rough experimental curve (black line) and the one obtained by using Savitzky-Golay smoothing (red line) is presented in Figure 4.8. It is obvious that having the filtered curve, the numerical computations of the parameters will be more efficient as we got rid of the disturbing noises.

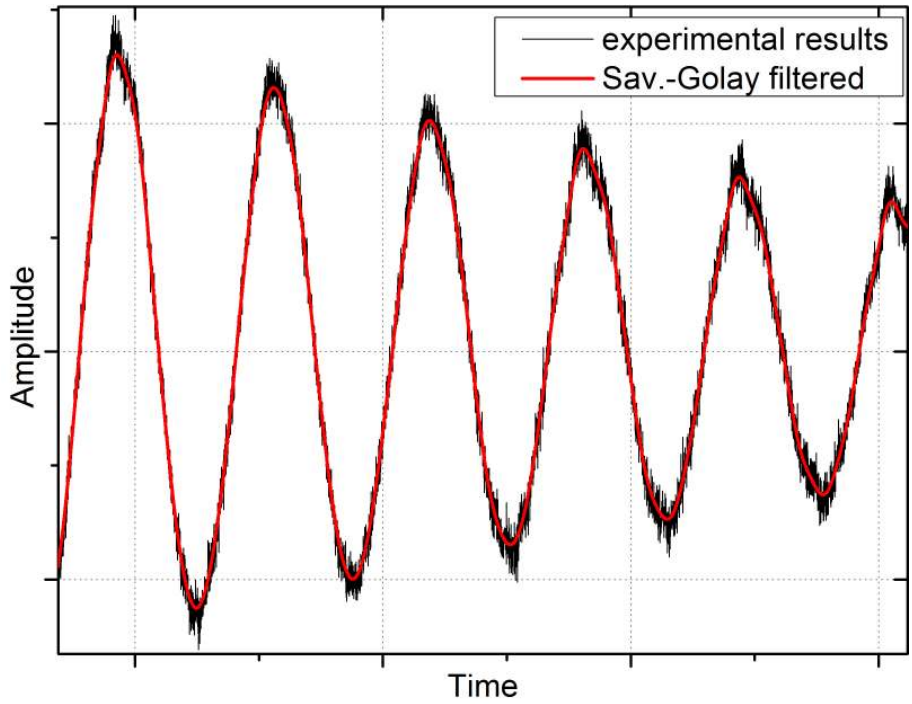

Figure 4.8: Comparison of the rough data and the plot smoothed with the Savitzky-Golay method.

The successive sub-sets of adjacent data points were fitted with the low-degree polynomial by the method of linear least squares. When the data points were equally spaced an analytical solution to the least-squares equations was found. The resulting adjusted

value g_i was determined according to the formula

$$g_i = \sum_{n=-n_L}^{n_R} c_n f_{i+n} \,, \tag{4.1}$$

where g_i is the new adjusted value for the time moment, n_L, n_R are the number of samples taken for computations, placed on left and right from the center point i, c_n is the filter convolution coefficient and f_i is the input data. The computations for every single point take place independently of others, so the result obtained after such treatment can produce a better representation of maxima and minima than the classic procedures of data smoothing. This prevents from the distortion of the original waveform which was important when analysing amplitudes for low displacements.

In some of the experimental results, the process of obtaining the curves "enveloping" the source data was performed. Envelope is tangent to every peak in the source dataset. The function obtains both the upper and the lower envelopes of the source data by applying a local maximum method combined with a cubic spline interpolation. In the first step the function finds out all the extreme values points whose first-order derivative is equal to zero in the source data. Then the cubic spline interpolation through these extreme values is performed with some Savitzky-Golay smoothing.

A fitting function was built to automatically initialize parameters and adjust initial parameter values to datasets. Pearson's χ^2 statistical value was computed to evaluate the goodness of the fit. The values of the data fitting variables are attached in the **Appendices**. The scheme of analysing all the collected data is presented in Figure 4.9.

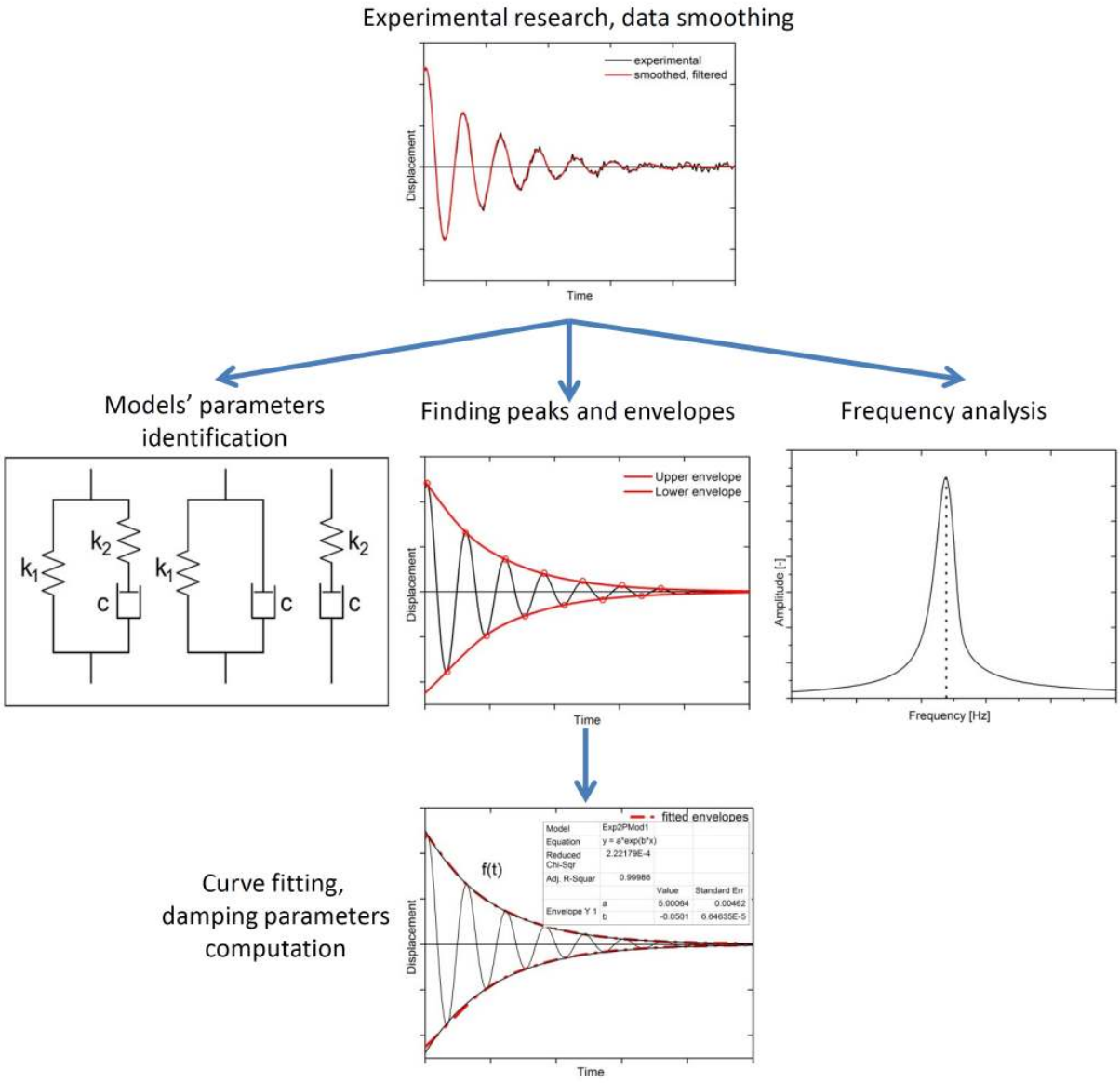

Figure 4.9: Consecutive steps of the experimental data analysis.

CHAPTER 5

Experimental Results

5.1 | Magnetorheological Elastomer in Vibration Damping

The presented results of the displacements in time are considered for the tip of the cantilever, where the maximum amplitude occurs (signal from the bottom laser sensor), as only the first mode of vibration was excited.

The On/Off control strategy was performed, switching the magnetic flux density between 0 and 700 mT in the particular moments obtained from the model, as presented in Figure 5.1. The control signal was computed by the PLC controller according to the

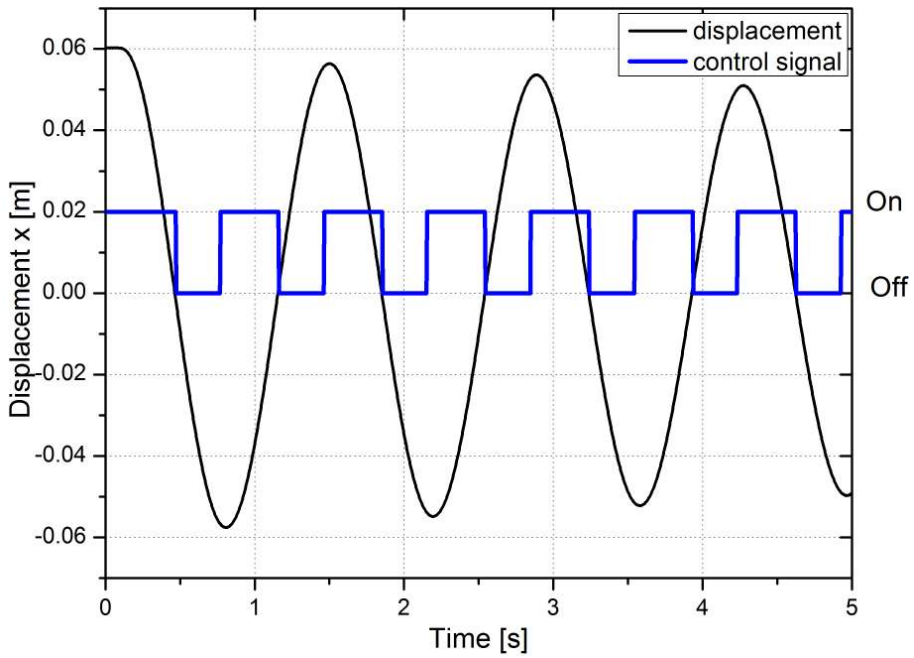

Figure 5.1: Displacement and control signal over time for the real beam with MRE.

numerically determined strategy, i.e. it achieved a high level at extreme deflection and a low value during a neutral displacement state. For comparison of the signals please refer

to **Chapter 3: Problem Formulation and System Modelling**).

The first 60 s of vibrations were acquired. This gave us enough information about the process. These results showed that if the smart material is embedded between the face layers, the overall damping of the beam enhances. Figure 5.2 illustrates the first segment of 30 s of vibration. The presented plots show how the magnetic field affects the amplitude of the displacement of the beam's tip for an initial deflection of 0.06 m, in three different cases: MRE not activated (0 V, black line), MRE turned on constantly (24 V, blue line), and MRE activated for selected moments (24 V control, red line), according to the control strategy. The case of free vibrations of a beam with the non-activated smart core is treated as the reference measurement.

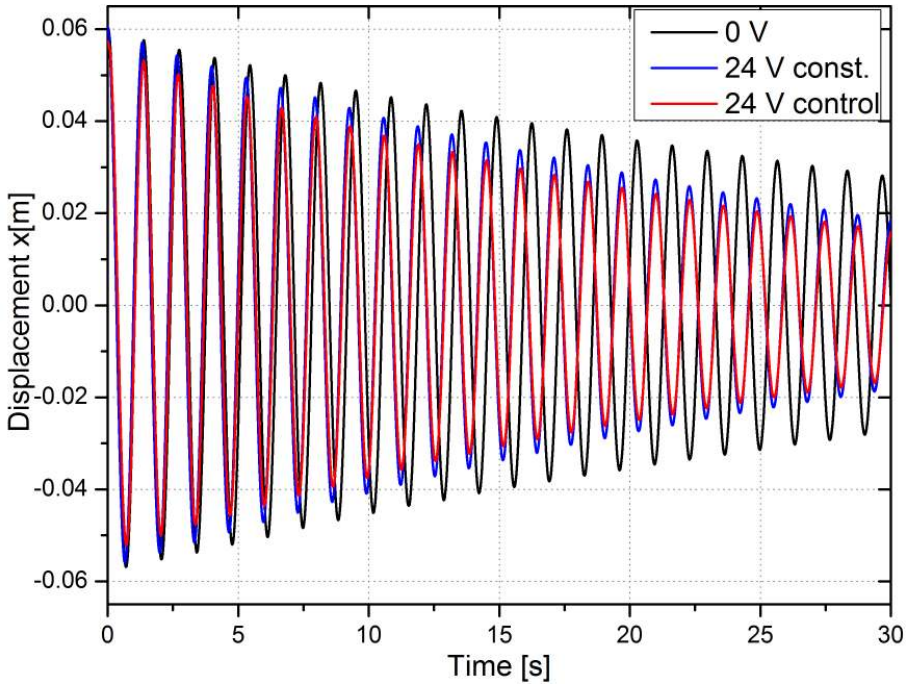

Figure 5.2: Displacement in time for different treatments of the beam with MRE damping member.

All three curves in Figure 5.2 exhibit damping. It has been observed that for no magnetic field applied, the response amplitude is the largest. Despite the elastomer merged locally in the sandwich beam, it caused a significant decrease of amplitudes for constant and periodic magnetic action. Although the experiment differs in this case from our theoretical analysis, the efficiency of the control with a small elastic inclusion, related to the entire length of the beam is effective.

It can be clearly seen that the controlled switching between active and non-active state of the MRE results in a more effective vibration damping in time than the one-time selection. The amplitude declines faster to the equilibrium point than for the previously

described cases. When the magnetic field is periodically switched, the response amplitude further decreases as the dynamic flexural rigidity of the beam increases with the shear modulus of the MRE core.

Longer observations allowed us to estimate the rate of damping. After 60 s, the amplitude of displacement for 0 V (0 mT magnetic field) is 12 mm, which is 20% of the initial deflection. If the MRE was constantly activated, the amplitude after 60 s of vibration decreased to 4.2 mm, which is 7% of the initial value. In the controlled switching case, the amplitude dropped to 2.6 mm, i.e. to 4% of the initial value.

The values of the logarithmic decrement of damping were computed in the process of fitting of the envelopes. The results obtained for the full time segment of 60 s and the envelopes of the displacement curves are plotted in Figure 5.3. It is apparent that the envelopes of the experimentally obtained signals can be very well fitted with exponential decay curves typical for systems with viscotic damping. The parameters of the fitted curves are presented in the **Appendices**. This enabled us to easily and precisely compute the value of the logarithmic decrement of damping

$$\delta = \beta \cdot T\,, \tag{5.1}$$

where β is the decay coefficient obtained in the curve fitting process and T is the period of the waveform.

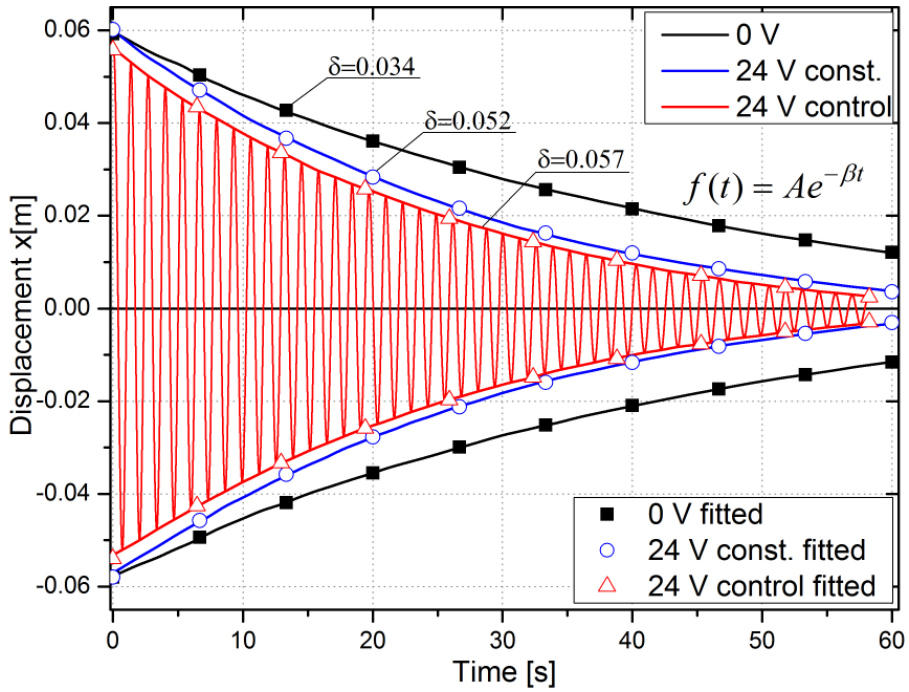

Figure 5.3: Fitted envelopes of the displacement amplitude for different damping treatments of the beam with MRE.

For the non-activated elastomer, the logarithmic decrement was $\delta = 0.034$, which is the reference value. As the material was constantly activated, the intensified dissipation resulted in a damping increased to $\delta = 0.052$. As the control strategy of switching the shear modulus is applied, the damping is increased by 67% compared to the basic value, up to $\delta = 0.057$.

Further analysis required to transform the time domain figures into the frequency dependencies. The Fourier Transform (FT) yields the average characteristics of the amplitude and the frequency contents over the full time span of the signal. The amplitude on the presented FT plots is the relative strength of the harmonic component present in the original signal. Since the strengths are related to the original signal value, the Y-scale of the graphs is unit-less.

The results in Figure 5.4 showed that the response of the cantilever consists of one intrinsic modal function, which corresponds to the first mode of vibrations with the frequency of 0.745 Hz for no magnetic field applied. The frequency slightly shifts toward higher frequencies (0.77 Hz) when the MRE member is activated permanently. From the above observations, it is evident that activating the material intensifies the global flexural rigidity of the system. When an external magnetic field is applied, the polarized particles tend to keep a chain-like linear structure while the rubber matrix moved in the direction of the shear force, and the rubber matrix and particles began to slip. For the controlled variant basically no frequency shift is observed. In fact the stiffness and frequency is increased just for a short period, and then it backs to the basic value, so the average frequency over the time span remains almost unchanged.

In the meanwhile, the peaks representing the vibration amplitudes decline due to the enhanced damping caused by the magnetic field presence. The damping ratio may be evaluated from the frequency spectrum as well, using the half-power band width method, which gives an overall idea about the damping of the system. In this method, the damping is evaluated from the frequencies on either sides of the peak in frequency spectrum observed at resonance condition. The non-dimensional damping ratio is defined as the ratio of the frequencies observed at two half power points of the natural frequency

$$\psi = \frac{\omega_1 - \omega_2}{2\omega_n} \tag{5.2}$$

where ω_1, ω_2 are the half power frequencies and ω_n is the natural frequency. The loss factor can be expressed as

$$\eta = \frac{\psi}{2\pi} \tag{5.3}$$

For the case when no magnetic field was applied, the damping ratio was ξ=0.0020. When

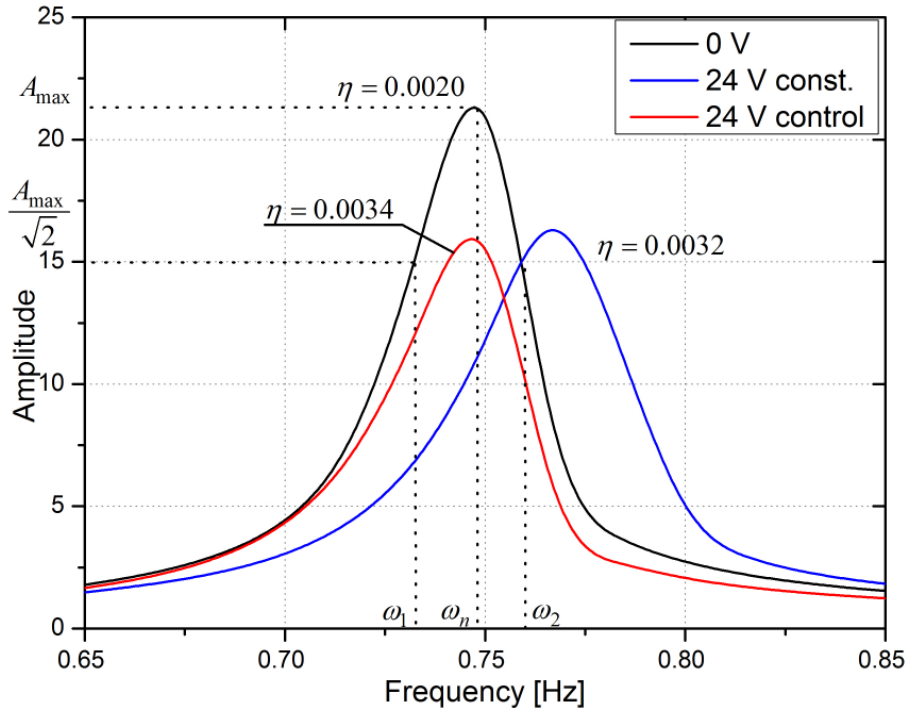

Figure 5.4: Frequency response of the cantilever with magnetorheological elastomer for different damping strategies.

the damping was turned on constantly the ratio was ξ_2=0.0032. As the temporary switching was performed, the damping raised up to ξ_3=0.0034.

5.2 | Granular Structure in Vibration Damping

For each type of granular material (Figure 4.7), the displacement's amplitude was recorded in order to measure the influence of the underpressure on the response of the cantilever. The underpressure value at the entrance of the hose connector was monitored during each measurement and was set to constant value chosen from the range 0 – 0.07 MPa. The atmospheric pressure was 100.3 kPa, so the examined underpressure values were equal to 0% and 70% vacuum. This part of the research was necessary to find the material which characterizes with the best damping properties. Also results of this part of the study were used for the identification of the parameters of the model.

5.2.1 Passive Damping for Constant Underpressure

Figure 5.5a illustrates the influence of the constant underpressure on the component of the amplitude of the displacement for initial deflection 0.06 m and zero initial velocity for the roller filling. First 60 s of the response are depicted. The negative pressure was set

individually before every measurement and remained constant during the vibrations, so that all of the measurements were performed after the initial jamming.

The obtained trial is a damped sine waveform, with frequency and amplitude depending on the set value of underpressure. The expanded view on Figure 5.5b gives details on the response for different constant values of the underpressure plotted as different colored lines.

By examining the free-decay time traces of the displacement, one may find that the displacement amplitude slightly increases when compared to the compliant state for 0 MPa, as the jammed state interactions are intensified by the higher underpressure value, which results in a slower reduction of the amplitude. The loss of the damping efficiency is rather small and is mainly related to the restriction on the movement of the granules, which can no longer slide easily. These observations were true for all of the types of the examined materials, so the individual plots were omitted in this part and disclosed in **Appendices**.

By analyzing the minimum and maximum beam deflections, the envelopes of the responses were obtained. The amplitude decreases exponentially at an almost constant rate, so the envelopes were approximated by the exponentially modulated decay curves - typically used for systems with viscous damping. This gave a very fine agreement. This was performed for all materials and every underpressure value. In Figure 5.6, the exemplary experimental curve (scatter) is plotted against the best fitted curve (solid line) for the roller granules subjected to 0.07 MPa. The detailed results and fitting parameters for different types of granules are disclosed in **Appendices**.

The comparison of the logarithmic decrement of damping for different filling materials is presented in Figure 5.7. The highest logarithmic decrement value was observed for the cubic granules. The second best damping performance was obtained for the rollers. Both types of the spheres exhibit slightly smaller logarithmic decrements of damping, with the steel spheres having the lowest damping value. This is a consequence of the fact that the small, cubic granules initially exhibit stronger force chains and high rolling resistance, compared to the other shapes. On the other hand, as the underpressure value is increased from 0 to 0.07 MPa, the absolute change of the logarithmic decrement is the most notable for the spherical granules while cubes exhibit minor change. The edgy, cubic particles initially form a highly ordered structure which is hard to reorganize. Spherical granules can be quite easily reorganized, as they have no edges that restrict certain movements. The performance of the roller granules can be located somewhere between the edgy and the spherical surfaces, giving high initial damping. Also the possibility to alternate the damping value is very fine.

Figure 5.8 presents the variation of the natural frequencies for a beam partially treated

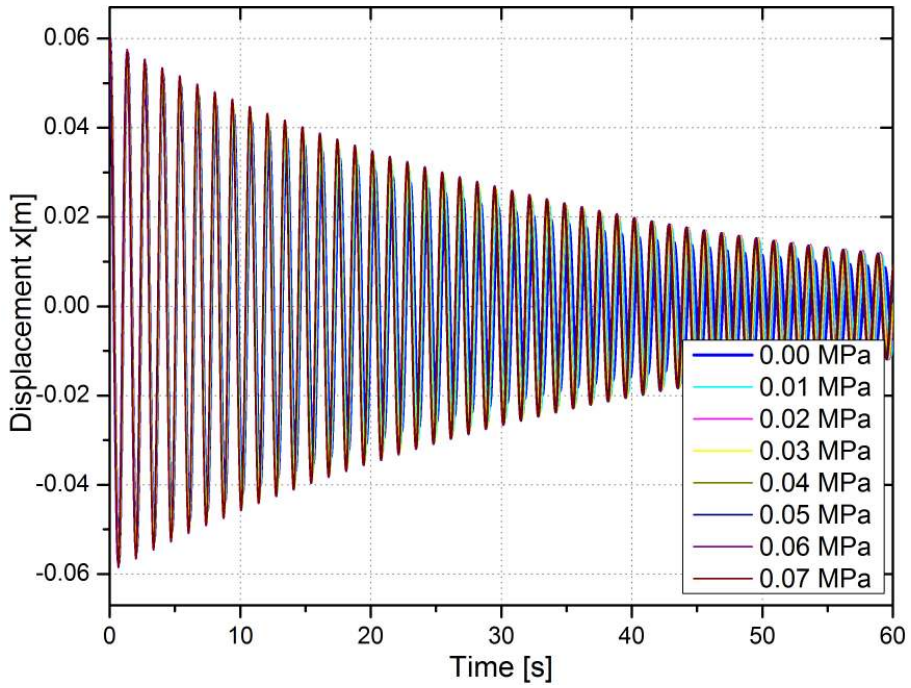

(a) Response of the beam

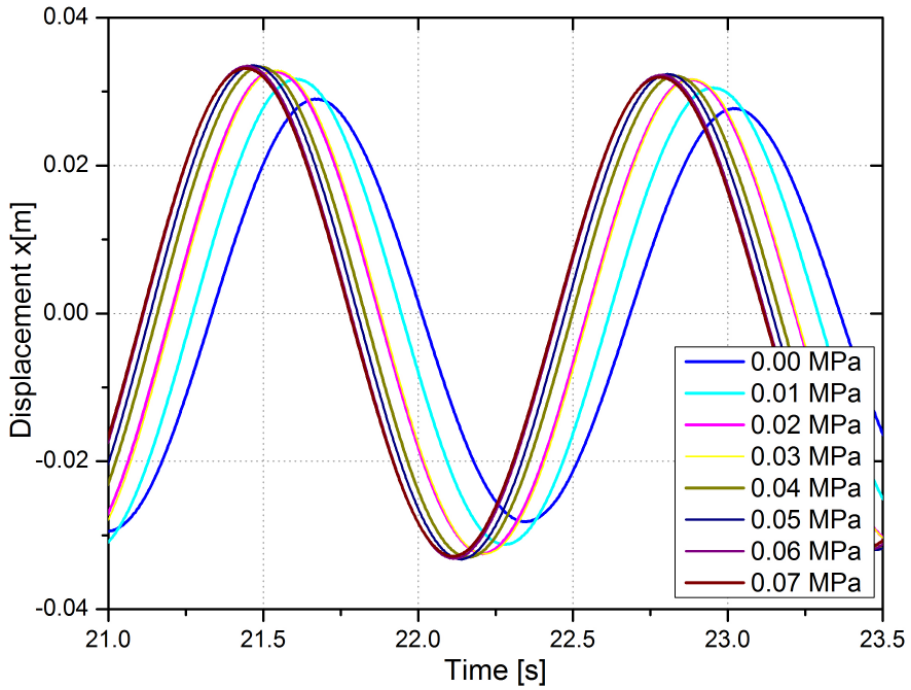

(b) Detailed view

Figure 5.5: Displacement over time for constant underpressure, granular structure filled with rollers.

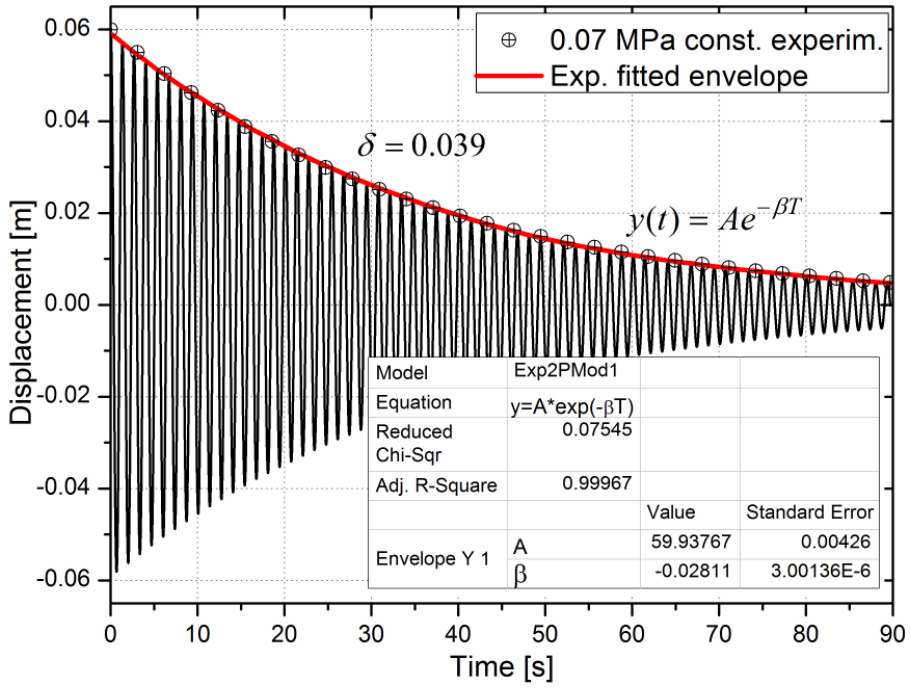

Figure 5.6: Envelope of the experimental response and the exponentially fitted curve for constant 0.07 MPa, roller granules.

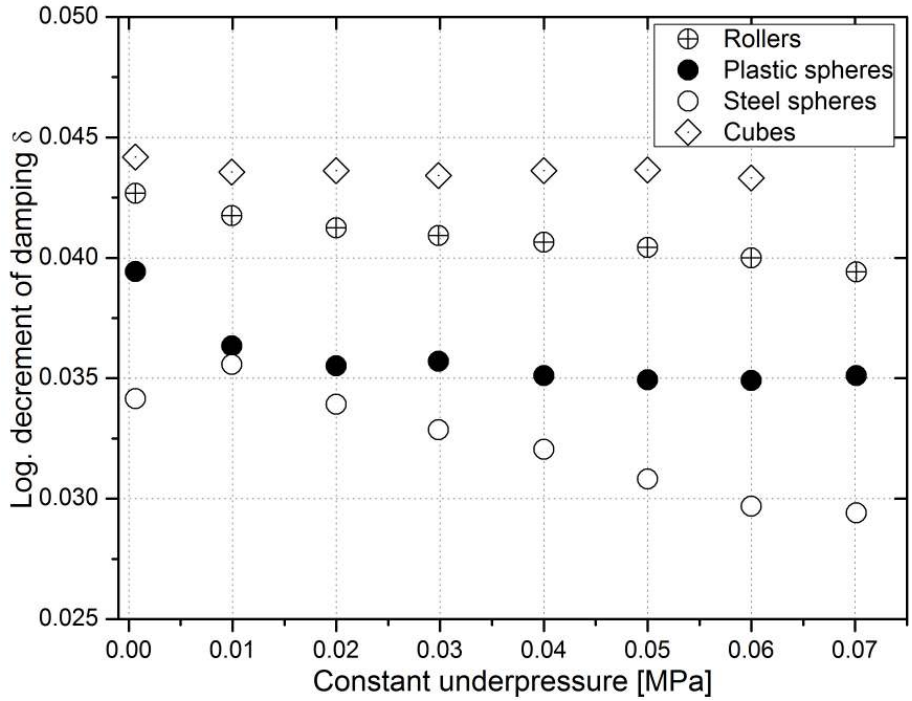

Figure 5.7: Logarithmic decrement of damping for constant underpressure for different types of granules.

with the granular structure with rollers. The amplitude on the FFT plot is the relative strength of the harmonic component present in the original signal. The frequency slightly shifts toward the higher values when the jamming is intensified by the negative pressure. The jammed material has a higher density of force chain network, and thus an intensified flexural rigidity. This was also true for all of the examined materials, but with different intensities - rollers exhibited the highest change.

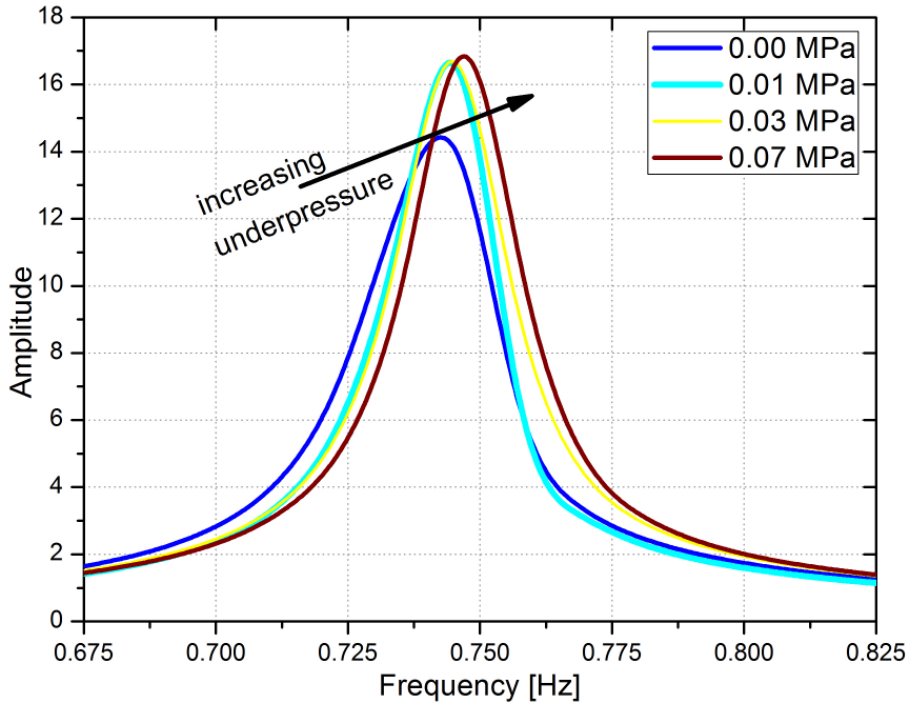

Figure 5.8: Frequency response for different values of constant underpressure, granular structure filled with rollers.

As can be seen from Figure 5.9, an intensified jamming shifts the natural frequencies to higher values when the underpressure is applied. The damping element filled with steel spheres was the heaviest one, so the frequency for it was the lowest. On the other hand, the cubic and roller fillings were the lightest, so they yielded the highest frequencies.

For the considered case, when only a part of the beam is treated with the granular damping member, the absolute frequency change is rather small, but the tendency seems to be clear. For the steel and plastic spheres, the increase reached 1%. For the roller and cubic shaped granules, the increase was 0.7% and 0.3%, respectively. The material that allows the highest change of the parameters seems to be the best to be used in the semi-active control based on periodical switching of the parameters. The roller granules were chosen for further investigation, as they allow large changes in their damping and frequency, exhibiting high values of these parameters.

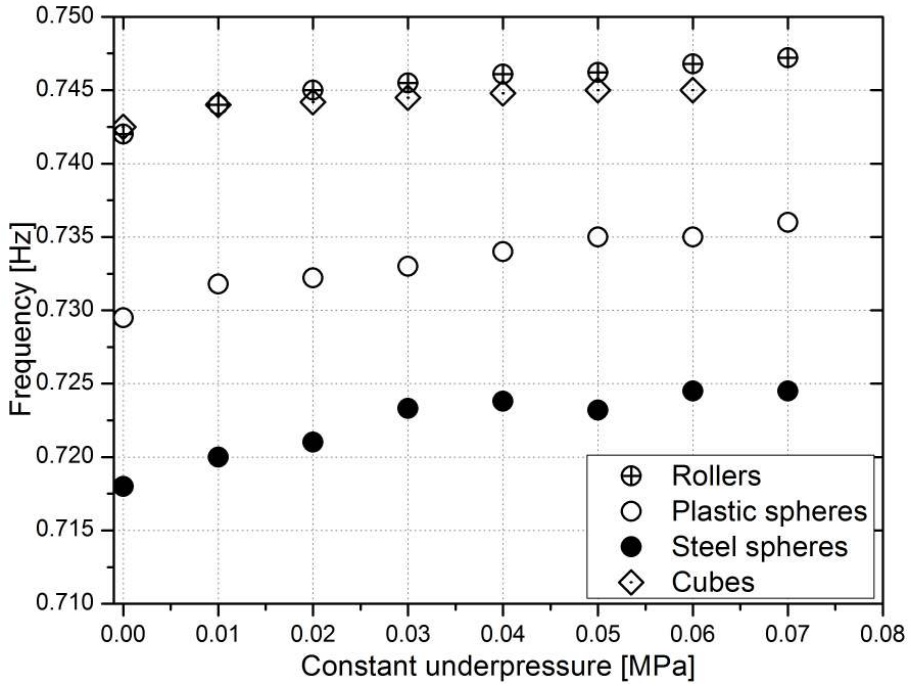

Figure 5.9: Frequency vs. underpressure for different granular materials.

5.2.2 Parameter Identification

This section describes the identification of the parameters of the model of the beam with granular structure presented in **Chapter 3: Problem Formulation and System Modelling**. The identification was based on the experimental results presented in the previous section.

A complex investigation of the non-trivial behaviour of a jammed granular structure and determination of all its parameters is a difficult issue. The problem of formulating the model of the real, complex, jammed granular structure with controllable properties requires considering contact, friction, rotation, slips, nonlinear large deflection phenomena, etc. Solving the reverse modelling problem would result in a significantly different results obtained for models considering different dominant interactions. Here, we analyse the problem for the one, dominant degree of freedom. Reasonable computational models for the mathematical simulations require knowing the values of the stiffness and viscosity. That is why we have chosen the Kelvin–Voigt, classic Maxwell, and a generalized Maxwell model [45] simplified to a Zener configuration (presented in Figure 5.10) to examine, which one is the best for modelling of the beam with granular damping element.

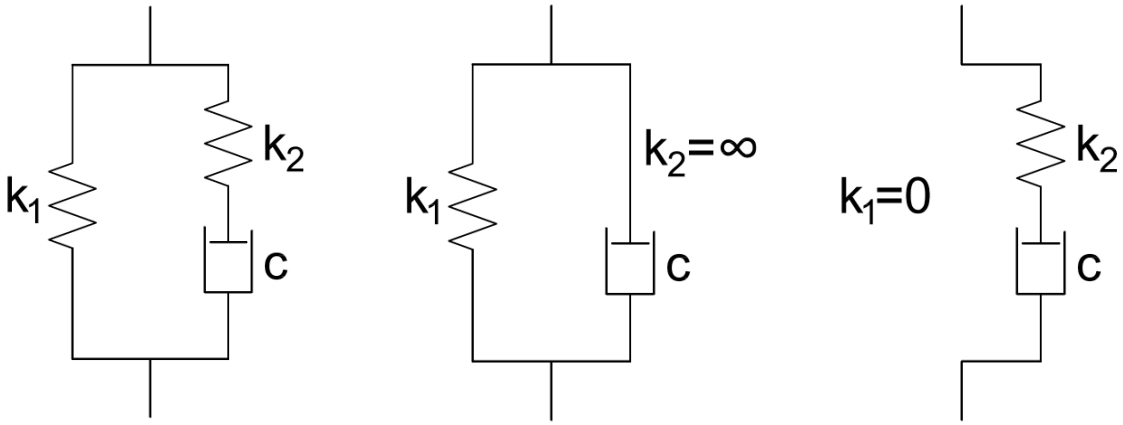

(a) Zener (b) Kelvin–Voigt (c) Simple Maxwell

Figure 5.10: Different models used for the parameter identification of the cantilever with granular damping member.

The reported estimation of the fit of the measured and computed displacements is denoted by ϵ and given by the relation

$$\epsilon = \frac{1}{\Delta t} \int_0^{t_f} \left(w(t) - \bar{w}(t)\right)^2 \mathrm{d}t \ , \tag{5.4}$$

where Δt is the time step of the registered data.

We assume displacements in time of the real beam (Figure 5.5a) as a reference function. The minimization problem allows us to determine the material parameters. We compare the first 30 seconds of vibrations with the chosen model of the structure. The computed parameters for the Kelvin–Voigt model are presented in Table 5.1. Furthermore, the Maxwell and Zener models (Table 5.2 and 5.3) also give a good aapproximation to the experimental curves.

The general Zener model reduces to the simplified models during the minimization procedure by assuming certain particular values of the model parameters. By assuming infinite value of the stiffness k_2 (Figure 5.10) the Kelvin–Voigt model is obtained. For the simple Maxwell model k_1=0 and parameters k_2 and c remain.

Figure 5.11 presents the estimation error of the models. Although the Zener combines features of the two other models and theoretically it should provide the best fit because it allows modifying more parameters, the computational identification for numerous parameters is less efficient than for the simple models. The generalized model approach is even less accurate than its equivalent Maxwell model with the same probability of establishing the minimum, i.e., for the same number of Monte Carlo attempts.

Table 5.1: Computed parameters for the Kelvin–Voigt model for the roller granules.

Δp [MPa]	k_1 [N/m]	c [Ns/m]	error ϵ
0.00	8.601	0.03082	427
0.01	8.633	0.03117	463
0.02	8.672	0.03162	598
0.03	8.682	0.03244	818
0.04	8.690	0.03180	669
0.05	8.705	0.03094	536
0.06	8.706	0.03037	463
0.07	8.707	0.03011	432

Table 5.2: Computed parameters for the Maxwell model for the roller shaped granules.

Δp [MPa]	k_2 [N/m]	c [Ns/m]	error ϵ
0.00	8.602	112.778	410
0.01	8.654	112.410	583
0.02	8.674	111.100	576
0.03	8.683	108.343	790
0.04	8.690	110.893	666
0.05	8.705	113.358	518
0.06	8.706	115.820	450
0.07	8.707	118.121	426

Table 5.3: Computed parameters for the Zener model for the roller shaped granules.

Δp [MPa]	k_1 [N/m]	k_2 [N/m]	c [Ns/m]	error ϵ
0.00	0.0538	8.542	112.12	410
0.01	0.0002	8.621	111.80	592
0.02	0.0040	8.660	110.60	576
0.03	0.0391	8.664	107.50	789
0.04	0.0073	8.672	110.31	666
0.05	0.0607	8.686	112.81	518
0.06	0.0760	8.697	115.56	449
0.07	0.0657	8.708	117.60	425

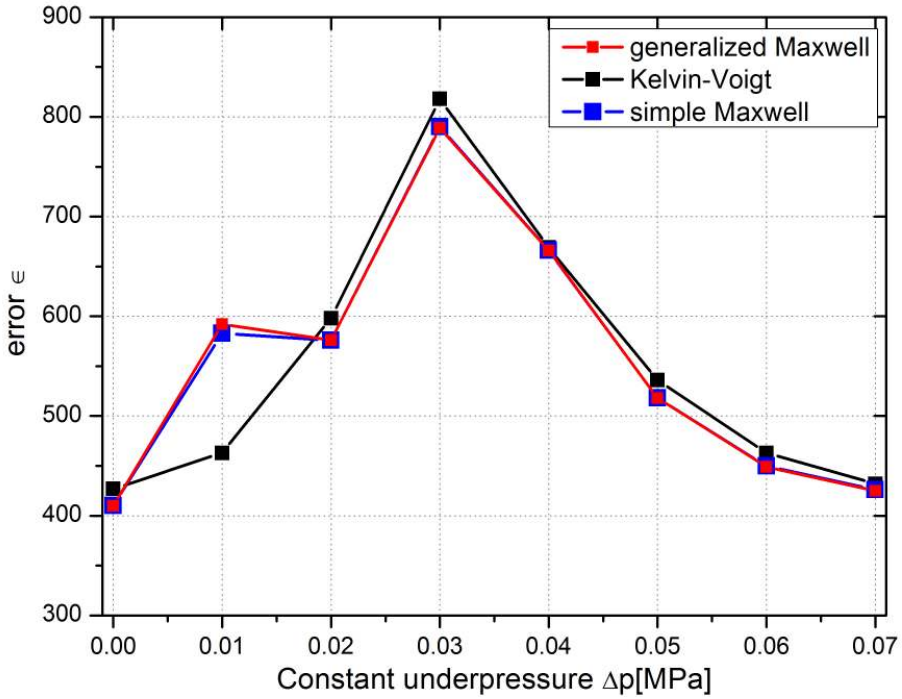

Figure 5.11: Error of the parameter fitting for different models.

The Zener model coincides with the simple Maxwell model for almost every value of Δp except small discrepancy for 0.01 MPa. This means that we can use simpler model for computations to get fair results. The Kelvin–Voigt model exhibits almost equally good results, and the error for 0.01 MPa is the smallest one for all the models.

For both of the simplified models the traces of the parameter k (Figure 5.12a and b) show that the stiffness increases with the underpressure in the range 8.60–8.71 N/m. The increase of the stiffness is nonlinear, however it seems that it tends to reach saturation, and further increasing of underpressure above 0.07 MPa is pointless. The influence of the damping c on the final displacement turns to be marginal. The damping c turns not to be a monotonic function of the underpressure. For both, Kelvin–Voigt and Maxwell models, it follows an opposed tendency since the role of the viscotic damper is different in each model.

It turns out that the Kelvin–Voigt model combines the fastest and simplest computations with a good accuracy. This is the reason why it was chosen for the optimization presented in **Chapter 3: Problem Formulation and System Modelling**.

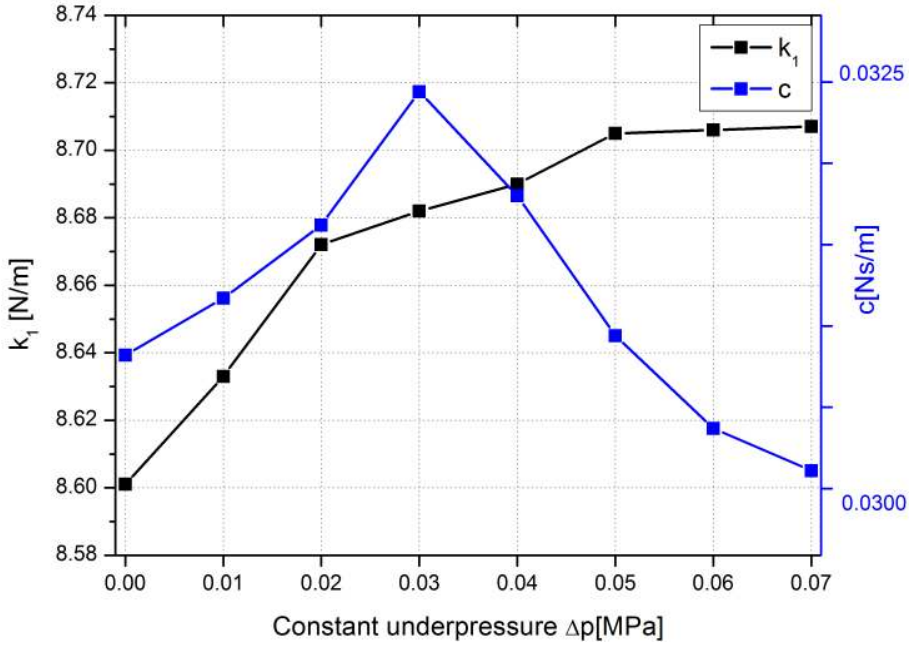

(a) Kelvin–Voigt

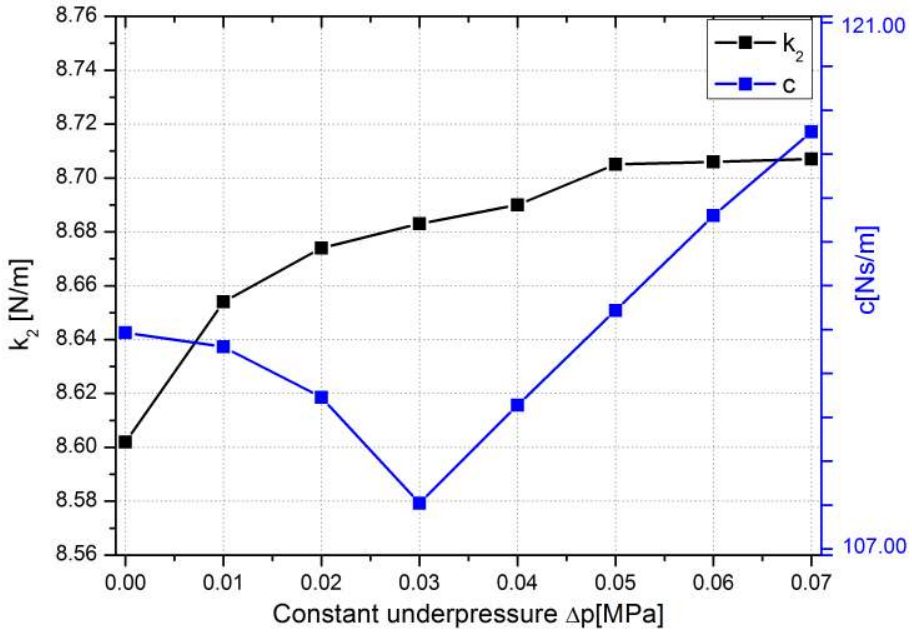

(b) Simple Maxwell

Figure 5.12: Results of the parameter identification for the Kelvin–Voigt and simple Maxwell model.

5.2.3 Semi–Active Damping for Selective Underpressure

The next step was to study the concept of the switched jamming treatment obtained with the granular damping structure. The control strategy involves switching the underpressure between 0 MPa and the selected threshold value. Any value from the range of 0–0.07 MPa may be chosen, however research showed that the highest change of the parameters is obtained for the maximum value of underpressure, so 0.07 MPa was selected as the extreme threshold value. Further analysis concerns the question whether the controlled switching between 0 MPa and 0.07 MPa may result in an efficient vibration suppression.

Figure 5.13 presents the controller-adapted version of the theoretically obtained strategies from **Subsection 3.3.3: Control Strategy for Granular Structure**. The first strategy named *optimal10* is the simplified version of the control signal from Figure 3.11 obtained for 10 time intervals. The second one, named *optimal20* is the simplified theoretical strategy which was obtained for 20 time intervals.

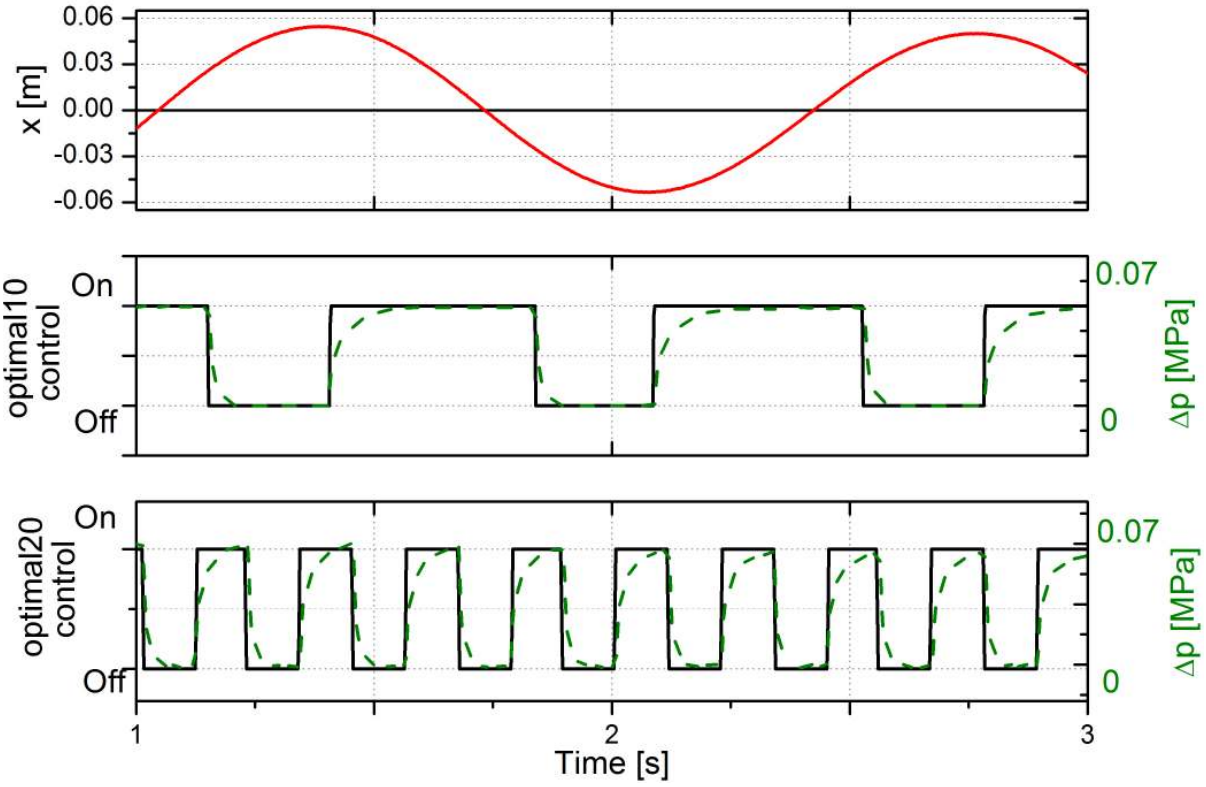

Figure 5.13: Displacement amplitude and simplified control signal sequences used for the experimental research study.

The figure also shows how the negative pressure inside the envelope (green line) change over time as the underpressure is switched. It turned out that the highest possible frequency of switching is 20 Hz and is limited by the inertia of the process of jamming, and

the time needed to remove the air from the envelope.

In Figure 5.14 the response of the controlled beam with the roller filling is compared with the reference results for a one-time selection of a constant underpressure of 0.07 MPa. The results clearly show that proper control of the underpressure and switching its value in particular moments may notably improve the efficiency of the proposed damping system. The efficiency of both control strategies is similar, however the beam exhibits faster vibration suppression for strategy *optimal20*.

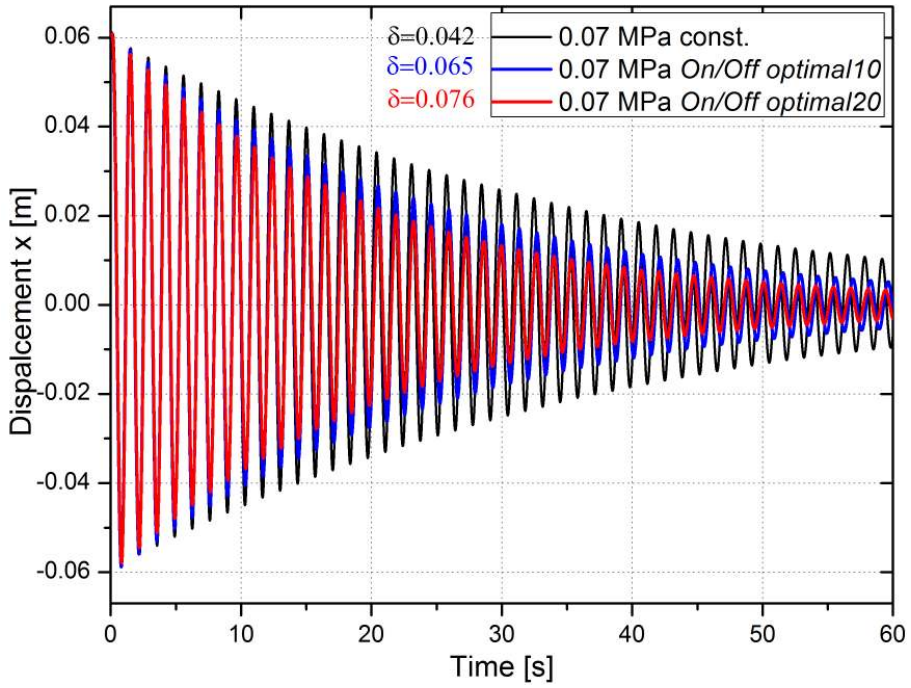

Figure 5.14: Comparison of the displacement for constant underpressure and different switching control strategies.

For constant damping, after 60 s of vibration the displacement was suppressed to 9.2 mm (15.3% of the initial value). For *optimal10* the displacement was suppressed to 3.2 mm (9.3% of the initial value), compared to 1.4 mm (5.3% of the initial value) obtained with strategy *optimal20*. The value of the logarithmic decrement of damping increased from 0.042 for constant underpressure 0.07 MPa, up to 0.065 for *optimal10* strategy and 0.076 (*optimal20*). The surplus is almost 80% compared with the case when structure is permanently jammed by constant underpressure.

Let us take a look how the damping efficiency change, when we switch the underpressure from 0 MPa to any other threshold values. The value of the logarithmic decrement obtained for the algorithm named *optimal10* is presented in Figure 5.15. The value of the logarithmic decrement obtained for algorithm named *optimal20* is presented in Figure 5.16.

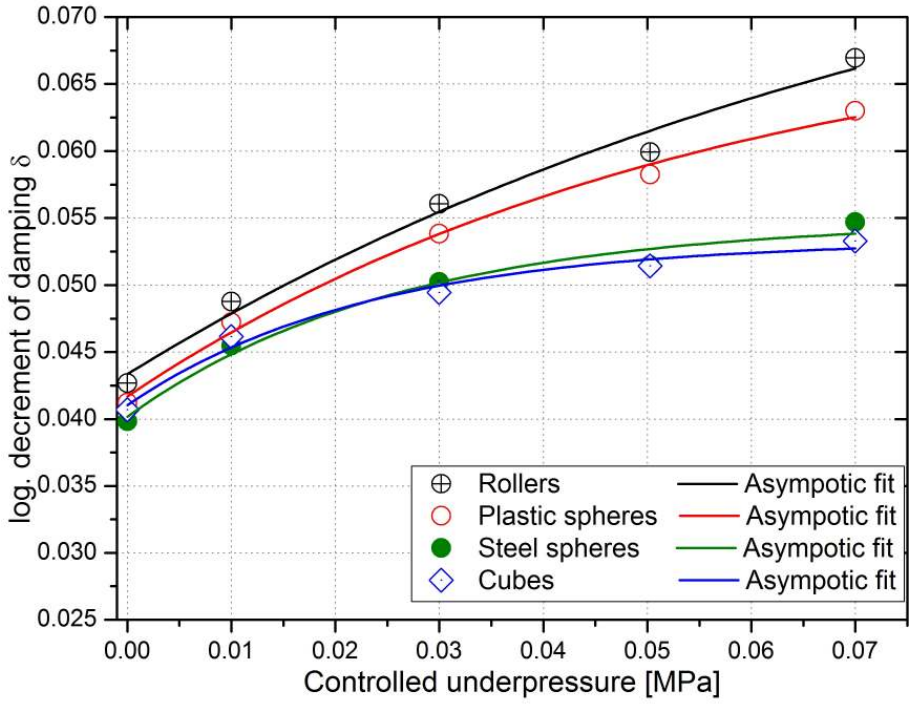

Figure 5.15: Logarithmic decrement of damping for the control algorithm *optimal10*, obtained for different threshold values of underpressure.

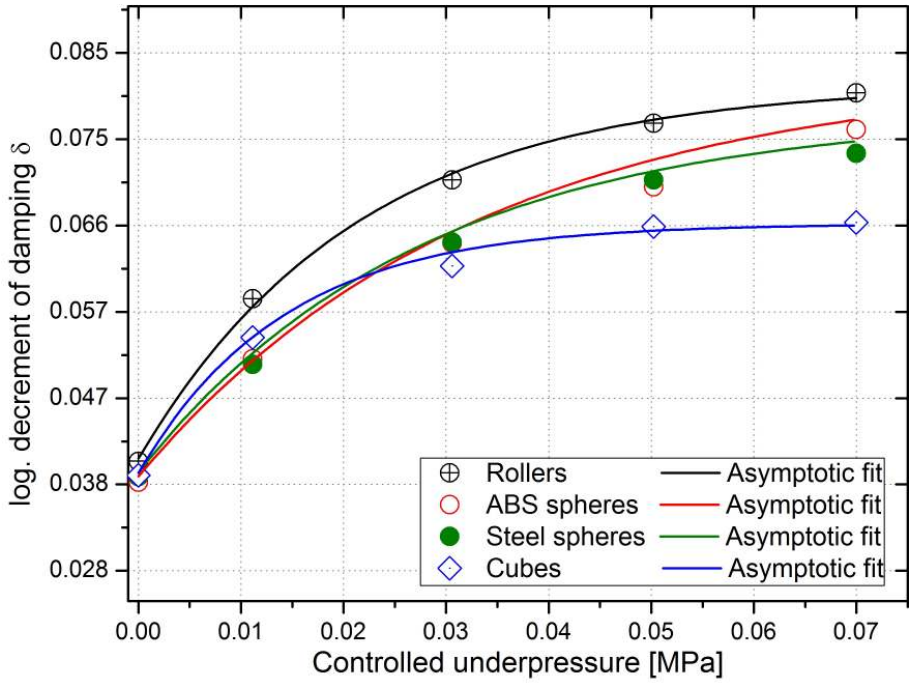

Figure 5.16: Logarithmic decrement of damping for the control algorithm *optimal20*, obtained for different threshold values of underpressure.

For each of the materials, the highest efficiency of damping was achieved with control algorithm *optimal20*. Rollers turned out to be the most effective material, that allows widest control of damping capacity, i.e. highest damping ratio in compliant state to damping ratio in jammed state. It can also be stated that for *optimal20*, the characteristic exhibits much more notable saturation than for the algorithm *optimal10*, escpecially when cubic granules are considered.

The frequency response for the most effective algorithm *optimal20* (Figure 5.17) showed that the response of the free vibrations of the beam consists mainly of one intrinsic modal function, which corresponds to the first mode of vibrations with the frequency of 0.74 Hz for no underpressure (for the roller granules). The frequency slightly shifts toward the higher values when the granular material is jammed permanently or temporarily. This is a natural consequence of the fact that the jammed material characterizes with intensified flexural rigidity as the force chains are formed.

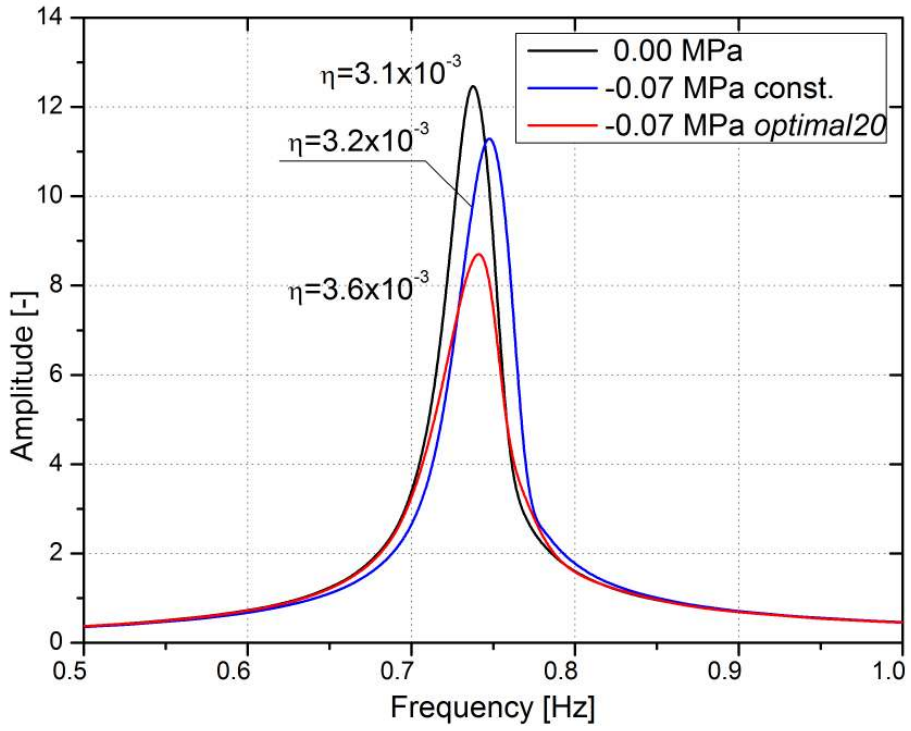

Figure 5.17: Frequency response of the beam with granular damping element filled with rollers, for the *optimal20* algorithm.

Alternatively the damping ratio was computed from the half-power bandwidth method. For no underpressure the damping ratio value was $3.1 \cdot 10^{-3}$. The value of damping ratio for constant 0.07 MPa was $3.2 \cdot 10^{-3}$. In the jammed state, intensified by the locking pressure, the dissipative interactions between the granules are much stronger. Then the damping ratio increases. For the controlled case, the damping is highest and reached

$3.5 \cdot 10^{-3}$, which is 13% greater than the value without control.

The mechanism was found to be effective in reducing the amplitude without significantly shifting the natural frequency of the cantilever. For no underpressure and switching underpressure, the frequency was almost identical, around 0.74 Hz. In the case of constant underpressure, the frequency shifts slightly to 0.75 Hz.

The experimental studies proved the efficiency of the elaborated algorithms. Rollers turned out to be the most versatile material, providing high damping and vast possibility of control. The presented results are justa a small piece of the experimental studies that had to be done to acquire the results. A very intrusting part of the further study on the control algorithms was devoted to searching for even more efficient strategies than the theoretical ones. Total of 8 empirical algorithms were examined and compared. That part of the study is presented in **Appendices**. It turned out that there are algorithms that exhibit even better vibration attenuation than the examined strategies. This clearly indicates that the modelling studies still needs to be expanded, which motivates further studies.

5.3 | Discussion of Results

From the laboratory research it was observed that both materials can be successfully used as a smart adaptive structures, and the proper momentary switching of their properties allows reducing the vibrations more effectively than if the treatment is passive. The coincidence between theoretical and experimental results obtained for magnetorheological elastomer and granular structure was satisfying, nevertheless, some discrepancies were noted.

For granules and elastomers, the damping capacity acquired by means of switching control was less effective than in obtained numerical results. This is the consequence of the modelling simplifications, differences between the assumed model and the real structure. The experimental cantilever with MRE was treated with the smart material only at the tip of the structure. In the mathematical model of the elastomer, the modelled beam was filled with the damping core all along the face sheets, which gives much greater increase in the rigidity of the structure. For simplicity of computation, the case of the cantilever beam supported from both sides was considered theoretically, and solved for the middle point. The experiments were carried on for a free-clamped configuration of the beam, which resulted in the better damping behaviour obtained numerically.

For the granular material the behaviour of the structure was simplified to a two degrees of freedom model, replacing the complex granular interactions with the Kelvin–Voigt

model, displaced axially. The theoretical control strategy was simplified to a more practical On/Off control algorithm. Moreover in much more complex practical problem smaller portion of the total energy can be released from the system in each cycle, nevertheless the strategy could be applied to mitigate the vibrations. Although the real application was less effective than theoretical one, the simplified strategy exhibited an improvement of the damping property. Further development of the material model and taking into consideration more interactions between granules could result in even better damping performance.

The thesis which states that changing of the damping properties of the magnetorheological elastomer or granular structure in selected moments, allows damping the vibration of the beam structures more effectively than when the damping is turned on constantly, was confirmed in theory any by the experimental investigation.

CHAPTER 6

Conclusions

Throughout this work, the semi-active damping method for transverse vibration of a vibrating sandwich beam, treated with two types of smart materials was investigated. For the beam with magnetorheological elastomer the distinctive feature is the ability to control the damping capacity by varying the magnetic field. For the beam with the granular damper the vibration attenuation is obtained by changing the underpressure value among the granules.

For both types of the damping materials, theoretical models of the systems have been developed. The mathematical model for the layered beam with MRE was based on the assumption of having a variable shear modulus material placed between purely elastic layers. Bending parts of the beam structure were described with the differential equations as layered elements of a sandwich structure, and the semi-analytical solution of the initial-boundary problem was obtained.

For the granular damper the phenomenological model was proposed to represent the complex behaviour of the system. The modified Kelvin–Voigt model was proven to be effective and accurate, however further model development is recommended. Models for both considered materials have allowed accurately describing the dynamic response of the concerned cantilevers. The optimal control problems were posed, considering the concept of periodically switched controllable capabilities of the systems in order to efficiently attenuate free vibration. The resulting control functions were simplified to a rectangular On–Off shapes, which are easy to realise on a classic electromechanical relay system.

The numerical analysis proved that the idea of periodical changing the material properties can be very efficient if the switching is presumed in a proper manner. To demonstrate the validity of the control strategy obtained numerically, the experiments were carried out for the real, initially deflected sandwich cantilever. The experimental verification was less efficient than the theoretical one, since the damping members were placed only locally at the tip of the beam, but the agreement between the theoretical and the experimental results was satisfactory.

The surplus of free vibrations of the real beams partially treated with either type of the smart material reached 10%–40% or more, depending on the material and the control strategy used. A detailed discussion of the experimental results concerning the amplitude of vibration, logarithmic decrement of damping, loss factor, stiffness, and natural frequencies has been provided. Both of the investigated functional materials have many applications prospect, which provides an impetus for continued research in this area.

6.1 | Perspectives

Designing lighter, safer and more efficient damping structures which are cost effective, has been in high demand in modern vibroisolation technology. Properly designed adaptive structures allow significant improvement of the dynamic properties of the systems, related to their passive equivalents. Unlike the passive type, the controllable system allows adapting to various loading conditions and excessive structural vibrations. Hence we obtain lower displacements, improved fatigue strength and the safety of the structure.

Both, the elastomers and the granular structures provide some flexibility in the shape design and material tailoring variation to obtain desired dynamical performance and functionality. The granular materials encapsulated in elastic envelopes can possess almost any suitable shape which allows installing them in irregular-shaped spaces.

The mechanism of triggering the jammed state in granular structure is reliable and relatively simple to apply, plus the cost of the structure is low. However, the structure itself is less robust due to the necessity of keeping the envelope hermetic, which is the weakest point of the solution. The applicably is limited to the applications with lower frequency excitations, since the granules need some time to reorganize, and it takes some time to evacuate the air from the envelope. The MRE provide better robustness, much quicker response, but require electrical supply system and the production cost is higher.

The change from one state of the elastomer to another takes a short time (order of milliseconds), therefore MRE are excellent for applications where strong dynamic features are required. One of the branches of applications of the MRE is the aerospace industry in which structures are mostly based on the metallic and composite layered solutions including carbon fibre-reinforced plastics, which have low internal damping. The ability to modify the internal layer parameters will influence dynamic properties of the structure. The proposed material and control strategy can be used to mitigate vibrating parts of the plane, and efficiently reduce wind flutter effects. The increase in capacity, and consequently the possibility of reduction of the weight of the airplanes will lower the fuel consumption.

(a) Civil engineering

(b) Traveling load

(c) Wind turbine towers

(d) Elastomeric bearings

(e) Wheel guiding transverse springs

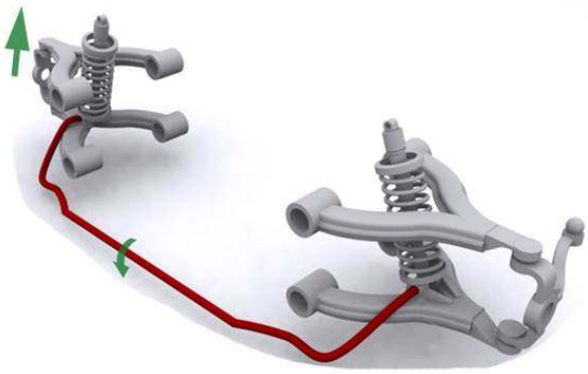

(f) Stabilizer bars

Figure 6.1: Areas of potential application of semi-active layered damping systems. Sources: barbarashdwallpapers.com, windaction.org, freyrom.ro, zf.com.

The automotive industry may also be a potential recipient of both of the proposed damping variants. Vibrations generated by the vehicle drive system and the suspension could be suppressed by the self-adaptive absorbers, or smart lightweight suspension beams (Figure 6.1e), stabilizer rods (Figure 6.1f) or suspension bushings in order to reduce the shudder effect. The electrical current could be supplied from the automotive electrical system, while the underpressure could be generated by one of the pumps. It would be particularly useful to adjust the vibration of the adjacent structures in response to present conditions such as vehicle speed, road type and whether conditions, vehicle load and similar.

The semi-active solution with an efficient control algorithm may also be used for applications where we have to deal with the fast traveling load such as train-track (Figure 6.1b), vehicle-bridge, crane-weight systems (Figure 6.1a) or robotic linear guideways which are of a special interest for practising engineers. Existing structures could be reinforced by supplementary supports with magnetorheological elastomers controlled externally to improve the stability of the structure. That type of control, when only a few of many MR fluid dampers are activated was described in [5]. The construction might benefit from incorporating magnetorheological elastomers as an alternative to fluid dampers.

The seismic performance efficiency of the base isolation system, which decouples the civil structures from the ground motion (Figure 6.1d) can be highly improved by adapting the concept of the smart materials controlled according to the switching strategy. The controlled elastomers with stiffness-tuning ability strive to alleviate limitations of existing passive-type base isolators, which works well on a site with a stiff soil condition, but are not be effective at all on a site with a softer soil.

Existing mechanical structures viability may be enhanced by the additional supports with one of the proposed, semi-active solutions. Only in the United States about 40% of bridges are obsolete or are not able to meet current requirements raised by the intensity of public transport. Studies prove that half of the cost of replacing the bridge is traffic redirection to another route, during its construction or reconstruction. For the massive structures MRE elastomers seems to provide enough strength, robustness and range of controllable stiffness. Although the problem at the closed Volga River bridge (please see **Chapter 1: Introduction**) was solved using magnetorheological dampers, application of smart elastomers with variable shear modulus would give a completely new possibility of overcoming such problems.

A granular-based system would be preferred in lightweight structures, for example in mitigating the low frequency vibrations of a tower pole of a wind turbine (Figure 6.1c) where they can be employed as an environmentally friendly solution operating in relation

to the time changing wind speed and variable speed mode used in a large scale turbines. For normal operating condition the structure could be damped by the loose granular material, while the switched jamming strategy would be active for an exceeded level of vibrations.

Properly adapted, smart granular damping elements may also be used as well in intelligent rail ties, speed bumps, marine dock buffers, loading bumpers, fenders in the warehousing industry, pedestrian walkways, pipeline systems, speed humps and many other types of structures. It is an attractive alternative in semi-active damping due to its conceptual simplicity, potential effectiveness and very low cost. In spite of these benefits, the proposed semi-active damping systems bears some drawbacks, primarily because they are more complex than the passive counterpart and require additional sensors, actuators and controllers.

6.2 | Recommendations

Although the idea presented in this work is in the initial phase, its potential seems to be very attractive and it deserves a major attention. The proposed approach opens a lot of new and interesting research problems and potential solutions for engineering applications. Numerous problems still seem to be open to further study.

The modelling section could be still significantly improved, considering more in-depth look at the material properties and additional laboratory material test. The optimal composition and geometric parameters of the damping members, and minimizing their weight by selecting their optimal placement can help in maximization of modal damping ratios and modal strain energies and can lead to significant saving in the amount of used material. The structures with MRE can benefit from the fact that the certain properties can be achieved in the manufacturing process. The methods include coating of the magnetizable particles for corrosion protection or improvement of the bonding between the particle and the matrix, different matrix choices and alignment of the particles in the curing process. This gives the possibility of tailoring material variation response to obtain desired dynamical performance and functionally in the structure, but also needs a complex investigation to find the optimal compositions. In order to study in details the possibilities of controlling the vibrations of the beams treated with smart material, it is necessary to analyse the response of the systems subjected to the dynamic exploitation loads and harmonic excitations, for example reproducing the excitation caused by the vehicle riding on the bumpy road, seismic vibrations or environmental load or an impulse-excited system. Versatility of the construction of the presented laboratory stand makes

it possible to take the advantage of the currently equipped elements and to utilize them on the test bench intended to investigate the dynamic loads response. The presented analysis will help the designers to estimate the damping capacity of structures vibrating under dynamic conditions in order to maximize it as per the requirements in the actual applications. Further study on the topic is to be highly recommended.

Appendices

APPENDIX A

Additional Experimental Results

In the main part of the work the most important results were showed and discussed. However, a major effort and a huge amount of time was spent to find the best materials used for the research, proper configuration of the specimens, calibrating the measurement system, etc. This appendix includes small part of the supplementary, most important results for the research presented in the **Chapter 5: Experimental Results**.

Although many interesting behaviour concerting granular materials and elastomers were noted, they were not published in this dissertation as they are not strictly significant for the topic of selective control. However, the author hopes that the collected experimental material will be soon published in form of scientific articles.

Magnetorheological Elastomer

The computed parameters of the fitted curves for the magnetorheological elastomer presented in Figure 5.3 are listed in the Figure A.1. The average error of the exponential decay curve fitting was sufficiently low to use the logarithmic decrement as measure of damping in the system.

Model	Asymptotic fit for 0V		
Equation	y = a-b*c^x		
Reduced Chi-Sqr	0.02287		
Adj. R-Square	0.99987		
		Value	Standard Error
Envelope Y 1	a	-4.01193	0.00929
	b	-63.28461	0.00811
	c	0.97749	6.06883E-6

Model	Asymptotic fit fpr 24 V const.		
Equation	y = a-b*c^x		
Reduced Chi-Sqr	0.03637		
Adj. R-Square	0.99985		
		Value	Standard Error
Envelope Y 1	a	-5.18558	0.00574
	b	-65.36077	0.0047
	c	0.96713	6.72223E-6

Model	Asymptotic fit for 24 V cotrol		
Equation	y = a-b*c^x		
Reduced Chi-Sqr	0.01255		
Adj. R-Square	0.99994		
		Value	Standard Error
Envelope Y 1	a	-5.81675	0.00342
	b	-61.60617	0.0028
	c	0.96613	4.37568E-6

Figure A.1: Parameters of the fitted envelopes for the beam with MRE.

Passive Damping for the Granular Structure

Time and frequency responses of the cantilever with the granular structure filled with different types of materials are presented in Figure A.2. The time analysis itself is not sufficient for the complex research so the Fourier Transform vibration analysis was applied. This allowed transforming the time domain data into the frequency domain.

The recorded waveforms allow drawing basic conclusions about the analysed process, such as the nature of the vibration amplitude at particular moment, phase shift or the envelope of the signal, for certain type of the granular material. The presented results were used to compute the logarithmic decrement of damping and calculate the frequency of vibrations for different underpressure values, described in **Section 5.2.1: Passive Damping for Constant Underpressure**.

The parameters of the fitted envelopes for the beam with the granular damping structure for the passive-damping case are presented in Figure A.3.

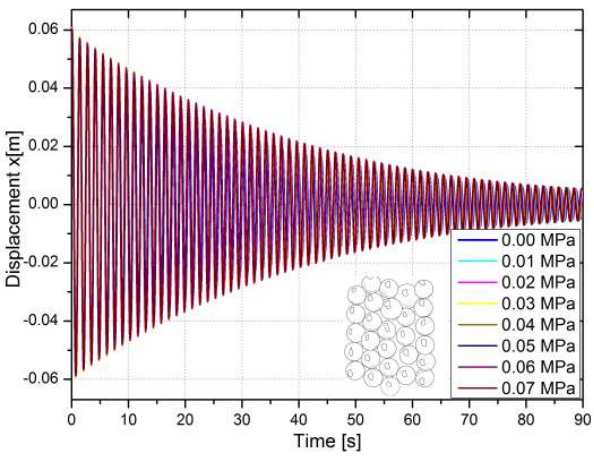

(a) Displacement for plastic spheres

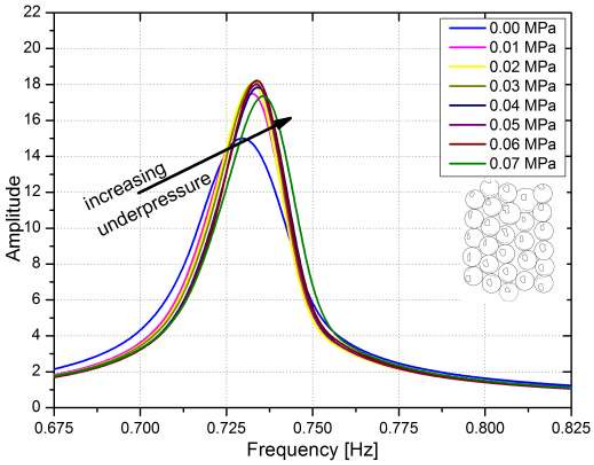

(b) Frequency for plastic spheres

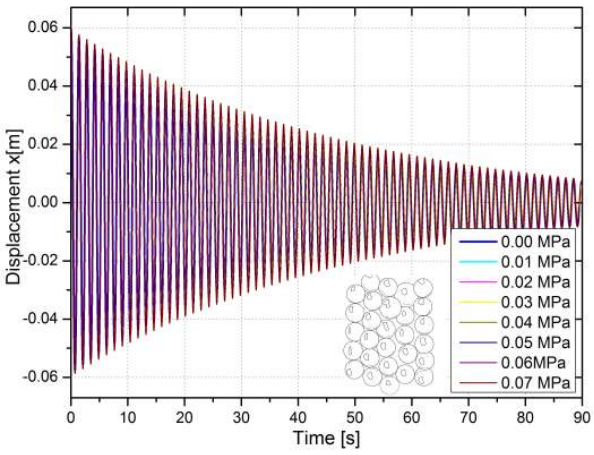

(c) Displacement for steel spheres

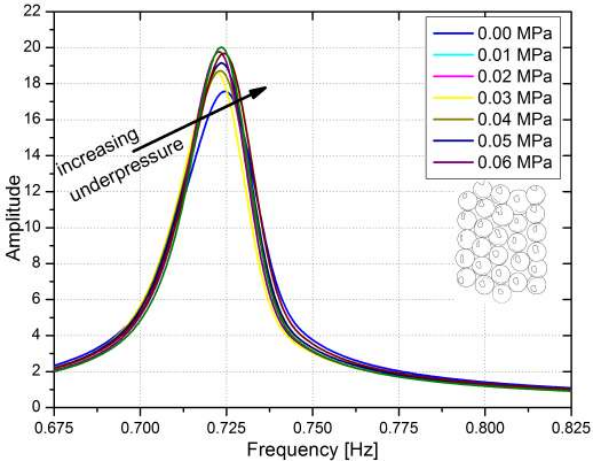

(d) Frequency for steel spheres

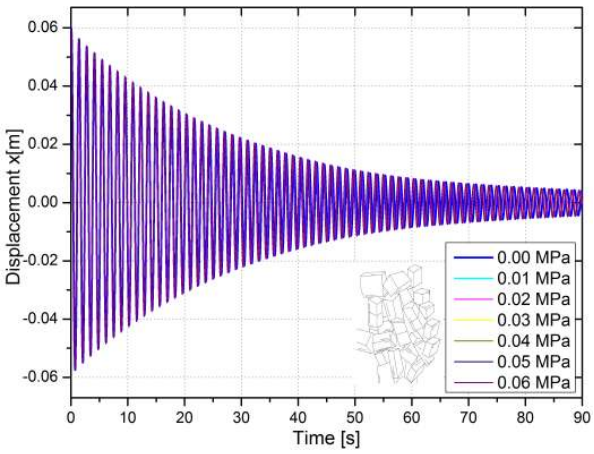

(e) Displacement for cubes

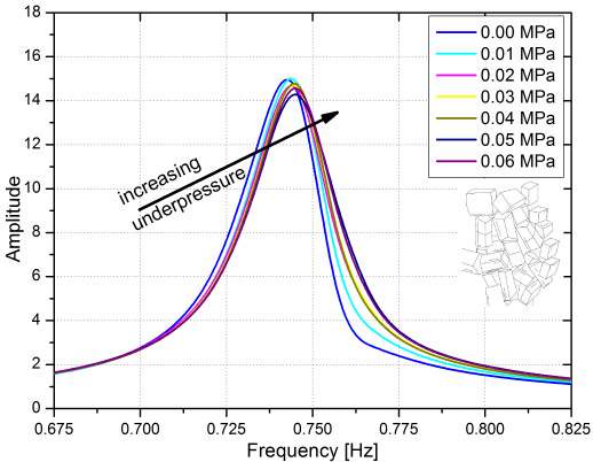

(f) Frequency for cubes

Figure A.2: Displacement and frequency response for constant value of underpressure for different types of granular materials.

Model	Exp2PMod1	Plastic spheres	Upper envelope					
Equation	y = a*exp(b*x)							
Reduced Chi-Sqr	0.05954	0.22272	0.30177	0.29562	0.28431	0.27563	0.26581	0.12055
Adj. R-Square	0.99973	0.99905	0.99874	0.99878	0.99876	0.99879	0.99886	0.99946
		Value	Standard Error					
Envelope Y 1	a	59.11462	0.00385		p=0.00			
	b	-0.02947	2.86092E-6					
	a	60.44761	0.00717		p=0.01			
	b	-0.02672	4.82057E-6					
	a	61.03958	0.00832		p=0.02			
	b	-0.02654	5.51189E-6					
	a	61.37214	0.00826		p=0.03			
	b	-0.02668	5.46095E-6					
	a	60.00034	0.00805		p=0.04			
	b	-0.02624	5.37791E-6					
	a	59.86148	0.00791		p=0.05			
	b	-0.02611	5.2774E-6					
	a	60.41896	0.00775		p=0.06			
	b	-0.02602	5.11444E-6					
	a	59.49009	0.00526		p=0.07			
	b	-0.02646	3.5687E-6					

Model	Exp2PMod1	Steel spheres						
Equation	y = a*exp(b*x)							
Reduced Chi-Sqr	0.10397	0.43774	0.26561	0.2738	0.26926	0.13446	0.0648	0.03846
Adj. R-Square	0.99947	0.99812	0.99884	0.99878	0.9988	0.99937	0.99969	0.99981
		Value	Standard Error					
Envelope Y 1	a	57.56791	0.00467					
	b	-0.02336	2.99534E-6		p=0.00			
	a	60.35587	0.01014					
	b	-0.02694	6.94585E-6		p=0.01			
	a	60.49571	0.00761					
	b	-0.02476	4.83348E-6		p=0.02			
	a	60.38137	0.00764					
	b	-0.02398	4.75721E-6		p=0.03			
	a	60.69738	0.00751					
	b	-0.02339	4.57325E-6		p=0.04			
	a	60.06728	0.00523					
	b	-0.02249	3.13574E-6		p=0.05			
	a	59.83477	0.00359					
	b	-0.02167	2.10875E-6		p=0.06			
	a	59.29398	0.00276					
	b	-0.02147	1.62388E-6		p=0.07			

Model	Exp2PMod1	Cubes	Upper envelope				
Equation	y = a*exp(b*x)						
Reduced Chi-Sqr	0.2123	0.16801	0.16696	0.1755	0.19076	0.18593	0.15502
Adj. R-Square	0.99905	0.99925	0.99926	0.99921	0.99915	0.99917	0.99931
		Value	Standard Error				
Envelope Y 1	a	58.69172	0.00758		p=0.00		
	b	-0.03254	6.14776E-6				
	a	58.81742	0.00673		p=0.01		
	b	-0.03241	5.43082E-6				
	a	58.72492	0.00671		p=0.02		
	b	-0.03245	5.42975E-6				
	a	58.57348	0.00687		p=0.03		
	b	-0.0323	5.54866E-6				
	a	58.75293	0.00718		p=0.04		
	b	-0.03245	5.80228E-6				
	a	58.70854	0.00709		p=0.05		
	b	-0.03248	5.73924E-6				
	a	58.98604	0.00645		p=0.06		
	b	-0.03229	5.17632E-6				

Figure A.3: Parameters of the fitted envelopes for the beam with MRE.

Empirical Control Strategies for the Granular Structure

Despite studying the response for the theoretically obtained strategies of switching the underpressure, additionally eight different empirical strategies were studied for comparison. The shape of the control signals and the moments for activating the underpressure are presented in Figure A.4.

Even small differences in the moment of jamming the granular material resulted in a notable change in the damping properties of the beam. From the presented strategies the most interesting results were obtained for the algorithm named *new20-100*. The results confirmed that the proposed controlled jamming system outperforms the passive one, and may be efficiently used in mitigating the response of the structure. It turned out that the empirical algorithm also outperforms the theoretical strategies studied in the main part of the dissertation.

Better damping behaviour is achieved when the material is constantly activated through the whole cycle of vibrations, and becomes unjammed just for very short moment near the maximum deflection points, as presented in Figure A.5.

Just a short time before the tip of the beam reaches the point where $\dot{x} = 0$, the material is switched to the unjammmed state. All the remaining, weak particle chains are removed. Then it is quickly switched at the maximum deflection point where $\dot{x} = 0$, so the large number of strong particle chains is recreated. The jammed beam is coming back to the equilibrium point, passes it and reaches maximum deflection point at the opposite site. This movement causes major dissipation caused by the breakage of the force chains, which are once again recreated at point $\dot{x} = 0$. This can be compared to periodically gluing particles at maximum deflection points, breaking the bonds during their movement, and gluing the material once again. Once again rollers turned out to be the most effective material. For the control strategy *optimal20* the decrement was $\delta = 0.076$ while the selective switching of 0.07 MPa according to *new20-100* allowed increasing it up to $\delta = 0.092$ as presented in Figure A.6.

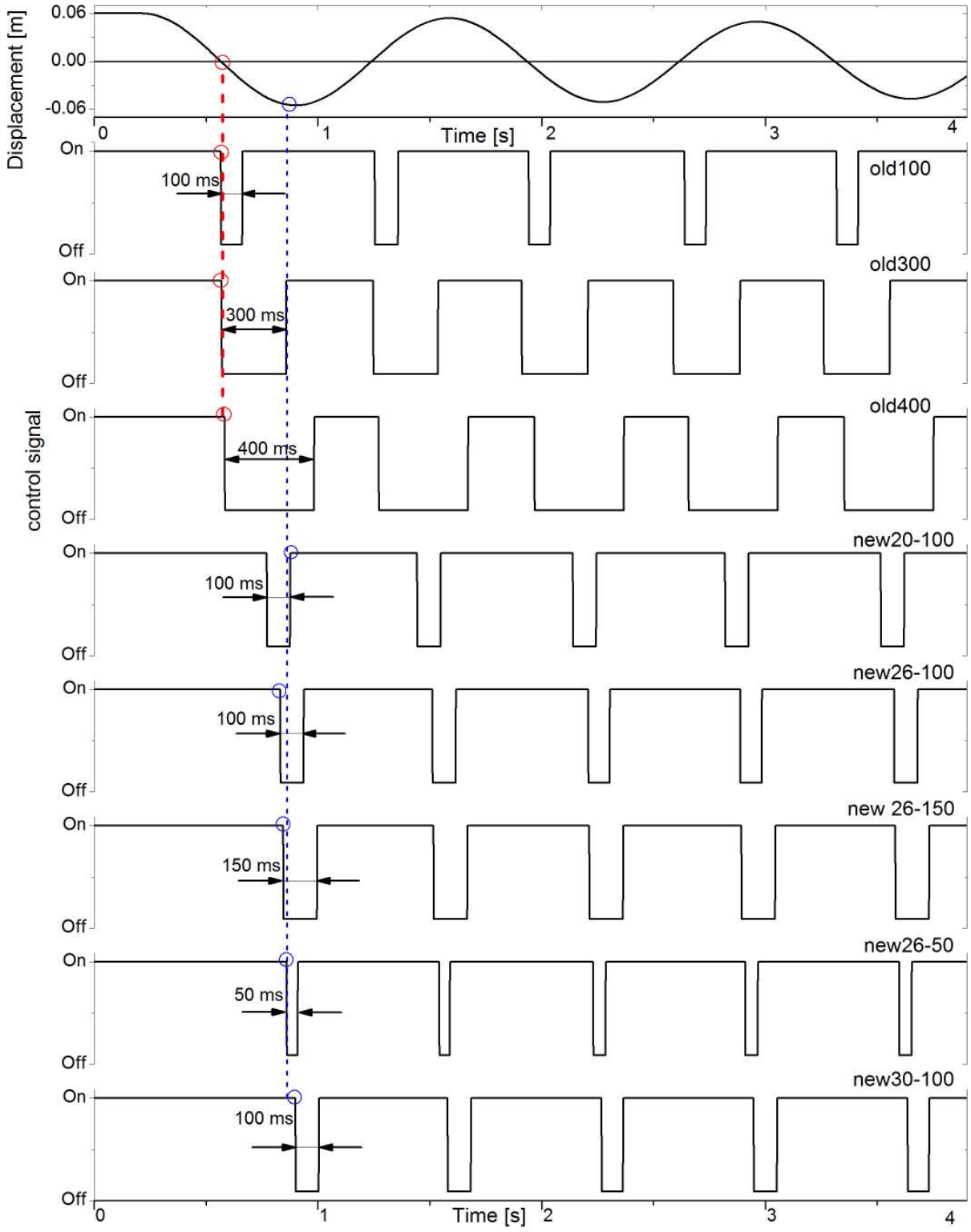

Figure A.4: Control signal sequences used for the experimental research study.

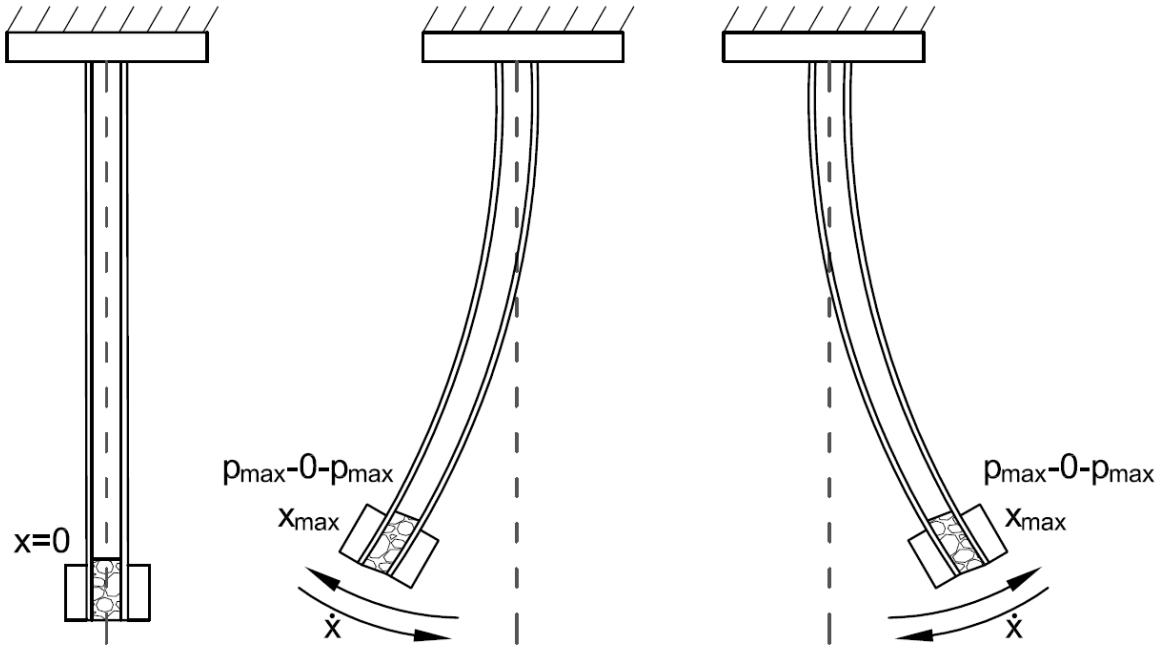

Figure A.5: Distinct moments for momentary switching the granular material state, obtained for the control strategy *new20-100*.

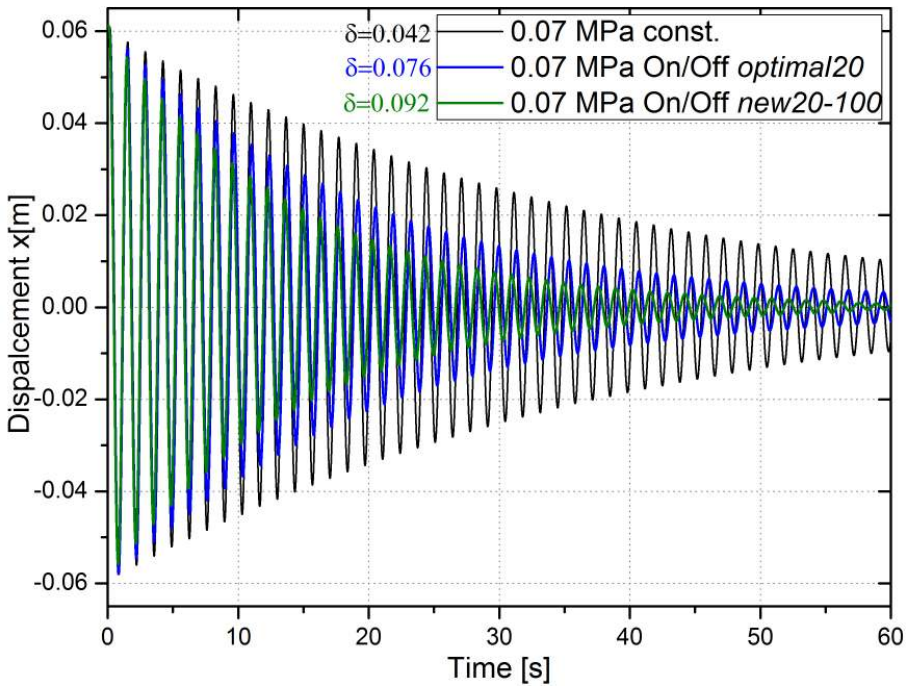

Figure A.6: Comparison of the best theoretical algorithm *optimal20* with the best empirical algorithm *new20-100* for the roller granules.

APPENDIX B

PLC Controller Algorithms

All of the programmable logic controller algorithms discussed in **Chapter 5: Experimental Results** were programmed using ladder diagram language in CX-Programmer 9.4, software dedicated to OMRON compact automatic controllers.

Figure B.1 presents the ladder diagram program used to switch the electromagnets acting as actuators for the cantilever beam with the embedded magnetorheological elastomer. Every ladder step of the algorithm was commented to give an idea how the program operates.

Figure B.2 and B.3 present the code used to switch the underpressure among the granular structure at selected moments to obtain the optimal control and maintain the operation of the electrovalve.

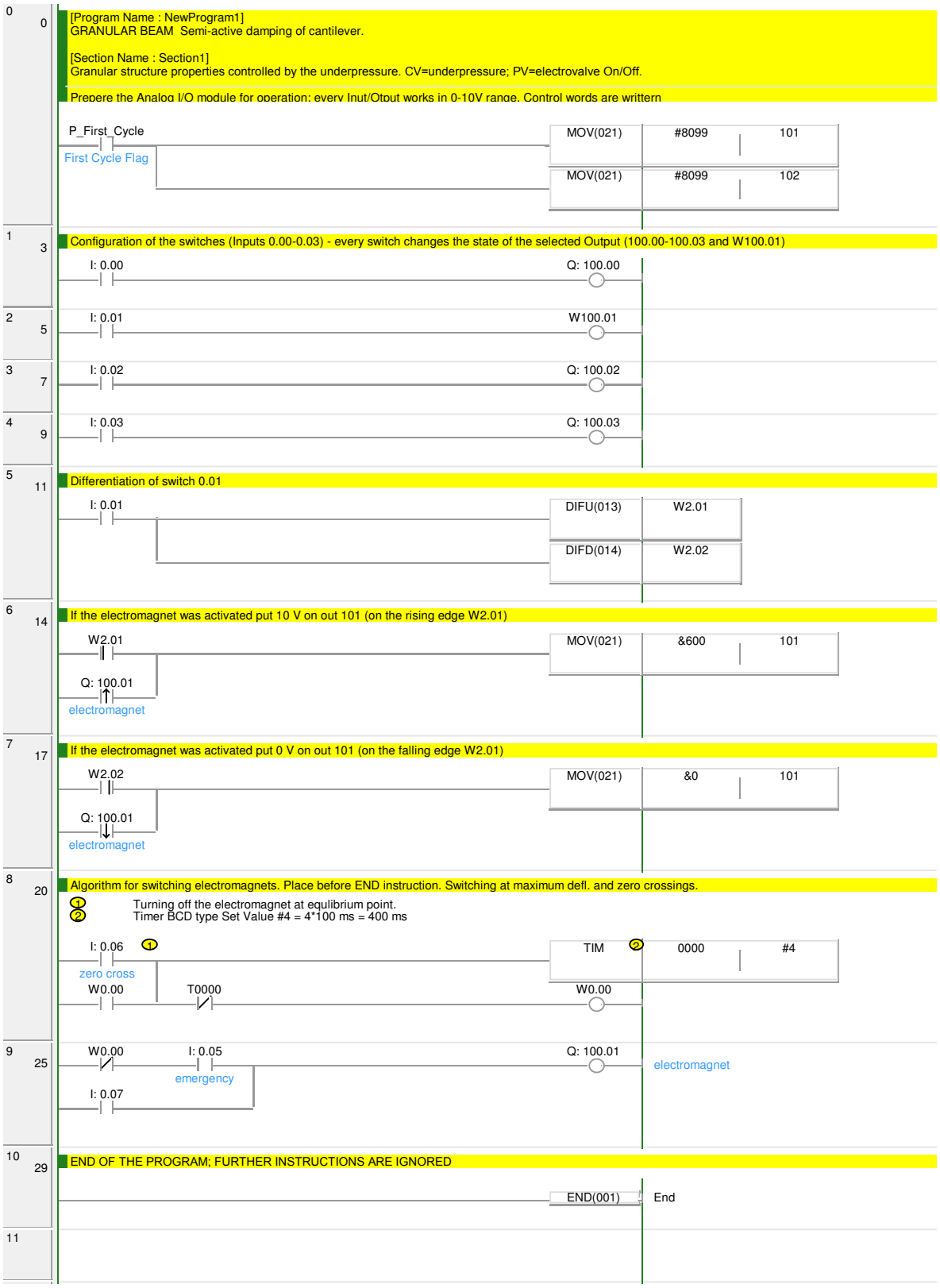

Figure B.1: PLC ladder diagram for the beam with MRE damping element.

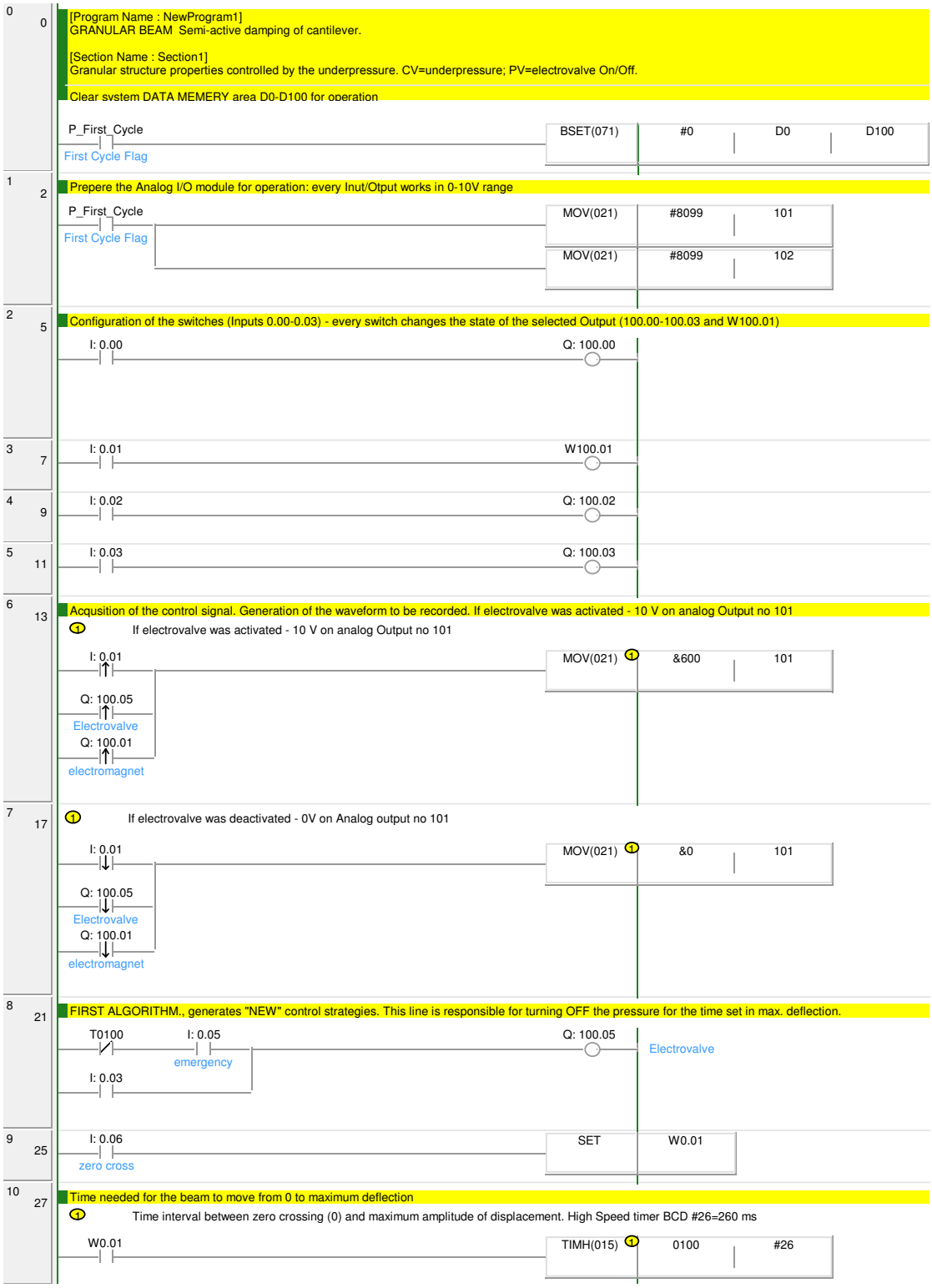

Figure B.2: Part 1 of PLC ladder diagram for the beam with granular damping structure.

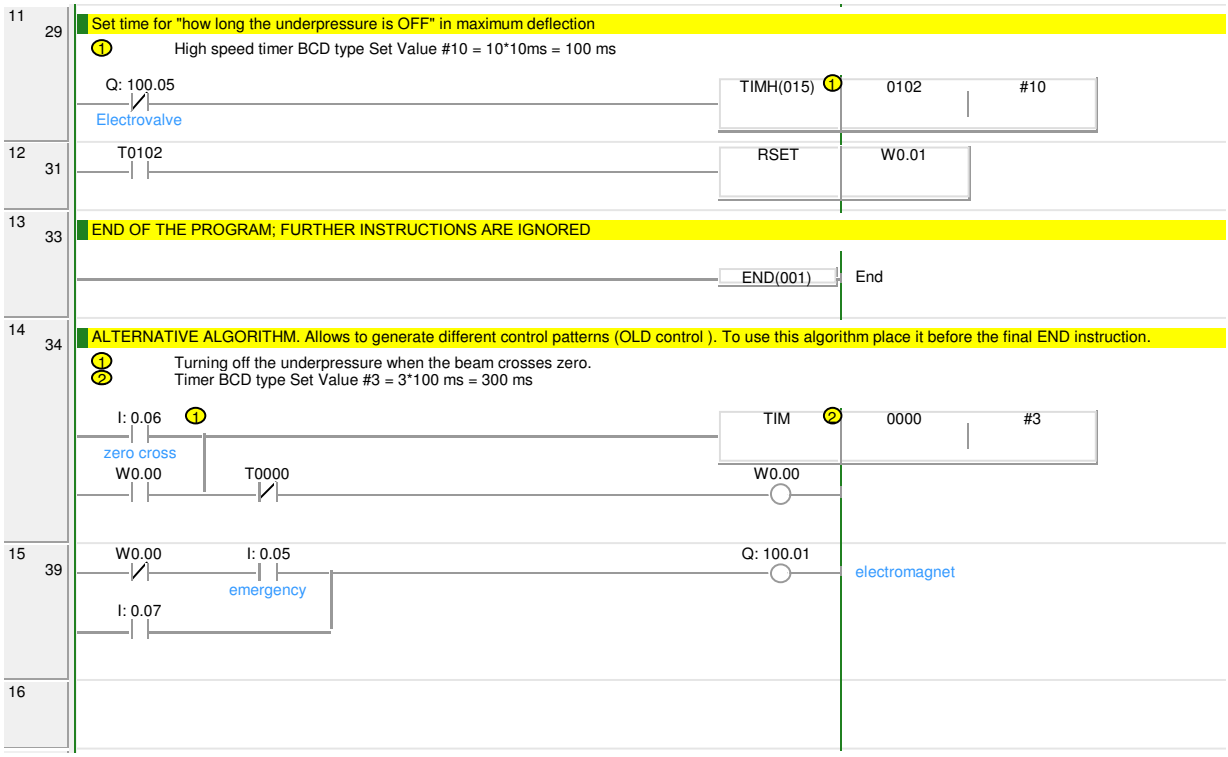

Figure B.3: Part 2 of PLC ladder diagram for the beam with granular damping structure.

Bibliography

[1] M. A. Aguirre, N. Nerone, I. Ippolito, A. Calvo, and D. Bideau. Granular packing: influence of different parameters on its stability. *Granular Matter*, 2(1):75–77, 2001. (Cited on page 25.)

[2] I. Ahmad. Smart structures and materials. In *Smart Materials, Structures and Mathematical Issues: The 15th World Conference On Earthquake Engineering*, pages 13–16, Virginia Polytechnic Institute and State University, 1988. (Cited on page 24.)

[3] L. A. Albanese and K. A. Cunefare. Performance of MRE based vibration absorbers. *Journal of Intelligent Material Systems and Structures*, 19:551–563, 2008. (Cited on page 21.)

[4] D. Backstrom and A. C. Nilsson. Modelling the vibration of sandwich beams using frequency-dependent parameters. *Journal of Sound and Vibration*, 300:589–611, 2007. (Cited on page 27.)

[5] C. Bajer and D. Pisarski. Semi-active control of 1d continuum vibrations under a travelling load. *Journal of Sound and Vibration*, 329(2):140–149, 2010. (Cited on pages 29 and 88.)

[6] J. Bajkowski and J. M. Bajkowski. Influence of temperature and rotational speed on the properties of magnetorheological brake. In *Proceedings of the Fifth International Conference Design and Modeling of Mechanical Systems, Lecture Notes in Mechanical Engineering*, pages 143–149, Springer-Verlag Berlin Heidelberg, 2013. (Cited on pages 19 and 21.)

[7] J. Bajkowski, W. Grzesikiewicz, M. Hać, B. Landjerit, and P. Tadzik. Propriétés mécaniques d'échantillons avec les materiaux granulaires ferme en surface avec sous-pression. In *IV French – Polish Seminar of Mechanics*, pages 1–7, Warsaw, Poland, 1999. (Cited on page 25.)

[8] J. Bajkowski, W. Grzesikiewicz, M. Hać, and P. Tadzik. Parameter determination of half-active damping of vibration of mechanical systems by using granulated mate-

rials. In *Mat. Internationale Congres DYCONS'99*, pages 67–74, Ottawa, Canada, 1999. (Cited on page 25.)

[9] J. Bajkowski, P. Tadzik, and R. Zalewski. New possibilities of the active damping of vibrations. *Mechanics*, 26(4):156–159, 2007. (Cited on page 25.)

[10] J. Bajkowski and R. Zalewski. Influence of a single grain material on isotropic hardening parameters of granular structures under compression in uniaxial tensil tests. *Proceedings of the Institute of Vehicles*, 63(4):119–126, 2006. (Cited on page 25.)

[11] J. M. Bajkowski and R. Zalewski. Transient response analysis of a steel beam with vacuum packed particles. *Mechanics Research Communications*, 60C(1):1–6, 2014. (Cited on page 26.)

[12] A. Bhimaraddi. Sandwich beam theory and the analysis of constrained layer damping. *Journal of Sound and Vibration*, 179(4):591–602, 1995. (Cited on page 27.)

[13] G. Biroli. Jamming: A new kind of phase transition. *Nature Physics*, 3:222–223, 2007. (Cited on page 24.)

[14] A. Boryga and B. Skórska. Immobilization (in Polish). *CIR Medical Catalog*, 1, 2003. (Cited on page 25.)

[15] E. Brown, N. Rodenberg, J. Amend, and A. Mozeika. Universal robotic gripper based on the jamming of granular material. *Proceedings of the National Academy of Sciences of the United States of America*, 107(44):18809–18814, 2010. (Cited on page 25.)

[16] M. E. Cates, J. P. Wittmer, J. P. Bouchaud, and P. Claudin. Jamming, force chains and fragile matter. *Physical Review Letters*, 81:1841–1844, 1998. (Cited on page 25.)

[17] B. Chakraborty and R. P. Behringer. Jamming of granular matter. *Encyclopedia of Complexity and System Science*, 4697:4997–5021, 2009. (Cited on page 24.)

[18] L. Chen, L. X. Gong, and W. H. Li. Microstructures and viscoelastic properties of anisotropic magnetorheological elastomers. *Smart Materials and Structures*, 16:2645–50, 2007. (Cited on page 21.)

[19] L. Chen, X. L. Gong, W. Q. Jiang, J. Yao, H. Deng, and W. Li. Investigation on magnetorheological elastomers based on natural rubber. *Journal of Materials Science*, 42(14):5483–5489, 2008. (Cited on page 21.)

[20] L. Chen, X. L. Gong, W. Q. Jiang, and J. J. Yao. Investigation on magnetorheological elastomers based on natural rubber. *Journal of Materials Science*, 42:5483–9, 2007. (Cited on page 21.)

[21] D. D. L. Chung. Modeling of vibration damping in composite structures. *Journal of Materials Science*, 36:5733–5737, 2001. (Cited on page 12.)

[22] R. M. Crane, A. L. Santiago, and C. P. Ratcliffe. Modeling of vibration damping in composite structures. *Advanced Materials for Vibro- Acoustic Applications*, 2:1–9, 1996. (Cited on page 12.)

[23] H. X. Deng and X. L. Gong. Application of magnetorheological elastomer to vibration absorber. *Communications in Nonlinear Science and Numerical Simulation*, 13:1938–47, 2008. (Cited on page 21.)

[24] H. X. Deng, X. L. Gong, and L. H. Wang. Development of an adaptive tuned vibration absorber with magnetorheological elastomer. *Smart Materials and Structures*, 15(1):N111–6, 2006. (Cited on page 21.)

[25] R. A. DiTaranto. Theory of vibratory bending for elastic and viscoelastic layered finite-length beams. *Journal of Applied Mechanics*, 32(4):881–886, 1965. (Cited on page 26.)

[26] R. A. DiTaranto and W. Blasingame. Composite damping of vibration sandwich beams. *Journal of Engineering for Industry*, 89(4):633–638, 1967. (Cited on page 26.)

[27] B. E. Douglas and J. C. S. Yang. Transverse compressional damping in the vibratory response of elastic-viscoelastic-elastic beams. *The American Institute of Aeronautics and Astronautics Journal*, 16(9):925–930, 1978. (Cited on page 27.)

[28] B. Dyniewicz, A. Pręgowska, and C. I. Bajer. Adaptive control of a rotating system. *Mechanical systems and signal processing*, 43:90–102, 2014. (Cited on page 43.)

[29] D. N. J. Els. *The Effectiveness of Particle Dampers under Centrifugal Loads*. Ph.D thesis, Stellenbosch University, 2009. (Cited on page 23.)

[30] J. M. Ginder, M. E. Nichols, L. D. Elie, and J. L. Tardiff. Magnetorheological elastomers: Properties and applications. In *Proceedings of the 1999 Smart Structures and Materials on Smart Materials Technologies*, pages 131–138, Newport Beach,USA, 1999. (Cited on page 20.)

[31] N. W. Hagoodand and A. Von Flotow. Damping of structural vibrations with piezoelectric materials and passive electrical networks. *Journal of Sound and Vibration*, 146(2):243–268, 1991. (Cited on page 12.)

[32] G. H. Hitchcock, F. Gordaninejad, and A. Fuchs. Controllable magneto-rheological elastomer vibration isolator, 2006. US Patent 7,086,507. (Cited on page 21.)

[33] M. W. Hyer, W. J. Anderson, and R. A. Scott. Non-linear vibrations of three-layer beams with viscoelastic cores. *Journal of Sound and Vibration*, 46(1):121–136, 1976. (Cited on page 27.)

[34] F. Jabbari and J. E. Bobrow. Vibration suppression with a resettable device. *Journal of Engineering Mechanics*, 128(9):916–924, 2002. (Cited on page 29.)

[35] A. Jiang, K. Althoefer, and P. Dasgupta. The core-snake, the variable stiffness laparoscopic camera. In *Proc. of the Hamlyn Symposium on Medical Robotics*, pages 7–9, London, UK, 2013. (Cited on page 25.)

[36] A. Jiang, A. Ataollahi, K. Althoefer, and P. Dasgupta. A variable stiffness joint by granular jamming. In *Proc. of ASME IDETC and CIE Conference*, pages 1–9, Chicago, IL, 2012. (Cited on page 24.)

[37] M. R. Jolly, J. D. Carlson, and B. C. Munoz. A model of the behaviour of magnetorheological materials. *Smart Materials and Structures*, 4(1):607–614, 1996. (Cited on pages 7 and 20.)

[38] D. Kadau, D. Schwesig, J. Theuerkauf, and D. Wolf. Influence of particle elasticity in shear testers. *Granular Matter*, 8(1):35–40, 2006. (Cited on page 25.)

[39] M. Kallio, T. Lindroos, S. Aalto, E. Järvinen, and T. Kärnä. Dynamic compression testing of a tunable spring element consisting of a magnetorheological elastomer. *Smart Materials and Structures*, 16:506–514, 2007. (Cited on page 21.)

[40] R. C. Kar and W. Hauger. Stability of a sandwich beam subjected to a non-conservative force. *Computers and Structures*, 46(5):955–958, 1993. (Cited on page 27.)

[41] E. M. Kerwin. Damping of flexural waves by a constrained viscoelastic layer. *Journal of the Acoustical Society of America*, 31(7):952–962, 1959. (Cited on page 26.)

[42] A. V. Krysko, M. V. Zhigalov, and O. A. Saltykova. Control of complex nonlinear vibrations of sandwich beams. *Russian Aeronautics Iz. VUZ*, 51(3):238–243, 2008. (Cited on page 27.)

[43] D. F. Ledezma-Ramirez, N. S. Ferguson, and M. J. Brennan. Shock isolation using an isolator with switchable stiffness. *Journal of Sound and Vibration*, 330(5):868–882, 2011. (Cited on page 29.)

[44] C. Lee. Finite element formulation of a sandwich beam with embedded electro-rheological fluids. *Journal of Intelligent Material Systems and Structures*, 6(5):718–728, 1995. (Cited on page 22.)

[45] R. Lewandowski and B. Chorazyczewski. Identification of the parameters of the Kelvin-Voigt and the Maxwell fractional models, used to modeling of visoelastic dampers. *Computers and Structures*, 88(1-2):1–17, 2010. (Cited on page 74.)

[46] A. J. Loeve, O. S. Van de Ven, J. G. Vogel, P. Breedveld, and J. Dankelmann. Vacuum packed particles as flexible endoscope guides with controllable rigidity. *Granular Matter*, 12(6):543–554, 2010. (Cited on page 25.)

[47] M. T. Lopez, A. Zugaldia, F. González-Caballero, and J. D. G. Durán. Sedimentation and redispersion phenomena in iron-based magnetorheological fluids. *Journal of Rheology*, 50(4):543–561, 2006. (Cited on page 20.)

[48] Y. P. Lu and B. E. Douglas. On the forced vibrations of three-layer damped sandwich beams. *Journal of Sound and Vibration*, 32(4):513—516, 1974. (Cited on page 27.)

[49] M. D. Luscombe and J. L. Williams. Comparison of a long spinal board and vacuum mattress for spinal immobilization. *Emergency Medicine Journal*, 20(1):476–478, 2003. (Cited on page 25.)

[50] K. Magnucki, P. Jasion, and M. Smyczyński. Modelling of five layer sandwich beams (in Polish). *Modelling in Engineering*, 45(14):90–98, 2012. (Cited on page 27.)

[51] A. Maher, F. Ramadan, and M. Ferra. Modeling of vibration damping in composite structures. *Composite Structures*, 46:163–170, 1999. (Cited on page 12.)

[52] K. M. Mao, M. Y. Wang, and Z. W. Xu ad T. N. Chen. Simulation and characterization of particle damping in transient vibrations. *Journal of Vibration and Acoustics*, 126:202–211, 2004. (Cited on page 22.)

[53] J. G. McDaniel and P. Dupont. A wave approach to estimating frequency-dependent damping under transient loading. *Journal of Sound and Vibration*, 231(2):433–449, 2000. (Cited on page 23.)

[54] D. J. Mead and S. Markus. The forced vibration of a three-layer, damped sandwich beam with arbitrary boundary conditions. *Journal of Sound and Vibration*, 10(2):163–175, 1969. (Cited on pages 26 and 31.)

[55] T. Mitsuda, M. Wakabayashi, S. Kawamura, and S. Kuge. Wearable haptic display by the use of a particle mechanical constraint. In *Proceedings of the 10th Symposium on Haptic Interfaces for Virtual Environment & Teleoperator Systems*, pages 1–6, Orlando, USA, 2002. (Cited on page 25.)

[56] S. O. Reza Moheimani. A survey of recent innovations in vibration damping and control using shunted piezoelectric transducers. *IEEE Transactions On Control Systems Technology*, 11(4):482–494, 2003. (Cited on page 12.)

[57] R. R. Mohler. *Bilinear control processes*. Academic Press, New York, 1973. (Cited on page 29.)

[58] R. A. S. Moreira and J. D. Rodrigues. A layerwise model for thin soft core sandwich plates. *Computers and Structures*, 84:1256–1263, 2006. (Cited on page 26.)

[59] R. A. S. Moreira, J. D. Rodrigues, and A. J. M. Ferreira. A generalized layerwise finite element for multi-layer damping treatments. *Computational Mechanics*, 37:426–444, 2006. (Cited on page 26.)

[60] A. Mroz, A. Orlowska, and J. Holnicki-Szulc. Semi-active damping of vibrations: Prestress accumulation-release strategy development. *Shock and Vibration*, 17:123–136, 2010. (Cited on page 29.)

[61] B. Nayak, S. K. Dwivedy, and K. Murthy. Vibration analysis of a three-layer magnetorheological elastomer embedded sandwich beam with conductive skins using finite element method. In *Proceedings of the Institution of Mechanical Engineers Part C*, Orlando, USA, 2012. (Cited on page 22.)

[62] A. S. Nayfeh, M. J. Verdirame, and K. Kripa. Damping of flexural vibration by coupling to low-density granular materials. *Smart Structures and Materials: Damping and Isolation*, 4697:158–167, 2000. (Cited on pages 23 and 24.)

[63] R. M. Nedderman. *Statics and Kinematics of Granular Materials*. Cambridge University Press, Cambridge, 1973. (Cited on page 25.)

[64] J. Onoda, T. Endo, H. Tamaoki, and N. Watanabe. Vibration suppression by variable stiffness members. *AIAA Journal*, 29(6):977–983, 1991. (Cited on page 29.)

[65] A. Ossowski. Semi-active control of free beam vibration. *Theoretical Foundations of Civil Engineering*, 11:557–566, 2003. (Cited on page 29.)

[66] W. Ostachowicz, A. Żak, P. Malinowski, and T. Wandowski. Control of properties of composite structures with the use of multi–functional materials. *Advances in Science and Technology*, 56:324–333, 2008. (Cited on page 29.)

[67] W. Ostachowicz, K. Majewska, and A. Zak. Magnetic shape memory alloys for forced vibration control of beam-like structures. *Smart Materials and Structures*, 16:2388–2397, 2007. (Cited on page 29.)

[68] R.A. Ottaviani, J. C. Ulicny, and M. A. Golden. Magnetorheological nanocomposite elastomer for releasable attachment applications, April 12 2005. US Patent 6,877,193. (Cited on page 21.)

[69] J. Park and D. L. Palumbo. Damping of structural vibration using lightweight granular materials. *Experimental Mechanics*, 49:697–705, 2009. (Cited on pages 23 and 24.)

[70] D. Pisarski and C. I. Bajer. Semi-active control of 1d continuum vibrations under a travelling load. *Journal of Sound and Vibration*, 329(2):140–149, 2010. (Cited on page 43.)

[71] D. Pisarski and C. I. Bajer. Smart suspension system for linear guideways. *Journal of Intelligent & Robotic Systems*, 62(3-4):451–466, 2011. (Cited on page 43.)

[72] K. Popp, P. B. Kosasih, X. Z. Zhang, and W. H. Li. Fabrication and characterization of MR elastomers with high MR effects. In *15th International Congress on Sound and Vibration*, pages 258–265, Daejeon, Korea, 2008. (Cited on page 21.)

[73] B. Posiadała. Free vibrations of uniform Timoshenko beams with attachments. *Journal of Sound and Vibration*, 204(2):359–369, 1997. (Cited on page 27.)

[74] J. Rabinow. The magnetic fluid clutch. *American Institute of Electrical Engineers Transcations*, 67:1308–1315, 1948. (Cited on page 19.)

[75] J. Rabinow. Magnetic fluid clutch. *National Bureau of Standards Technical News Bulletin*, 32(4):54–60, 1948. (Cited on page 19.)

[76] V. Rajamohan, R. Sedaghati, and S. Rakheja. Vibration analysis of a multi-layer beam containing magnetorheological fluid. *Smart Materials and Structures*, 19(1):1–12, 2010. (Cited on page 22.)

[77] M. Rak, M. Ichchou, and J. Holnicki-Szulc. Identification of structural loss factor from spatially distributed measurements on beams with viscoelastic layer. *Journal of Sound and Vibration*, 310:801–811, 2008. (Cited on page 27.)

[78] A. Ramaratna, N. Jalili, and D. M. Dawson. Semi-active vibration control using piezoelectric-based switched stiffness. In *Proceedings of the 2004 American Control Conference*, pages 5461–5466, Boston, Massachusetts, 2004. (Cited on page 30.)

[79] M. Romaszko. Free vibration control of a cantilever MR fluid based sandwich beam. In *Proc. of 14th International Carpathian Control Conference (ICCC)*, pages 311–314, Rytro, 2013. (Cited on page 30.)

[80] D. Ross, E. E. Ungar, and E. M. Kerwin. Damping of plate flexural vibrations by means of viscoelastic laminate. *Structural Damping*, 3:49–88, 1959. (Cited on page 26.)

[81] O. Sadovskaya and V. Sadovskii. *Mathematical modelling in mechanics of granular materials*, volume 21 of *Advanced Structured Materials*. Springer, 2012. (Cited on page 25.)

[82] M. Saeki. Impact damping with granular materials in a horizontally vibrating system. *Journal of Sound and Vibration*, 251(1):153–161, 2002. (Cited on page 22.)

[83] M. Sanchez, G. Rosenthal, and L.A. Pugnaloni. Universal response of optimal granular damping devices. *Journal of Sound and Vibration*, 331:4389–4394, 2012. (Cited on page 22.)

[84] A. Savitzky and M. J. E. Golay. Smoothing and differentiation of data by simplified least squares procedures. *Analytical Chemistry*, 36(8):1627–1639, 1964. (Cited on page 62.)

[85] A. S. Semisalova, N. S. Perov, G. V. Stepanov, E. Kramarenkoa, and A. R. Khokhlova. Strong magnetodielectric effects in magnetorheological elastomers. *Soft Matter*, 9:11318–11324, 2013. (Cited on page 21.)

[86] M. A. Silva and R. Brasil. Optimization of impact damping for a non-ideal structural systems. In *Proc. of Congress on Numerical Methods in Engineering*, pages 1–20, Porto, Portugal, 2007. (Cited on page 22.)

[87] C. L. Sisemore and C. M. Darvennes. Transverse vibration of elastic-viscoelastic-elastic sandwich beams: compression-experimental and analytical study. *Journal of Sound and Vibration*, 252(1):155–167, 2002. (Cited on page 27.)

[88] E. Steltz, A. Mozeika, J. Rembisz, and N. Corson. Jamming as an enabling technology for soft robotics. *Electroactive Polymer Actuators and Devices*, 7642:225–229, 2010. (Cited on page 25.)

[89] F. Svaricek, Ch. Bohn, P. Marienfeld, H.-J. Karkosch, and T. Fueger. *Automotive Applications of Active Vibration Control.* Vibration Control. SCIYO, Rijeka, Croatia, 2010. (Cited on page 12.)

[90] M. D. Symans and M. C. Constantinou. Passive fluide viscous damping systems for seismic energy dissipation. *Journal of Earthquake Technology*, 35(4):185–206, 1998. (Cited on page 12.)

[91] J. C. Ulicny and M. A. Golden. Releasable fastener system and process, April 22 2004. US Patent 0074066. (Cited on page 21.)

[92] B. Wang and M. Yang. Damping of honeycomb sandwich beams. *Journal of Materials Processing Technology*, 105:67–72, 2000. (Cited on page 23.)

[93] K. Wei, W. Zhang, P. Xia, and Y. Liu. Nonlinear dynamics of an electrorheological sandwich beam with rotary oscillation. *Journal of Applied Mathematics*, 2012:1–17, 2012. (Cited on page 22.)

[94] Z. B. Xu, X. L. Gong, G.J. Liao, and X. M. Chen. An active-damping-compensated magnetorheological elastomer adaptive tuned vibration absorber. *Journal of Intelligent Material Systems and Structures*, 21:1039–47, 2010. (Cited on page 21.)

[95] M. Yalcintas and J. P. Coulter. Analytical modeling of electrorheological material based adaptive beams. *Journal of Intelligent Material Systems and Structures*, 6:488–97, 1994. (Cited on page 27.)

[96] M. Yalcintas and J. P. Coulter. Electrorheological material based non-homogeneous adaptive beams. *Smart Materials and Structures*, 7:128–143, 1998. (Cited on page 27.)

[97] M. Yalcintas and H. Dai. Magnetorheological and electrorheological materials in adaptive structures and their performance comparison. *Smart Materials and Structures*, 8:560–573, 1999. (Cited on page 27.)

[98] M. Yalcintas and H. Dai. Vibration suppression capabilities of magnetorheological materials based adaptive structures. *Smart Materials and Structures*, 13:1–11, 2004. (Cited on page 22.)

[99] N. Yamaguchi, M. Nakao, T. Furuta, and T. Mikoshiba. Development of cylindrical passive damper using high damping rubber. In *Proceedings Of The Fifteenth World Conference On Earthquake Engineering*, pages 1–10, Lisbon, Portugal, 2012. (Cited on page 12.)

[100] J.-Y. Yeh. Vibration analysis of sandwich rectangular plates with magnetorheological elastomer damping treatment. *Smart Materials and Structures*, 22(3):035010, 2013. (Cited on page 22.)

[101] J.-Y. Yeh, L.-W. Chen, and C.-C. Wang. Dynamic stability of a sandwich beam with a constrained layer and electrorheological fluid core. *Composite Structures*, 64:47–54, 2004. (Cited on page 22.)

[102] Z.G. Ying and Y. Q. Ni. Micro-vibration response of a stochastically excited sandwich beam with a magnetorheological elastomer core and mass. *Smart Materials and Structes*, 18(1):1–13, 2009. (Cited on page 22.)

[103] R. Zalewski. Constitutive model for special granular structures. *International Journal of Non-Linear Mechanics*, 45(3):279–285, 2010. (Cited on page 25.)

[104] R. Zalewski and J. M. Bajkowski. Experimental analysis of beam vibrations damping with the special ABS granular structure. *Machine Dynamics Research*, 35(3):98–106, 2011. (Cited on page 26.)

[105] R. Zalewski and Ł. Skoniecki. Six parameters rheological model for special granular structures. *Machine Dynamics Research*, 35(3):107–116, 2011. (Cited on page 26.)

[106] X. Z. Zhang and W. H. Li. Adaptive tuned dynamic vibration absorbers working with MR elastomers. *Smart Structures and Systems*, 5:517–529, 2009. (Cited on page 21.)